Voice Coil Actuated Variable Valve Timing System for Spark Ignition Engines

Md Forhad Khandaker

A Thesis

in

The Department

of

Mechanical and Industrial Engineering

Presented in Partial Fulfillment of the Requirements

for the Degree of Master of Applied Science at

Concordia University

Montreal, Quebec, Canada

March, 2006

Your file Votre référence
ISBN: 0-494-14308-8
Our file Notre référence
ISBN: 0-494-14308-8

ABSTRACT

Voice Coil Actuated Variable Valve Timing System for Spark Ignition Engines

Md Forhad Khandaker

Electromechanical valve actuators have been investigated in recent literature to implement variable valve timing (VVT) in spark ignition vehicle engines. Various types of electromechanical actuators are being investigated to control engine valves independently from crankshaft and ultimately get full benefits from variable valve timing. This thesis investigates a new type of electromechanical actuator - voice coil actuator (VCA). The thesis addresses the modeling of the voice coil actuated engine valve system and proposes a novel control strategy using pulse width modulation (PWM) that achieves fast transitions and low seating velocities. A Lyapunov-based stability analysis of a discrete-time model of the closed-loop PWM system as well as an experimental validation of the static force characteristics of the VCA are also presented in the thesis.

The novel switching control strategy performs better than current strategies using electromechanical valve actuators to implement variable valve timing (VVT). The main improvement over electromechanical actuators is the fact that the novel control strategy achieves the conflicting performance requirements of very fast transition times while simultaneously exhibiting low contact velocities. The experimental results validated the bi-directional motion ability of the voice coil actuator, which is an essential property of an electromechanical actuator to control engine valves.

DEDICATION

To my beloved Parents

Abdul Mannan Khandaker

And

Rabeya Begum

ACKNOWLEGEMENTS

I would like to start with the name of almighty ALLAH, Who deserved all praise and gratitude from His amazing creatures.

This research work was a great opportunity for me to develop my academic carrier in a completely new field of electromechanical system modelling, simulation and control system design.

My thanks go first to my supervisors, Dr. Henry Hong and Dr. Luis Rodrigues. It was impossible for me to finish this research work without their continuous guidance, support and encouragement.

I would like to thank Robert Oliver and Gilles Huard of the Department of Mechanical and Industrial Engineering, for their technical support to develop the experimental setup. I want to thank my lab-mates Dagang, Girish, and Donfang for their help during my study period and I wish them the best. I also would like to thank some of my friends who have inspired me and have greatly contributed in the research project.

I also greatly acknowledge the Natural Sciences and Engineering Research Council of Canada (NSERC) for the funding of this research project.

And, Finally, my thanks go to my loving family members – my wife, Shahana Parvin, my son, Nazmus, my daughter, Shati and my parents for their support and tolerance of the many late nights.

Md Forhad Khandaker

TABLE OF CONTENTS

PAGE

LIST OF FIGURES

FIGURE NO **PAGE**

LIST OF TABLES

NOMENCLATURE

c	- Viscous damping between the moving parts in the air medium (?)
d	- Pulse Width Modulation duty ratio (-)
dT	- The pulse width for the *(k+1)th* sampling period.
e	- System position error (mm)
f	- Frequency (Hz)
h	- Pulse Width Modulation voltage amplitude (V)
i	- Applied current (A)
l	- Length of the conductor (m)
m	- Lumped mass of valve subsystem (kg)
m_1	- Mass of the engine valve (kg)
m_2	- Mass of the moving coil (kg)
n	- Number of wire turns
p	- Desired pole location
r	- Reference input of the system
u	- Pulse width modulated control input
y	- Controlled variable of the system (output)
BDC	- Bottom dead center
B	- Magnetic induction flux density (Weber/m^2)
BSFC	- Brake specific fuel consumption
CO	- Carbon Monoxide
D	- Total valve traveling distance (mm)

DIG - Direct Injection Gasoline

DOHC - Double Overhead Camshaft

EEVC - Early exhaust valve closing

EEVO - Early exhaust valve opening

EIVC - Early intake valve closing

EIVO - Early intake valve opening

EGR - Exhaust gas recirculation

EMF - Electromotive force

EMV - Electromechanical / Electromagnetic valve

EVA - Electromechanical valve actuator

EVC - Exhaust valve close

EVO - Exhaust valve open

EVVT - Electronically variable valve timing

F - Force produced in VCA (N)

$G(s)$ - System transfer function

$G_c(s)$ - Controller transfer function

$G_o(s)$ - Overall transfer function

HC - Hydrocarbons

IVC - Intake valve close

IVO - Intake valve open

I_{PWM} - Current drawn by the pulse width modulation system

K_b - Back EMF constant (Volts/(m/s))

K_F - Force constant (N/A)

L - Coil inductance (mH)

LEVC - Late exhaust valve closing

LEVO - Late exhaust valve opening

LIVC - Late intake valve closing

LIVO - Late intake valve opening

M - Constant of actuating signal limit

NOx - Nitrogen oxides

PV - Pressure - Volume

PWM - Pulse Width Modulation

PO - Percent Overshoot

$P_{analogue}$ - Input analogue power to the system (Watts)

P_{PWM} - Input power of the PWM signal to the system (Watts)

R - Coil resistance (Ω)

RGF - Residual gas fraction

SI - Spark Ignition

SOHC - Single Overhead Camshaft

T - Sampling period (ms)

T_r - Rise time (ms)

T_s - Settling time (ms)

TDC - Top dead center

UBHC - Unburned Hydrocarbons

V - Applied voltage to the voice coil actuator (V)

VTEC - Variable Valve Timing and Lift Electronic Control

VCA - Voice coil actuator

VVA - Variable valve actuation

VVT - Variable valve timing

V_b - Back electromotive force voltage (V)

$V_{\max}$ - Maximum PWM voltage

φ_m - Phase margin (degree)

θ_p - Angle of the undetermined pole

ω_n - Natural frequency

ξ - Damping ratio

CHAPTER 1

INTRODUCTION

1.1 Engine Valve Control Technology

Automobile engine designers are seeking methods for minimizing fuel consumption, vehicular emissions and enhancing engine efficiency. For a conventional camshaft controlled engine configuration, the duration and the timing of the valve events are usually fixed to correspond directly to the crankshaft rotation. However, for efficient engine operation, the valve timing, lift and duration must correspond optimally to the engine load and speed requirements. As a result, conventional engine combustion performance, and hence engine efficiency, is often compromised under all operating conditions because the valve positions are significantly different from the optimal. Unlike conventional SI engines, a variable valve timing (VVT) engine has the ability to control the intake and exhaust valve events independently of the crankshaft rotation, allowing for reduced pumping losses and increased engine overall efficiency [1]. VVT controlled engines also have the ability to reduce the emissions of harmful hydrocarbons and nitrogen oxides (NO_X), which are pollutants of major environmental concern [2]. With proper variable valve actuation (VVA) design and control it is expected that the pressure-volume (PV) cycle of any VVT engine can achieve near-zero pumping losses, maximum volumetric efficiency, and the minimization of exhaust pollutants [3].

Although mechanically operated VVT's exist [4], the technology is still new and their operation is limited with respect to their phasing strategy for the variation of valve

lift and duration. Nonetheless they have shown a dramatic impact on engine performance [1].

The highest degree of flexibility and the fastest VVT capability are achieved in truly camless engines with either electrohydraulic or electromechanical actuators [2]. The electromechanical valve actuators (EVA) are becoming increasingly popular to actuate engine valves due to their ability to achieve continuously variable lift, duration, and phasing of the valves [5]. A developing technology using electronic and electromechanical actuators provides complete control of all valve-timing events that will simplify the complex design and enhance the limited operations of mechanically operated VVT's. The novel electronically variable valve timing (EVVT) strategy allows the continuous and rapid position control of intake and exhaust valve lift and duration at any point of time during an engine cycle [5]. Significant improvements in engine performance can be achieved through individual control of the valve timing and different versions of the electromechanical valvetrain (EMV) actuators are under development at several major automotive manufacturers [6]. The concept of camless engine technology has existed for several years. However, the problem of ensuring accurate transition timing with small impact velocities has prevented the technology from being implemented [7]. Meeting such requirements is the main objective of the proposed system design in this thesis.

Independent control of the intake and exhaust valves offers the possibility to operate the engine efficiently over a wide operating range. Voice coil actuators (VCA) are the ideal linear actuators for such an application as they are compact in size, cog-free, hysteresis-free and have fast response time compared to other actuators.

1.2 Fundamentals of Spark Ignition (SI) Engine

In a four stroke spark ignition engine the strokes correspond to Intake (suction), Compression, Power / Expansion and Exhaust. A typical pressure-volume (PV) diagram of the spark ignition engine is shown in fig.1.1. Initially, the piston is up close to the top of the cylinder and both the intake and exhaust valves are closed. The piston travels from top dead center (TDC) to bottom dead center (BDC) on the intake and power strokes, and travels from BDC to TDC on the compression and exhaust strokes. Mechanical energy is only produced during the power stroke and all other strokes are completed by the crankshaft inertia. The following subsections describe the fundamentals of all the strokes of a four stroke SI engine.

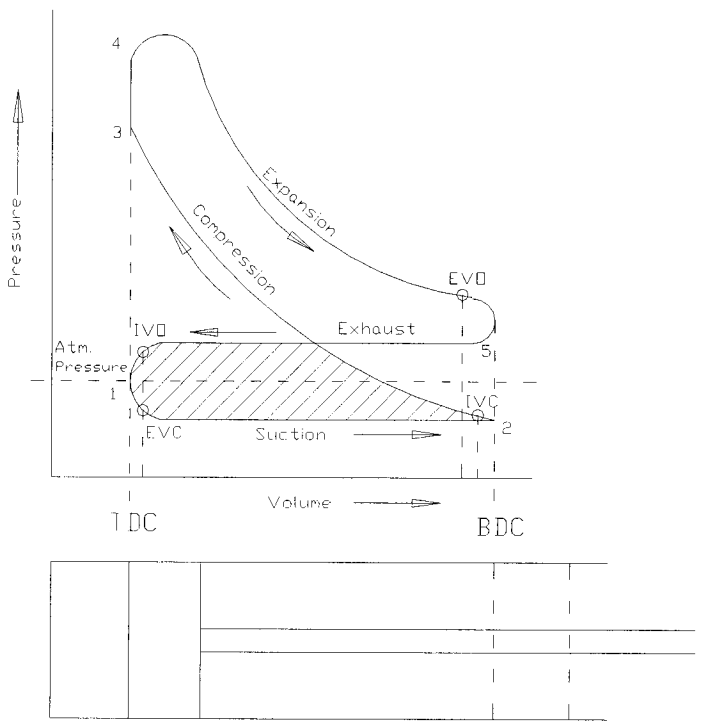

Fig. 1.1 PV diagram for a conventional four stroke SI engine

1.2.1 Intake Stroke

With reference to fig. 1.2 for the intake stroke, the piston moves downward from TDC; the exhaust valve is nearly closed; the intake valve begins to open (IVO) and the air-fuel mixture is sucked into the cylinder, while the exhaust is passed out through the

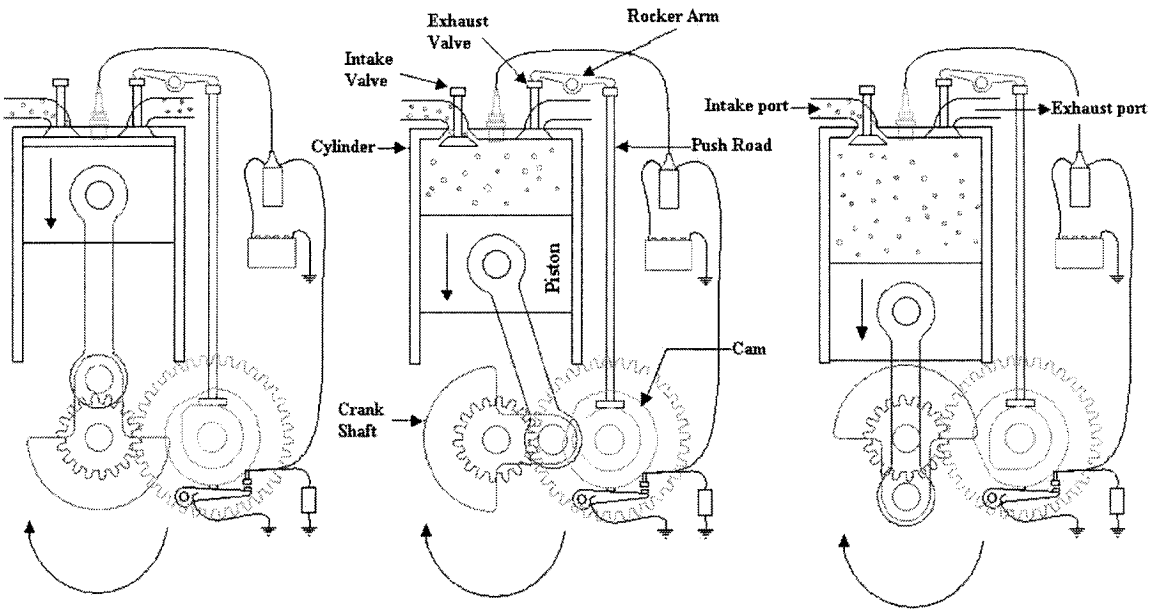

Fig. 1.2 Intake Stroke (Snap shot taken from the animated four stroke (Otto) engine [6])

exhaust valve. This period while the intake and exhaust valves are both open, is termed the "overlap". As the piston reaches to TDC and moves down the exhaust valve closes (EVC) and more fuel is sucked in. When the piston is traveling to the BDC, the intake valve closes (IVC), trapping the air-fuel mixture in the cylinder.

1.2.2 Compression Stroke

During the compression stroke, as shown in fig. 1.3, the piston moves from BDC to TDC and compresses the trapped air-fuel mixture. The amount of compression

depends on the compression ratio of the engine, which is usually in the range of 8:1 to 10:1. Both valves are closed during the compression stroke so that no air-fuel mixture escapes out of the cylinder when the air-fuel mixture is compressed. Then the mixture is ready for igniting.

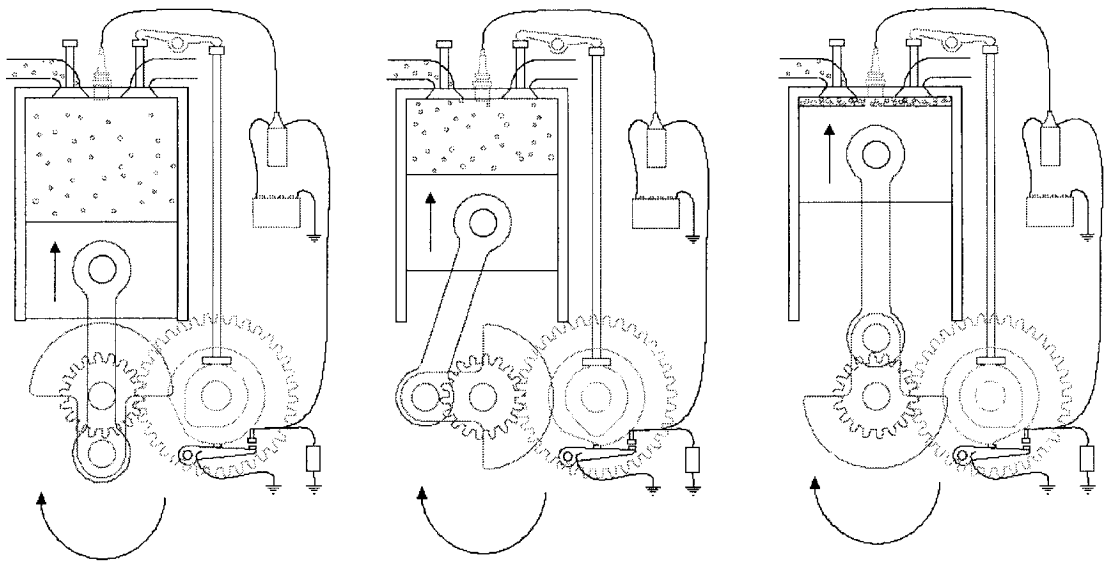

Fig. 1.3 Compression Stroke (Snap shot taken from the animated four stroke (Otto) engine [6])

1.2.3 Power Stroke

In this stroke (fig. 1.4) the compressed air-fuel mixture is ignited by the spark plug and produces a powerful expansion of the gases. This process pushes the piston down to the BDC with great force and provides power to the crankshaft. During this stroke both valves remain closed so that the expanding air can transmit its force completely to the piston.

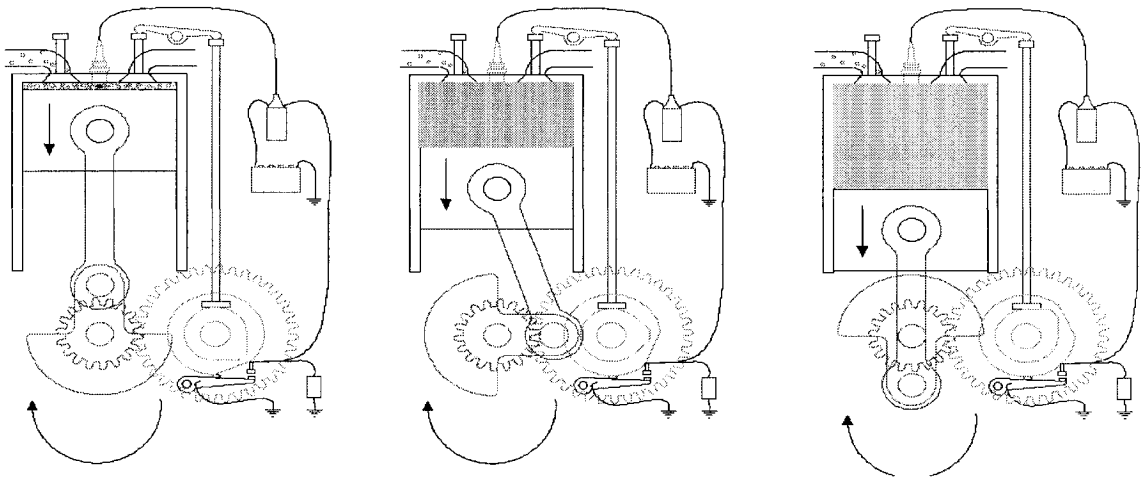

Fig. 1.4 Power Stroke (Snap shot taken from the animated four stroke (Otto) engine [6])

1.2.4 Exhaust Stroke

As the piston nears the BDC the exhaust valve begins to open (fig. 1.5). Most of the fuel has been burnt and the cylinder pressure will begin to push the exhaust out through the valve. The piston then passes through BDC and begins to rise towards the TDC; the exhaust valve opens (EVO) and allows the burned gases to be expelled from the engine cylinder.

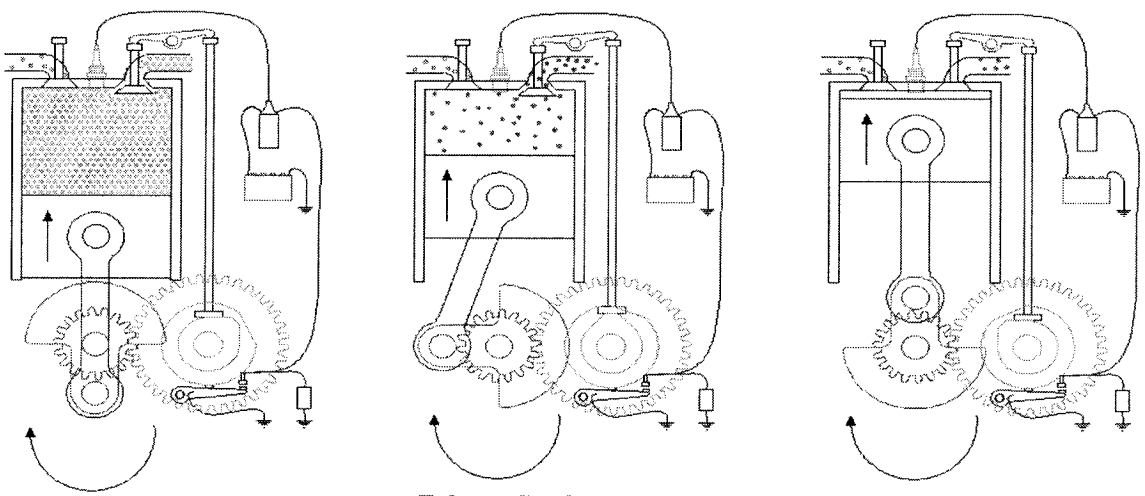

Fig. 1.5 Exhaust Stroke (Snap shot taken from the animated four stroke (Otto) engine [6])

The duration of each engine stroke can be determined by manipulating the engine speed with 180 crankshaft degrees. The camshaft is synchronized with the crankshaft so that it makes one revolution for every two revolutions of the crankshaft. This means that every intake and exhaust valve opens once every two revolutions of the crankshaft or one revolution of the camshaft. Therefore, the required valve lifting, opening and closing time can be found directly from the engine speed. The duration of the valve lifting, opening and closing is an important design criterion for an electromechanical valve actuator.

1.2.5 Valve Timing

The sequence of the opening, closing, overlapping, and lifting of the engine valves, has a great effect on engine performance at a given speed [14]. These parameters are controlled by the cam design, but until recently, they were fixed for all engine speeds. The result is varying engine efficiency at different speeds. The valve overlap period, while the exhaust valve is closing and the intake valve is opening (fig.1.1), is the main area of improvement to optimize the engine efficiency. This overlap is used to create a siphon effect to draw fresh mixture into the cylinder while forcing the exhaust out of it. It is not possible to expel all of the burnt fuel from the cylinder in a very small overlap period and power will be compromised. Conversely, in the case of long overlap period some of the fresh mixture will pass through into the exhaust manifold and be wasted. Variation in the overlap period is required for different engine speed and driving conditions. This overlap period cannot be readily changed by the current mechanically actuated valve system. Instead, the electronically actuated valves can achieve the optimum overlap period for different engine speed and driving conditions.

A recent development in valve train design is to use more than one intake and/or exhaust valve per cylinder because the total opening available for the same valve lift is greater. Most engines have two valves per cylinder, one intake valve and one exhaust valve. Some newer engines are using multiple intake and exhaust valves per cylinder for improved engine power and efficiency. These engines are sometimes named for the number of valves that they have such as "24 Valve V6" which indicates a six cylinders (V-6) engine with four valves per cylinder. Modern engine designs can use anywhere from 2 to 5 valves per cylinder [6] to increase valve opening area. However, the multiple engine valves reduce the strength of the cylinder head and increase the complexity of engine design. Another development is that recent car models are now featuring a variable cam timing (using multiple cam) that tries to maintain optimum engine performance and efficiency by compensating for the different valve timing required at various engine speeds and loads [36]. Existing valve trains include several mechanical parts, so the variable cam timing makes the engine design more complicated and it increases production cost. The mechanical valve actuating technique is described in the next section.

1.3 Valve Train

In a spark ignition engine, the group of parts that changes the type of motion to operate the engine valves is called the valve actuating mechanism. This mechanism may vary considerably in construction and design, even though its function remains the same. With reference to fig. 1.6 as an example, a valve actuating mechanism includes the camshaft, cam followers, pushrods, rocker arms, and valve springs. The valve actuating

mechanism receives power from the drive mechanism and transmits the power to the engine valves (see fig. 1.6). The intake and exhaust valves are of the poppet type, because the poppet valves have cone-shaped heads and similar shaped seats that give the valves a self-centering action.

The valves are opened and closed by a camshaft. A camshaft is a rotating shaft that has individual lobes for each valve. The key parts of any camshaft are the lobes. As the camshaft spins, the lobes open and close the intake and exhaust valves in time with the motion of the piston. The valves are maintained closed by springs. The pushrods and rocker arms transfer the reciprocating motion generated by the camshaft lobes to open the valves. As the valve is opened, it compresses the valve spring. The energy stored in the valve spring is then used to close the valve as the camshaft lobe rotates out from under the follower.

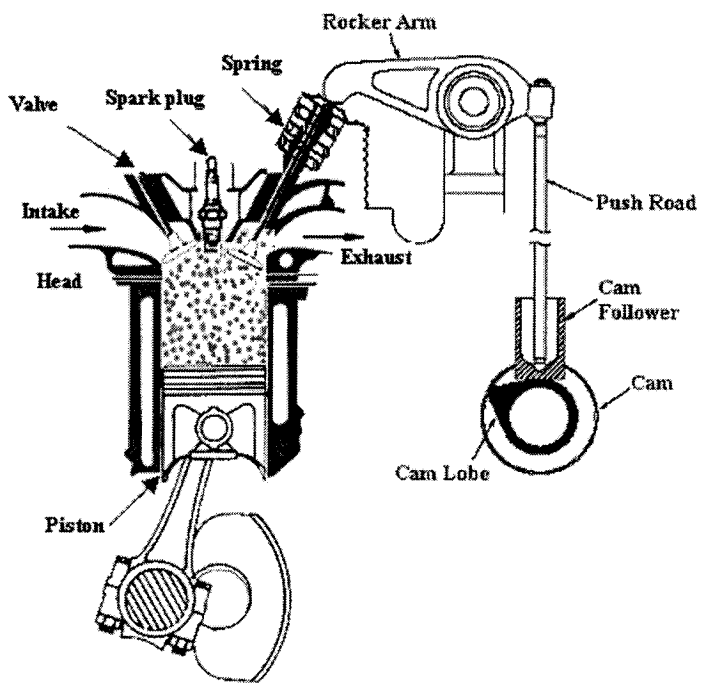

Fig. 1.6 Engine Valve Train [6]

In most engines, the synchronization between camshaft and crankshaft is done by a "timing chain or belt" that connects the camshaft with the crankshaft. Newer engines have the camshaft located in the cylinder head directly over the valves. This design is more efficient but it is more costly to manufacture and requires multiple camshafts. Some engines have two camshafts on each head, one for the intake valves and one for the exhaust valves. These engines are called Dual Overhead Camshaft (D.O.H.C.) Engines while the other type is called Single Overhead Camshaft (S.O.H.C.) Engines. Like SOHC and DOHC engines, the valves in a pushrod engine are located in the head, above the cylinder, but the camshaft on a pushrod engine is inside the engine block, rather than in the head.

The next section reviews the literature of variable valve timing (VVT) and the valve actuation technology to achieve VVT. The literature review is divided in two subsections. The first subsection describes the technology of intake and exhaust strategies of VVT and their effects on the engine performance and emissions. The second subsection describes the various techniques of valve actuation to achieve VVT.

1.4 Review of Previous Work

1.4.1 Variable Valve Timing

Variable Valve Timing (VVT) provides improvements in engine efficiency, emissions, and performance by changing the valve lift and timing as a function of engine overall conditions. Compromises inherent with fixed valve lift and timing have prompted engine manufacturers to consider Variable Valve Actuation (VVA) systems on spark

ignited engines for many decades. These systems have good potential to meet future power-train requirements for improved fuel economy, emissions, and performance [3]. Unlike lean-burn Direct Injection Gasoline (DIG) technology, VVA does not require lean after treatment technology and is therefore significantly lower risk in the face of increasingly stringent emissions regulations [2]. One of the greatest advantages of VVT is that, by the manipulation of valve timing it is possible to get internal exhaust gas recirculation (EGR), which has the potentials to reduce NO_x emissions [4].

Several engine manufacturers are performing research on systems that would allow variability in valve timing. There are a couple of novel ways to vary the valve timing. One system used on some Honda engines is called Variable Valve Timing and Lift Electronic Control (VTEC) [29]. VTEC is an electronic and mechanical system that allows the engine to have multiple camshafts. VTEC engines have an extra intake cam with its own rocker, which follows this cam. The profile on this cam keeps the intake valve opened longer than the other cam profile. At low engine speeds, this rocker is not connected to any valves. At high engine speeds, a piston locks the extra rockers that control the two intake valves. Another technology uses a device that can advance the valve timing [30]. This does not keep the valves opened longer; instead, it opens them earlier and closes them later. This is done by rotating the camshaft ahead a few degrees.

Variable Valve Timing (VVT) can also be achieved by cam-less actuation technology. Various studies have shown that optimization of the valve timing of a spark ignition engine results in higher fuel efficiency, lower emissions and improved torque performance [9]. Variable Valve Actuation (VVA) systems vary the valve lift and timing

continuously over the operating range and may be electro-hydraulically actuated, electro-magnetically actuated, or electro-mechanically actuated. Most continuous VVA system use Early-Intake-Valve-Closing (EIVC) as the primary strategy to reduce pumping work and improve fuel economy. Control of valve seating velocity, high power consumption, and speed limitations continue to present significant challenges for many continuously VVA systems [2].

The engine valve control objective is to ensure accurate valve opening and closing with small contact velocity V_c of all moving parts. The small contact velocity, also known as "soft landing", is a very important consideration because high contact velocities correlate with noise and component wear. The opening and the closing of the valves have to be achieved within a very small travel time or, otherwise, engine operation at high speed will deteriorate. These two requirements are obviously conflicting [3]. Also the control difficulties arise from 1) the nonlinear characteristics of the actuator; 2) the limited range of actuation and control input saturation; and 3) unknown and varying gas flow forces acting on the valves [16].

A variety of VVA strategies exist, such as

1) Late Intake Valve Closing (LIVC)
2) Early Intake Valve Closing (EIVC)
3) Late Intake Valve Opening (LIVO)
4) Early Intake Valve Opening (EIVO)
5) Early Exhaust Valve Closing (EEVC)
6) Late Exhaust Valve Closing (LEVC)

7) Early Exhaust Valve Opening (EEVO)

8) Late Exhaust Valve Opening (LEVO).

These strategies represent different ways to control the airflow into and out of the engine cylinder to reduce pumping losses during the gas exchange process [3]. Each one of these strategies will now be described in detail.

1) A late intake valve closing (LIVC) system on a single cylinder SI engine with three modified cams can reduce pumping losses by 40 % during part load conditions, and NO_X emissions by 24 % at mid load with no changes in hydrocarbons (HC) [10]. According to Saunders *et al.* [11], two methods can be used to improve the engine efficiency. One is VVT by LIVC to reduce the pumping losses, and the other is variable compression ratio (VCR) to increase the expansion ratio. The combination of these two methods results in an Otto-Atkinson cycle engine. Saunders *et al.* [11] obtained LIVC by using a secondary camshaft driven by a variable-geometry timing belt. VCR was obtained by using connecting rods with different length, modifications to the cylinder head and by using gaskets. The authors claimed that 13 % brake specific fuel consumption (bsfc) could be obtained by using LIVC. Using LIVC with VCR, bsfc can be improved up to 20 %. The LIVC serves the purpose of reducing the pumping losses, and the VCR is used to vary the amount of air-fuel mixture according to load and speed conditions. This combined strategy results in up to 20 % of fuel consumption savings over a conventional engine at low speeds/loads [12].

2) Using the early intake valve closing (EIVC) concept in a single cylinder SI engine with three modified cams can reduce pumping losses by 40 % as compared to a

conventional engine. Also it can reduce fuel consumption by 7 % and NO_X emission by 24 % at half load [13]. This system requires more number of cams, which leads to added complexity in the VVT mechanism.

3) The late intake valve opening (LIVO) causes the cylinder pressure to dip momentarily below the intake manifold pressure and the pumping loss is increased because of the reduced pressure in the first part of the intake stroke [14]. From their experimental results, Badami *et al.* [31] claimed a 6% of reduction in fuel consumption for a fixed mass of delivered fuel and 20% of reduction in fuel consumption at a fixed throttle position can be achieved with the combination of spark advance and adopting the LIVO strategy.

4) Early intake valve opening (EIVO) allows some amount of burnt gases to go back into the intake manifold because of the cylinder-intake manifold pressure gradient. This back flow is also used for internal exhaust gas recirculation (EGR), which is helpful to reduce NO_x [32, 33]. EIVO also reduces the pumping losses because some of the exhaust gases go into the intake manifold and less burnt gases are being expelled during the exhaust stroke.

5), 6) According to Law *et al.* [34] in an early exhaust valve closing (EEVC), a small amount of pumping losses can occur due to the compression and expansion of trapped residual gases. In the case of late exhaust valve closing (LEVC), there is more exhaust gas backflow because of the increase in overlap, which reduces the volumetric efficiency and also the pumping losses [14]. Moreover, LEVC is less effective in reducing HC emissions as compared to EEVC [32].

7), 8) Siewert [32] tested a single cylinder engine for an EEVO strategy that results in an increase of exhaust hydrocarbons and Asmus [35] mentioned that if the cylinder pressure during the exhaust stroke does not rise appreciably above the exhaust manifold then pumping losses will be minimized in EEVO engines. On the other hand late exhaust valve opening (LEVO) reduces the power output because the majority of the work is from the exhaust stroke that is used to expel the burnt gases from the engine cylinder and a greater pumping losses results [36].

The effects of the various strategies of VVT technology on the engine performance and emissions are summarized in Table 1.1.

Table 1.1 Effects of the various strategies of VVT technology on the engine performance

Strategy	**Effects on engine performance and emissions**
LIVC	Reduces pumping losses up to 40% and NO_X emissions up to 24%
EIVC	Reduces pumping losses up to 40%, fuel consumption up to 7% and NO_X emissions up to 24%
LIVO	Increases pumping losses and reduces fuel consumption up to 6~20%
EIVO	Reduces NO_X and pumping losses
EEVC	Reduces pumping losses by a small amount
LEVC	Reduces pumping losses and HC emission but also reduces volumetric efficiency
EEVO	Increases HC exhaust
LEVO	Reduces the power output and increases the pumping losses

1.4.2 Mechanical and Electronic Valve Actuation for VVT

Quite a few models and control mechanisms of independently valve actuation have been proposed to achieve VVT. Pierik *et al.* [5] explained the design features and operation of the mechanism of a mechanical variable valve actuation (VVA) system. The mechanical VVA system simultaneously varies lift, duration and phase. The capabilities of this mechanism of reduced lift, EIVC and LIVO were provided the best pumping loss reduction for partial load. The authors claimed that the VVA mechanism reduced the brake specific fuel consumption (BSFC) of approximately 12% at idle, 7~10% at low to middle load and 0~3% at middle to high load. Also the peak torque improved by an average of 3% over the engine speed range 1200 ~ 3200 rpm.

The author of [38] describes the implementation of the variable valve timing system in a 1.8 liter version of the Rover K16 engine. The VVA engine shows superior volumetric efficiency of 7% at high engine speed (6000 rpm). However, at a lower speed of 2500 rpm, the volumetric efficiency of the VVA engine is 4% less than that of the base engine. Stefanopoulou *et al.* [39] designed a model-based controller that coordinates variable camshaft timing and fuel charge in an internal combustion engine to reduce feed gas emission, regulate A/F ratio and maintain torque response similar to that of a conventional engine. Their simulation results demonstrated the potential performance improvements achieved by the variable cam timing (VCT) engine. A simple nonlinear model of hydraulic VCT actuators was developed and published in [41] on a dual-independent VCT engine under closed loop operation, which achieved superior performance compared to linear PIDs. The authors mentioned in the analysis of

experimental results that the overshoot in the response can be reduced significantly and the speed of the response can be increased by more than 50% with the nonlinear controller.

The nonlinear uncertain dynamics and stringent performance requirements of the solenoid valve actuators make modeling and control of these devices a challenging problem. A finite-element analysis (FEA) model is proposed in [40] to generate experimentally accurate static force and flux data as well as voltage transient data for a real prototype actuator. The authors claimed that the FEA-based linear programming (LP) model can be used as a plant model for simulating model-based control algorithms.

Wang *et al* [2] proposed a dynamic model of an electromechanical valve actuator. They developed a physics-based model for an electromechanical camless valve actuator. In this model, the actuator consists of a set of springs and electromagnets to control the opening and the closing of the engine valve. Different model formats were constructed for the linear and the saturation regions. However, the linear region model was used for control design. They took special care to ensure model validity in the small gap between the armature and the coil, where high contact velocities are responsible for noise production. The experimental data show the smooth change of velocity at extreme ends, but the simulation shows an acceleration followed by a large contact velocity. Stubbs [15] also proposed a similar type of EVA model including the consideration of resistance variations due to temperature.

A control methodology is developed based on a nonlinear state-space description of the actuator, which is derived based on physical principles and parameter identification

in [16]. Experiments were conducted to measure valve release timing, transition times, and closed-loop control schemes. Their experimental data show bouncing after the armature hits the lower coil. They showed that for typical engine speeds (5000 rpm ~ 7000 rpm), the delay time for valve release is much longer than the valve lift duration required for unthrottled engine operation. They applied a reverse polarity voltage with high amplitude (-180V) to cancel the current created by the electromotive force (EMF) . This strategy enabled a fast valve release, achieving the reduced delay time of 1.2 ms. The authors mentioned that the soft landing is fundamentally difficult to achieve because their system is (i) highly nonlinear, (ii) unstable with low control authority, and (iii) uncertain with varying parameters and disturbances. They designed a position feedback controller that reduced the impact velocity to 0.16 m/s with a consistent transition time of 3.42 ms.

Butzmann *et al* [17] proposed an adaptive feedback control algorithm. The average seating velocity they achieved from laboratory tests was below 0.1 m/s. The desired performance on the impact velocity and transition time is achieved by keeping a predefined constant ratio of the rate of change of current to the actual current. However, this performance is effective only under laboratory conditions and the authors point out potential problems when the system experiences large disturbances. Peterson *et al* [4] presented a linear design control methodology that reduces the impact velocities between the valve, valve seat, and the actuator. Experimental results show the open-loop impact velocity is approximately 1m/s and the closed-loop controller achieves a reduction of a factor of six in the impact velocity.

Tai *et a* [18] published a control-oriented electromechanical valve actuator model for small contact velocity with improved experimental results. They also considered the valve backlash (defined as the gap between the armature and valve stem) dynamics in their model and designed a robust H_{∞} loop-shaping controller method to stabilize the actuator. The experimental results show an average seating velocity of 0.057 m/s, which is quite remarkable. The main negative point in their result is that the valve closing time was too long at a high engine speed due to the use of a weak spring. Based on a measure of the sound intensity, an extremum-seeking controller was designed to reduce the magnitude of the impact velocity (Peterson *et al*, Automatica 2004). A small microphone was used to measure the sound intensity, which the controller then minimizes. The reduced sound intensity results in decreased impact velocities. Their experimental results achieved a transition time of 4.0 ms and an impact velocity of less than 0.1 m/s. Peterson *et al* [26] designed a nonlinear self-tuning controller that achieved a mean impact velocity of 0.16 m/s and a transition time of less than 4 ms.

In June 2003, Tai and Tsao [28] published a feed forward and Linear-Quadratic Regulator feedback controller to control the electromechanical camless valvetrain (EMCV) actuator for soft seating. Then a repetitive learning control was designed to improve tracking performance by a cycle-to-cycle learning process. The different control strategies were tested on their experimental system, which led to a reduced seating velocity of 0.061 m/s with a standard deviation of 0.028 m/s. Peterson *et al.* [9] presented a paper in which they considered the valve backlash effect, which plays a critical role in the operation of the electromechanical valve actuator. They used a combination of feed forward and iterative learning controllers, which is capable of bounding the impacts by

0.4 m/s through trajectory tracking. However, to achieve the controller to improve the tracking of the bounded impact velocity, the real-time iterative learning methodology required thirteen iterations.

Wang *et al.* [37] formulated the idle speed control problem for a SI engine equipped with a camless-electrohydraulic valvetrain and showed that unthrottled camless operation results in unstable open-loop dynamics at idle. Using theoretical derivations, they demonstrated that the unstable pole and controller hardware delay impose limitations in the achievable disturbance rejection performance of the closed loop system. A nonlinear controller, which renders the electromechanical valve actuator globally asymptotically stable without assuming linearity was presented in [3]. Stability was proven mathematically and was also shown experimentally. Experimental results showed that the nonlinear controller stabilizes the armature against the magnetic coil while achieving a mean impact velocity of 0.12 m/s.

As seen in the previous paragraphs, most researchers considered very similar types of electromechanical actuators that present significant nonlinear characteristics. Their proposed electromechanical valve mechanisms consist of two electromagnets that catch and hold the armature to moves between two extreme positions under the forcing of two springs. Valve motion is controlled via the voltage applied to both magnetic coils consecutively. In addition, for faster release of the armature, each time an opposite polarity voltage must be applied to the electromagnet that hold the armature during that time. However, a voice coil actuator is a linear bi-directional electromechanical actuator with low hysteresis and it offers the potential to be a very suitable actuator to control the

engine valve independently from the crankshaft. So far, no work has been performed on voice coil actuators (VCA) to control the inlet and exhaust valves for VVT. This thesis will address this problem and will suggest a novel variable valve timing system for spark ignition engines.

1.5 Research Objectives and Contributions

The main objective of this research is to propose a new type of fast responding bi-directional actuator to control the engine valve events independently from the crankshaft and ultimately achieve variable valve timing. In previous research it was shown that variable valve timing could potentially improve the engine efficiency and could reduce engine emissions. Therefore the research reported in this thesis concentrates on the following items:

1. To develop a mathematical model of the voice coil actuated engine valve system and analyze the transient and steady state performance of the system.

2. To propose a novel control strategy using pulse width modulation to achieve very fast transient response with low contact velocity between valve and valve seats.

3. To perform a Lyapunov-based stability analysis for a discrete-time model of the closed-loop voice coil actuated engine valve system.

4. To design and implement an experimental setup to validate the theoretical static physical characteristics of the voice coil actuator using experimental data.

1.6 Thesis Outline

The structure of this thesis is as follows. Chapter 1 reviews the literature associated with the variable valve timing and the mechanical / electronic valve actuation. It also includes the research objectives, contributions and the thesis outline. Chapters 2 and 3 describe the mathematical modeling of the voice coil actuated engine valve system and the novel control strategy by using pulse width modulation, respectively. Chapter 3 also includes the simulation results of the system for VVT and unthrottled engine operation. In chapter 4, a Lyapunov-based stability analysis is performed to prove the stability of a discrete-time model of the proposed pulse width modulated VCA system. Chapter 5 covers the experimental setup of the voice coil actuator and the analysis of the experimental results for the determination of static physical characteristics of a VCA. Finally, Chapter 6 presents the conclusions and the recommendations for further research in this domain.

CHAPTER 2

MATHEMATICAL MODELING OF A VOICE COIL ACTUATED ENGINE VALVE SYSTEM

2.1 Introduction

Voice-coil actuators (VCA) are versatile direct drive electromechanical devices. The voice-coil provides non-commuted limited motion servo-actuation with linear control characteristics. Its motion capability is of high precision position sensitivity, limited only by the feedback sensor used to close the control loop. A voice coil employs a permanent magnet field assembly in conjunction with a coil winding to produce a force proportional to the current applied to the coil. It has very low electrical and mechanical time constants and high power to weight ratio. The next section will describe VCAs in more detail.

2.1.1 Description of VCA

VCAs are ideal linear actuators as they are electro-mechanical devices that can be driven in both directions (Fig.2.1). The conventional VCA consists of a cylindrical moving coil, a permanent magnet, and a soft iron core. The coil is free to move axially in the air gap formed between the permanent magnet and the iron core.

VCAs are ideal electromechanical actuators for applications that require high frequency actuation, high velocity and acceleration, and linear control characteristics. Cog free, hysteresis free, smooth and fast response characteristics make it an ideal servomotor [19].

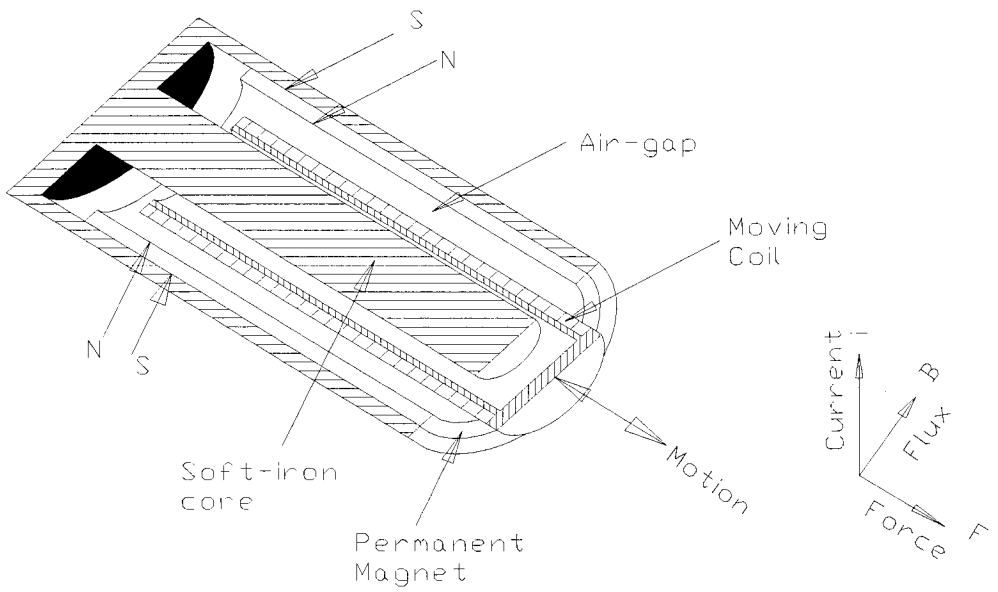

Fig.2.1 Sectional view of voice coil actuator

2.1.2 Working Principle of the VCA

The voice coil actuator has a free coil in the middle of a static permanent magnetic field to produce a force proportional to the applied current to the coil. The direction of the force depends on the polarity of the voltage applied to the two terminals of the coil. An easy way to find the direction of motion is to apply Fleming's left hand rule (Fig.2.2) [58].

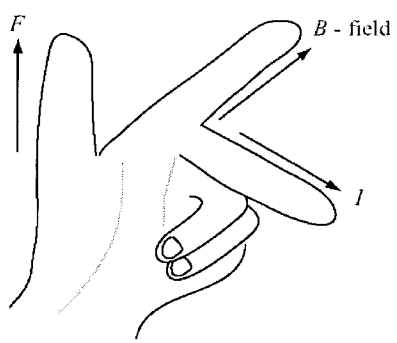

Fig. 2.2 Flemings left hand rule for magnetism [58]

Fig.2.3 shows the direction of the developed force in a voice coil actuator. The direction of force is out of the page if the current flows counterclockwise and the direction of the force is into the page if the current flows in clockwise.

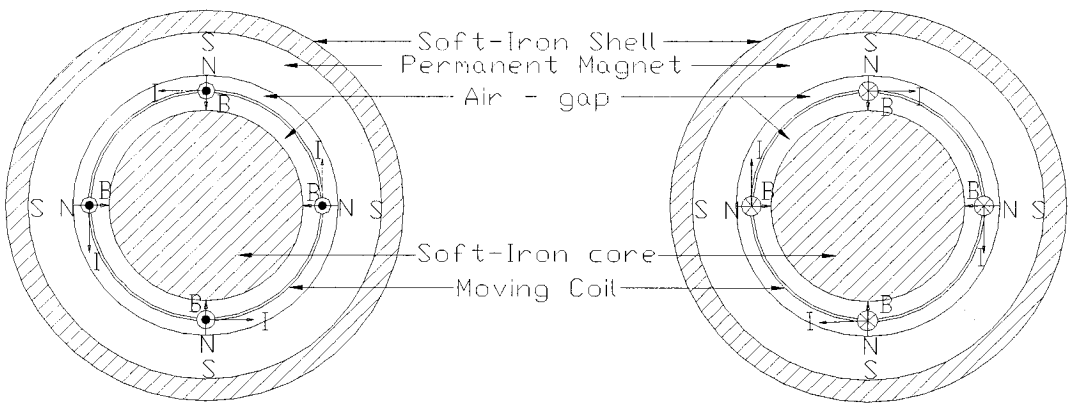

Fig.2.3 Cross section view of a VCA, (a) direction of current with force pointing out of page, (b) direction of current with force pointing into page

Fig. 2.4 presents the magnetic field lines of a voice coil actuator. The magnetic flux density vector comes from the north pole (the inner side of the permanent magnet), passes through the moving coil and soft iron core and comes back to the south Pole to complete a continuous closed field line. From this figure it is very clear that the force is produced in the same direction at every point on the moving coil and only depends on the current direction. If the current flows in the reverse direction the force will be produced in the opposite direction.

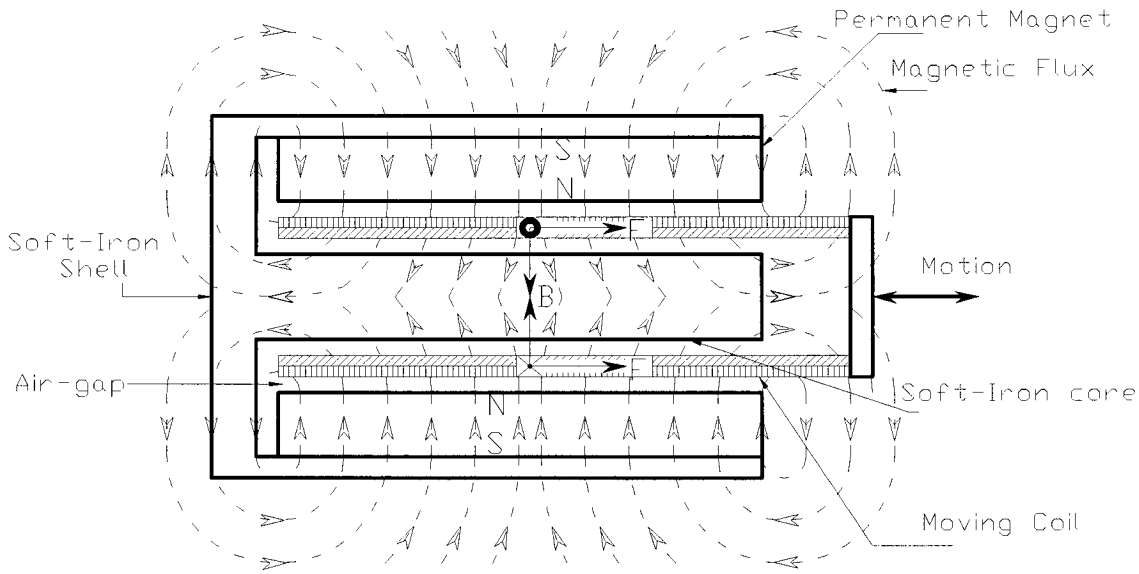

Fig. 2.4 Longitudinal section view of a VCA, magnetic field lines, and direction of the force generated during excitation

2.1.3 Design of the VCA

A conventional design of a voice coil actuator is depicted in fig.2.5. The voice coil actuator consists of a cylindrical coil that is free to move axially in the air gap. The air gap is formed between a cylindrical center pole and a permanent magnet that surrounds it. A soft iron shell houses both the magnet and the pole.

In some cases the axial length of the coil exceeds that of the magnet, by the amount of coil travel. In other cases the magnet is longer than the coil, by the travel length. The long coil configuration provides a superior force to power ratio and dissipates

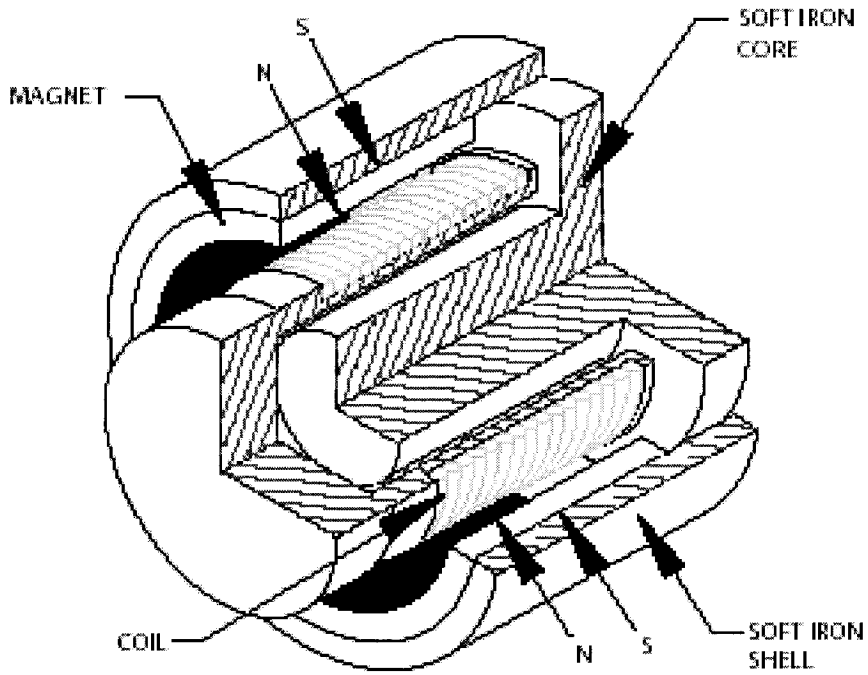

Fig.2.5 Conventional construction of VCA [20]

heat better, compared to the short coil configuration. However, the short coil configuration has a lower electrical time constant, smaller mass, and produces less armature reaction force. Neither arrangement provides a perfectly linear force versus travel characteristic.

2.1.4 Comparison of the VCA and the Solenoid Actuators

Solenoids

A **solenoid** is an electromagnetic device for creating a short pushing or pulling force. The solenoid usually consists of a current carrying coil, a magnetic steel core and a movable iron core called the *plunger* or *armature*. In a solenoid, the pulling or pushing force is created by energizing the coil of wire. A simple schematic of a solenoid is shown

in figures 2.6-a and 2.6-b. The current carrying coil creates a magnetic field, which produces a force on the magnetized plunger.

When current flows through the wire, a strong magnetic field is developed around the coil and through its center. Consider the coil of the solenoid is energized with current flowing in a direction such that the magnetic field creates a north pole on the plunger and a south pole on the static iron core at the facing ends (see fig.2.6-a). These opposite poles then create a magnetic pulling force to attract each other; hence the plunger moves towards the static core and reduces the air gap between the cores. The generated pulling force is proportional to the square of the current in the windings and inversely proportional to the square of the length of the air gap [43].

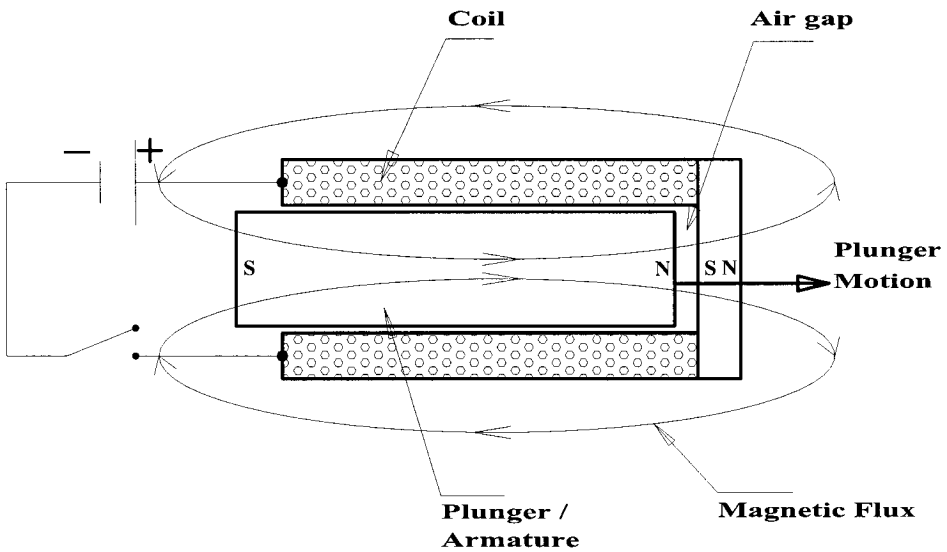

Fig.2.6-a: Schematic diagram of a solenoid actuator (direction of the flux with the current flowing counterclockwise when solenoid is viewed from the right).

Conversely, when the solenoid current flows in the opposite direction, the south pole is created on the plunger and the north pole is created on the static iron core (see fig.2.6-b). Again the resulting magnetic force attracts the plunger towards the iron core. This means that the force developed in a solenoid always has the same direction, even if the direction of the current in the coil is reversed. Therefore, a spring is usually used to allow the plunger to retract when the current is switched off. Due to an additional spring, the solenoid needs a large space that must be accounted for when the system is designed. Also the position of the solenoid plunger with a spring is less controllable because the return stroke in a solenoid valve is done by the spring force.

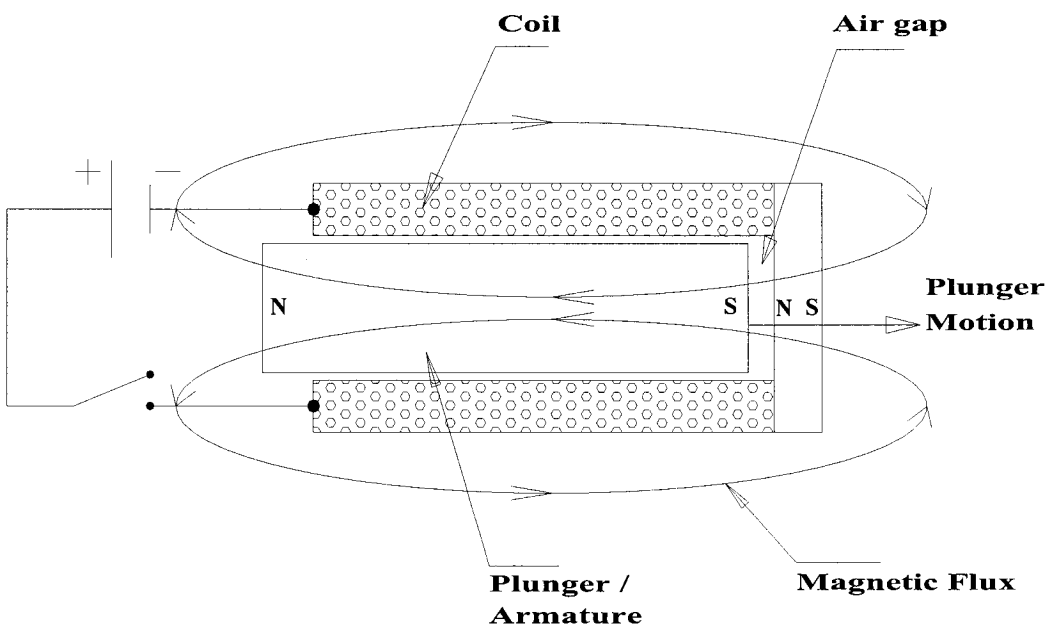

Fig.2.6-b: Schematic diagram of a solenoid actuator (direction of the flux with the current flowing in the reverse direction of the one in fig. 2.6-a).

Comparison to solenoid

The relation between the force characteristics versus displacement for a VCA and a solenoid are shown in Fig 2.7. The force versus stroke curve of a VCA is almost flat, which is a very useful characteristic for high precision control applications. In a VCA, the degradation of the force at the two travel extremes with respect to the mid-stroke force might be below 5% [19, 20].

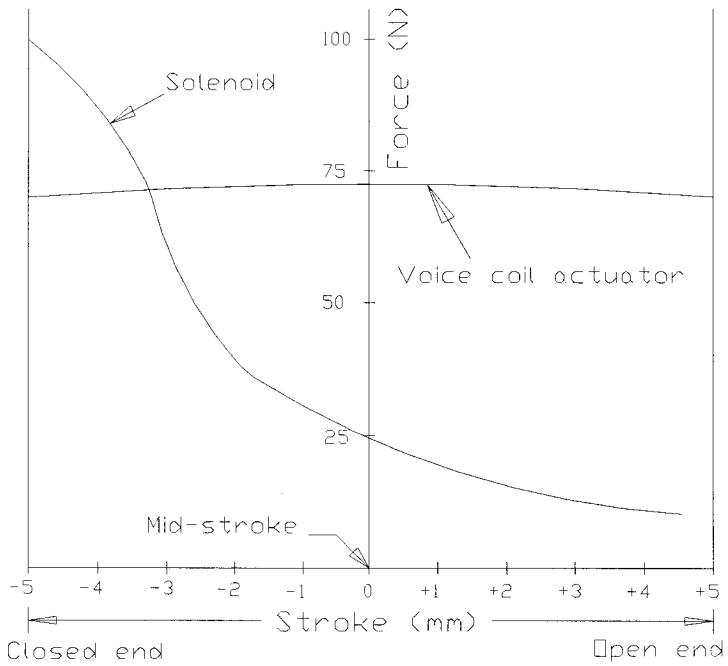

Fig.2.7 Force characteristics versus displacement [21]

In a solenoid the developed force varies inversely with the distance between the core and the pole face. The maximum force occurs when the core is attached to the pole. In addition a spring is used to develop a return force in a solenoid that makes it complicated to control.

Furthermore, in a VCA the direction of the force changes with the polarity of the voltage or the current direction, whereas in a solenoid the force is developed only in one direction and does not depend on the polarity of the voltage or the current direction (Fig. 2.8).

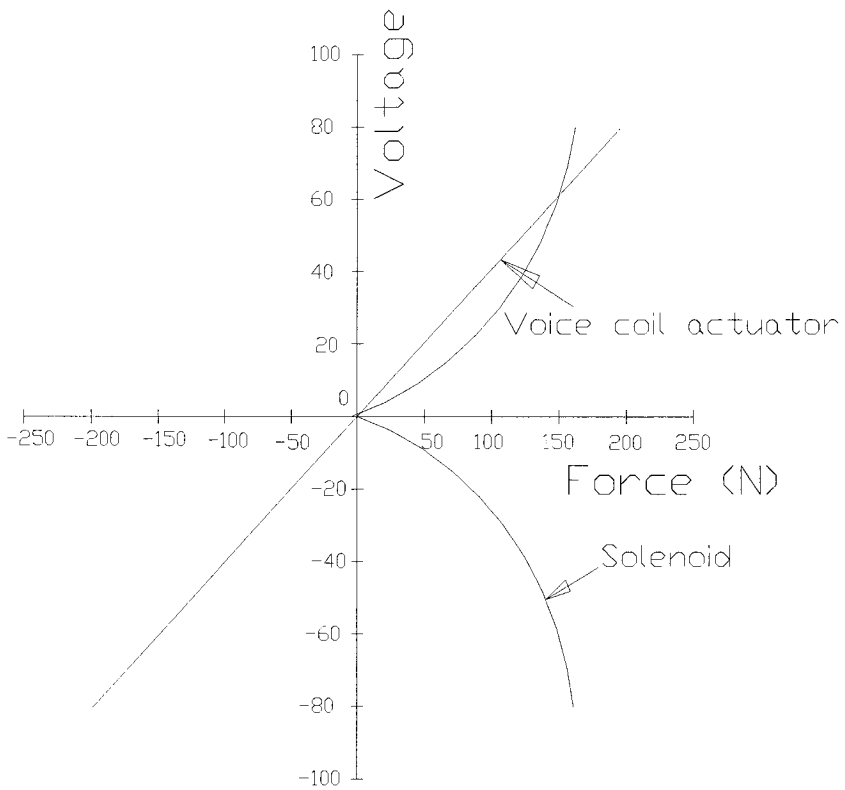

Fig.2.8 Force versus excitation characteristics [21]

Furthermore, hysteresis in solenoid devices can be as great as 10% or more of the developed force, whereas in voice coil motors it is typically much smaller than 1% of the developed force [20]. Low hysteresis enables precise and repeatable position control to

be realized. The characteristic features of the voice coil actuator are summarized in Table 2.1. The next section will describe the proposed architecture for the VCA controlled engine valve and its feedback control loop.

Table 2.1 Summary of the main features of the VCA.

• Low Inertia	• Low Hysteresis
• Quick Response Time	• Compact Design
• High precision Position Sensitivity	• Smooth and Cog Free
• Linear Force Response	• Wide Bandwidth
• Highly Efficient	• Long Life

2.2 Voice Coil Actuated Engine Valve System

Fig. 2.9 shows a schematic diagram of the proposed architecture for the VCA controlled engine valve and its feedback control loop. The VCA consists of a fixed permanent magnet and a moving coil for opening and closing the engine valve. The moving coil is attached to the engine valve by a connector, which also works as a physical stopper. The moving coil and the engine valve are both held by the physical stopper without a voltage being supplied. At this point the valve is fully open and in startup position. The next section describes the mathematical model of the voice coil.

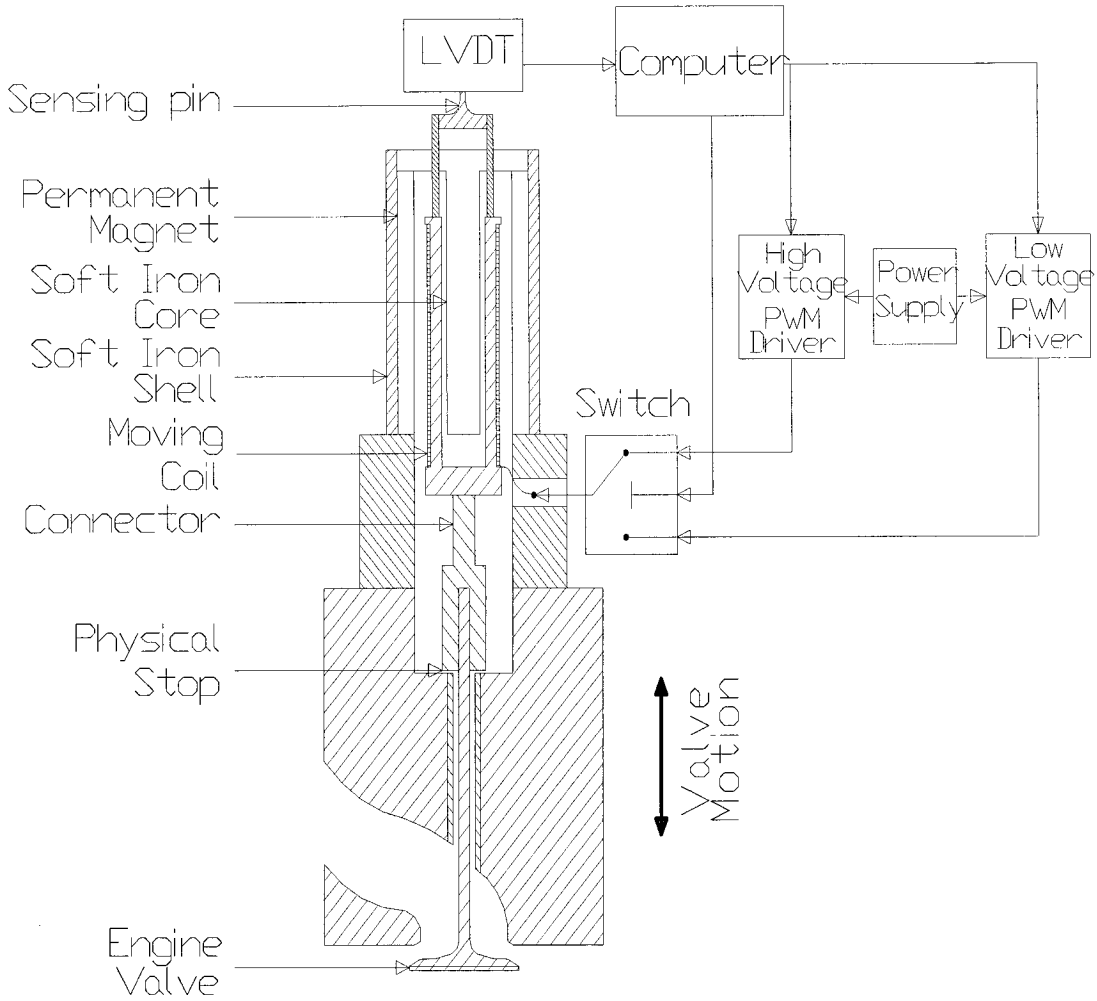

Fig. 2.9 VCA assembly - engine valve and feedback loop.

2.3 Mathematical Modeling

The electrical subsystem of a VCA actuated engine valve contains a power supply unit, two PWM voltage regulators and a moving coil surrounded by a strong magnetic field created by a permanent magnet. The force produced in the VCA is proportional to the applied current *i(t)* through the coil and can be expressed as

$$F(t) = K_1 Blin \tag{2.1}$$

where K_1 is a constant depending on the VCA design, B is the magnitude of the magnetic flux density vector, l is the conductor length and n is the number of wire turns, which are all constants. The expression (2.1) can thus be written as:

$$F(t) = K_F i(t) \tag{2.2}$$

where $K_F = K_1 Bln$ is defined as the force sensitivity constant, which is a positive number.

In the Laplace domain,

$$I(s) = \frac{1}{K_F} F(s) \tag{2.3}$$

The relationship between the current *I(s)*, the applied voltage *V(s)* and the back EMF $V_b(s)$, is found by the circuit loop equation from fig. 2.10:

$$V(s) = RI(s) + LsI(s) + V_b(s) \tag{2.4}$$

where R and L are the resistance and inductance of the VCA coil, respectively. The back electromotive-force (EMF) $V_b(s)$ is proportional to the coil velocity $\dot{x}$ and can be expressed in the Laplace domain as:

$$V_b(s) = K_b sX(s) \tag{2.5}$$

where K_b is the back EMF constant. Combining equations (2.3), to (2.5) yields:

$$V(s) = R\frac{1}{K_F} F(s) + Ls\frac{1}{K_F} F(s) + K_b sX(s)$$

$$V(s) = (R + Ls)\frac{F(s)}{K_F} + K_b sX(s) \tag{2.6}$$

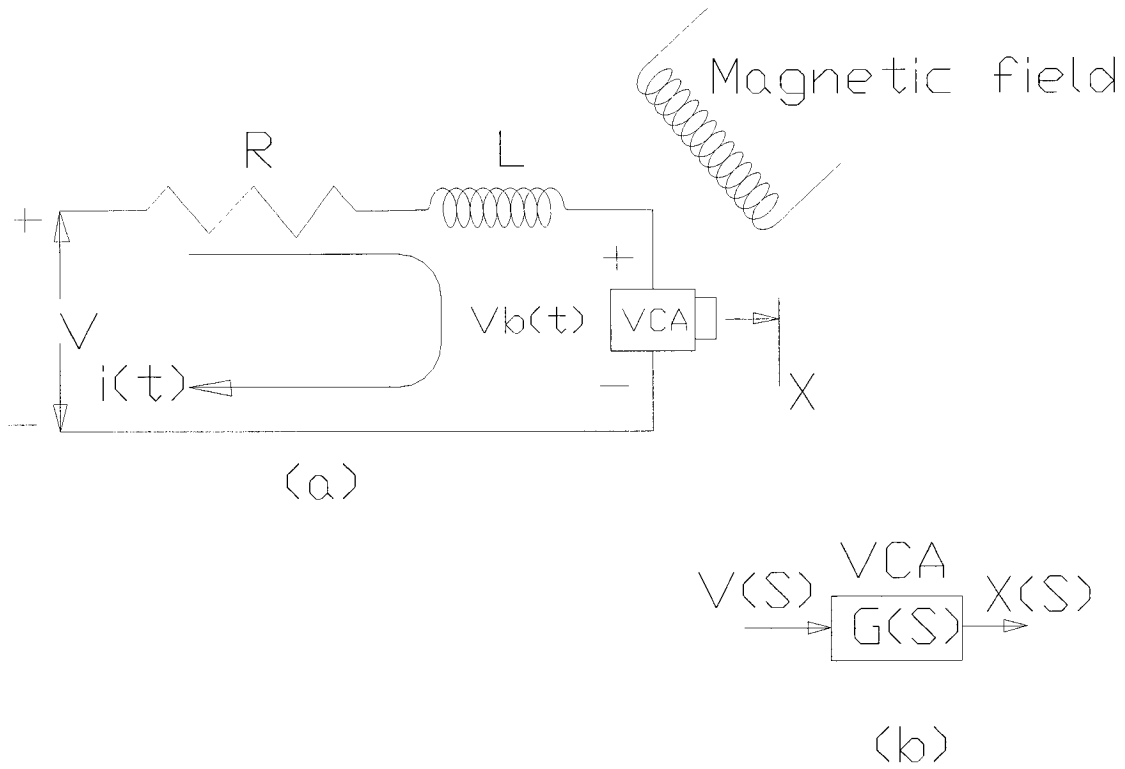

Fig. 2.10 (a) Schematic diagram of electrical subsystem of VCA, (b) Block diagram

The moving parts of the mechanical subsystem include the engine valve, a moving coil, a connector, and a sensing pin (see Fig. 2.9). For simplicity, these masses can be considered as a single lumped mass *m*. Also the gas forces, friction forces and valve-lash are not considered in the mathematical modeling of this thesis. Fig. 2.11 shows a model of this system as an equivalent mass-damper subsystem, and its equation of motion can be written as:

$$F(s) = ms^2X(s) + csX(s) \tag{2.7}$$

where c is the viscous damping coefficient.

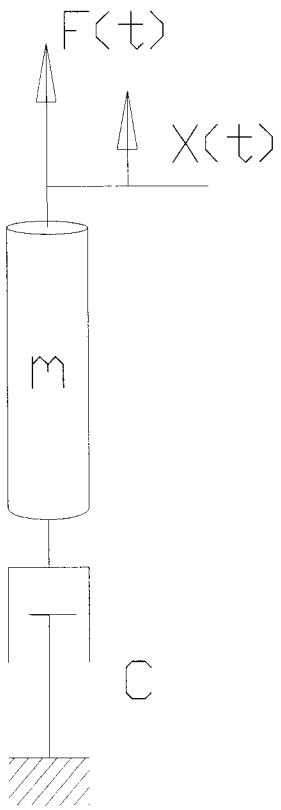

Fig. 2.11 Equivalent mechanical subsystem

Using equations (2.6) and (2.7), the transfer function between the applied voltage *V(s)* and the moving coil position *X(s)* can be written as:

$$G(s) = \frac{X(s)}{V(s)} = \frac{K_F}{s\{(R + Ls)(ms + c) + K_b K_F\}}$$

$$= \frac{K_F}{s\{mLs^2 + (mR + cL)s + Rc + K_b K_F\}}$$

$$\therefore G(s) = \frac{\frac{K_F}{mL}}{s\left\{s^2 + (\frac{R}{L} + \frac{c}{m})s + \frac{Rc + K_b K_F}{mL}\right\}} \qquad (2.8)$$

2.3.1 Block Diagram of the Voice Coil Actuated Valve System

Equation (2.4) can be rewritten in the following format,

$$V(s) - V_b(s) = [R + Ls]I(s)$$

$$\Rightarrow \frac{I(s)}{V(s) - V_b(s)} = \frac{1}{R + Ls} \tag{2.9}$$

From equation (2.7) the transfer function can be written as,

$$\frac{X(s)}{F(s)} = \frac{1}{ms^2 + cs} \tag{2.10}$$

From equations (2.3), (2.9) and (2.10), the block diagram in fig.2.12 results,

$$G(s) = \frac{\frac{K_F}{mL}}{s\left\{s^2 + (\frac{R}{L} + \frac{c}{m})s + \frac{Rc + K_b K_F}{mL}\right\}}$$

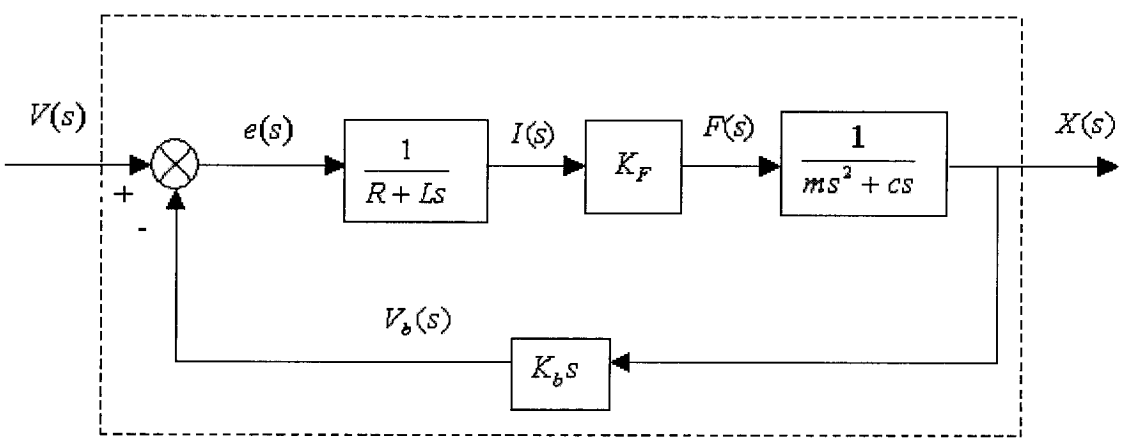

Fig. 2.12 Block diagram of the voice coil actuated valve system

It can be seen from the block diagram of the voice coil actuated valve system that the input to the system is the voltage and the output is the valve position. This output can be controlled by designing a feedback controller. A suitable voice coil actuator is chosen for an engine valve with a total movement of 10 mm and the manufacturer's specifications are used to simulate the system, which is discussed in the next section.

2.3.2 Parameters used in Simulation of a Voice Coil Actuated Valve System

The model parameter values are taken from the specifications of a suitable size VCA LA17_28_000A [20]. The parameter values used in the simulation are shown in Table-2.2. For simplification, the viscous damping between the moving parts in the air

Table 2.2 Parameter values used in simulation

Force Constant	$K_F = 4.0$ *lb/amp* $= 4.0 \times 4.4482$ *N/amp* $= 17.79$ *N/amp*
Back EMF constant	$K_b = 1.356 \times K_F = 5.42$ *volt/(ft/sec)* $= 5.42 \times 3.281$ *volts/(m/sec)* $= 17.78$ *volts/(m/sec)*
Weight of valve	$m_1 = 0.2$ *lbs* $= 0.89$ *N* $= 0.091$ *kg (mass)*
Weight of coil	$m_2 = 1/16$ *lbs* $= 0.28$ *N* $= 0.029$ *kg (mass)*
Resistance	$R = 6.7$ *ohms*
Inductance	$L = 1.7$ *mH* $= 1.7 \times 10^{-3}$ *Henrys*
Total weight	$m = m_1 + m_2 = (0.091 + 0.029) \times 1.2 = 0.15$ *kg (mass)* (Consider the safety factor of 1.25 times. Note that this is a design constraint normally considered in the literature)

medium is neglected, thus c = 0. Therefore the transfer function of the voice coil actuated engine valve system is (Note: the terms on c should be taken out),

$$G(s) = \frac{K_F}{s\{mLs^2 + (mR + cL)s + Rc + K_b K_F\}}$$

$$= \frac{17.79}{s\{0.15 \times 1.7 \times 10^{-3} \times s^2 + 0.15 \times 6.7 \times s + 17.79 \times 17.78\}}$$

$$\therefore G(s) = \frac{69765}{s\{s^2 + 3941 \times s + 1240416\}} \tag{2.11}$$

The step response of the voice coil actuated engine valve system is shown in fig.2.13. where it can be seen that the reference is not followed. A controller will be designed in chapter 3 to follow valve position references.

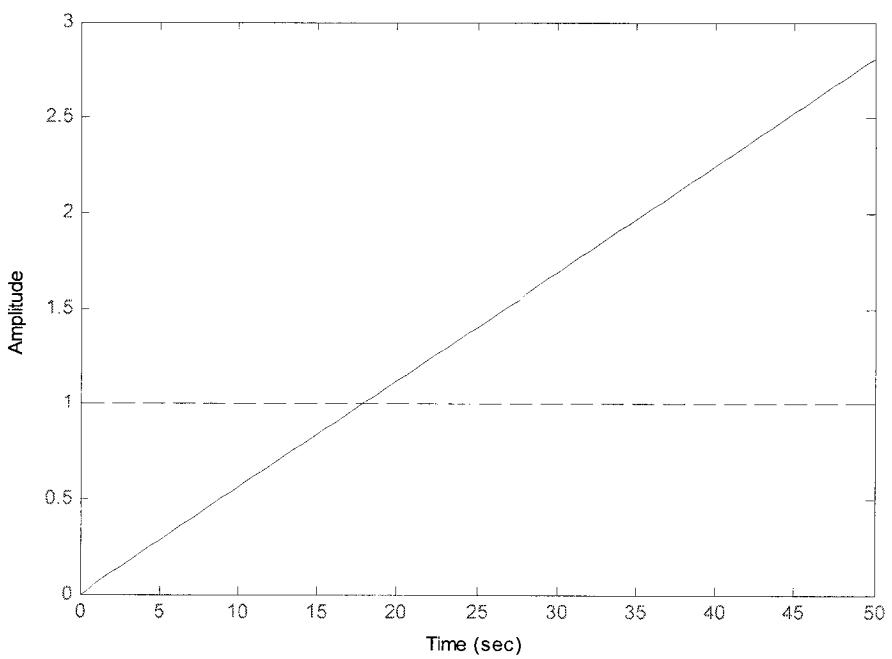

Fig.2.13 Step response of the open loop VCA system

CHAPTER 3

CONTROLLER DESIGN AND SIMULATION PERFORMANCE OF A VOICE COIL ACTUATED ENGINE VALVE SYSTEM

3.1 Introduction

In a conventional valve train system, the valve motion is controlled by a cam profile that is carefully designed to give low seating velocities for durability and low noise. An electromechanical valve (EMV) system introduces a difficult motion control problem with valve timings, fast transients, and low seating velocities (soft landing) [16]. This chapter proposes and simulates a novel closed-loop VCA position control methodology, where the objective for the VCA system is similarly to achieve very low contact velocities while maintaining fast system transient response.

3.2 Voice Coil Actuated Engine Valve System Characteristics and Performance

Referring to equation (2.11) in Chapter 2, the voice coil actuated valve system is a third order linear system. It has three poles without any zeros. All the poles of the system are in the left half *s*-plane except one that is at the origin (fig.3.1). This means that the VCA system by itself is marginally stable. If the VCA system is implemented in a unity feedback configuration, then the closed-loop VCA system will be of type one and thus can track a step input with zero steady state error. However the transient performance is the prime interest for the analysis of the VCA valve system. The desired transient response of the closed-loop VCA system consists of the following specifications (the minimum requirement to control the valve according to engine speed of 3000rpm):

1. Rise time < 5 ms

2. Settling time ≤ 5 ms

3. Overshoot < 5%

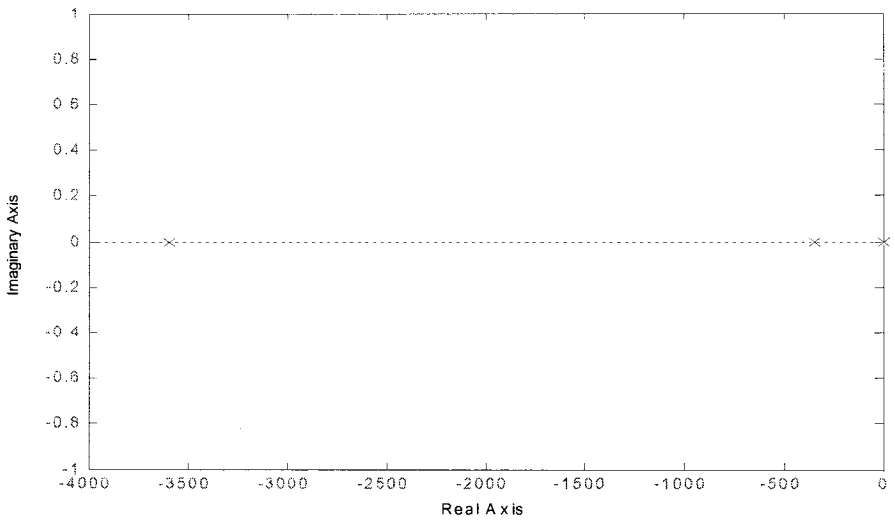

Fig.3.1 Pole-zero map of the open-loop VCA system

Fig. 3.2 shows the voice coil actuated engine valve system model in unity feedback configuration. The model diagram is in SIMULINK (Trademark of Mathworks Inc.) format that is used to determine the system dynamic response.

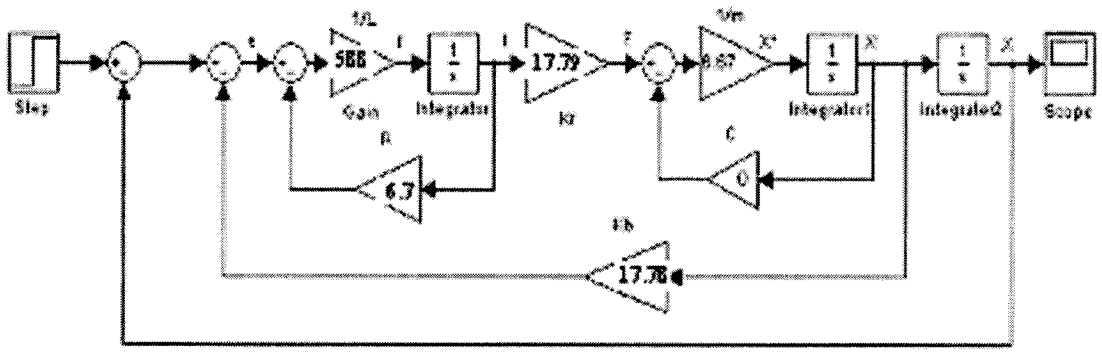

Fig. 3.2 Simulation diagram of unity feedback closed-loop VCA system

As shown in figure 3.3, the unity feedback closed-loop VCA system can track a reference step input without any overshoot but the system is too slow with a rise time around 40 sec and a settling time around 100 sec. The step response implies that the system performance is not satisfactory at all. Therefore, instead of a unity feedback, a suitable compensator should be introduced in feedback to decrease the rise and settling times while keeping the overshoot below the desired value to meet the VCA system performance criteria.

To meet the conflicting requirements of low seating velocity and fast settling time a novel switched control strategy for VCA systems is proposed in this thesis using the concept of pulse width modulation (PWM). This novel control strategy will achieve the required control performance criteria of the engine valve system and will be discussed in detail in the next section.

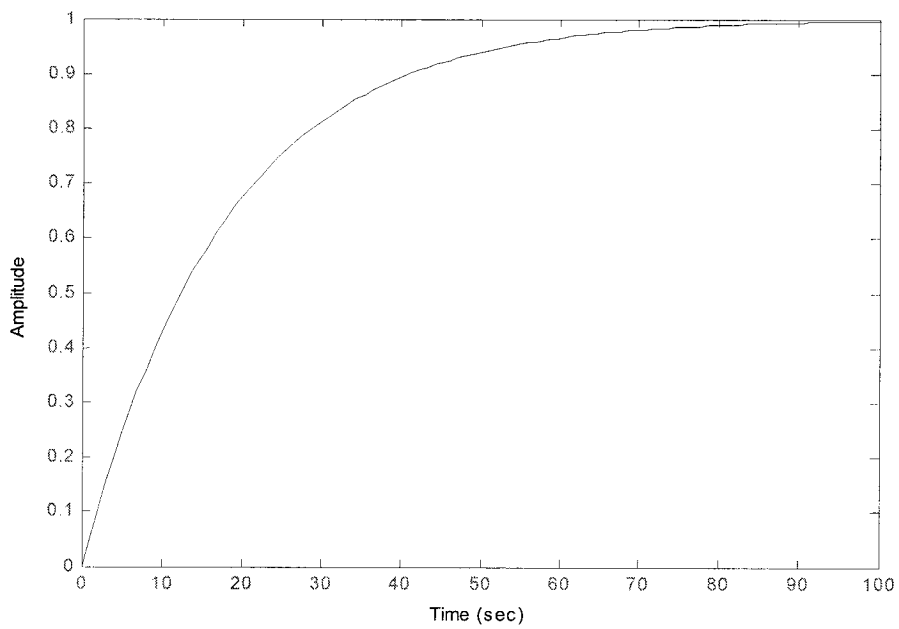

Fig.3.3 Step response of the unity feedback VCA system

3.3 Control Strategy of the Voice Coil Actuated Valve System

In conventional spark ignition engines, the pumping losses depend upon the opening and closing position of the throttle valve and are inversely proportional to the engine load [14]. The position control ability of a VCA valve-train system can eliminate the throttle valve, hence reducing a significant amount of pumping losses and increasing the engine volumetric efficiency. The proposed feedback control strategy for the VCA controlled engine valve system is shown in Fig. 3.4. Two different pulse width modulation (PWM) voltage drivers are used in this system to excite the VCA. The first PWM driver, with high voltage (100V) amplitude, is applied during the transient period for high velocity response. The second PWM driver, with low voltage (5V) amplitude, is applied in the steady state period for holding the engine valve in the desired position.

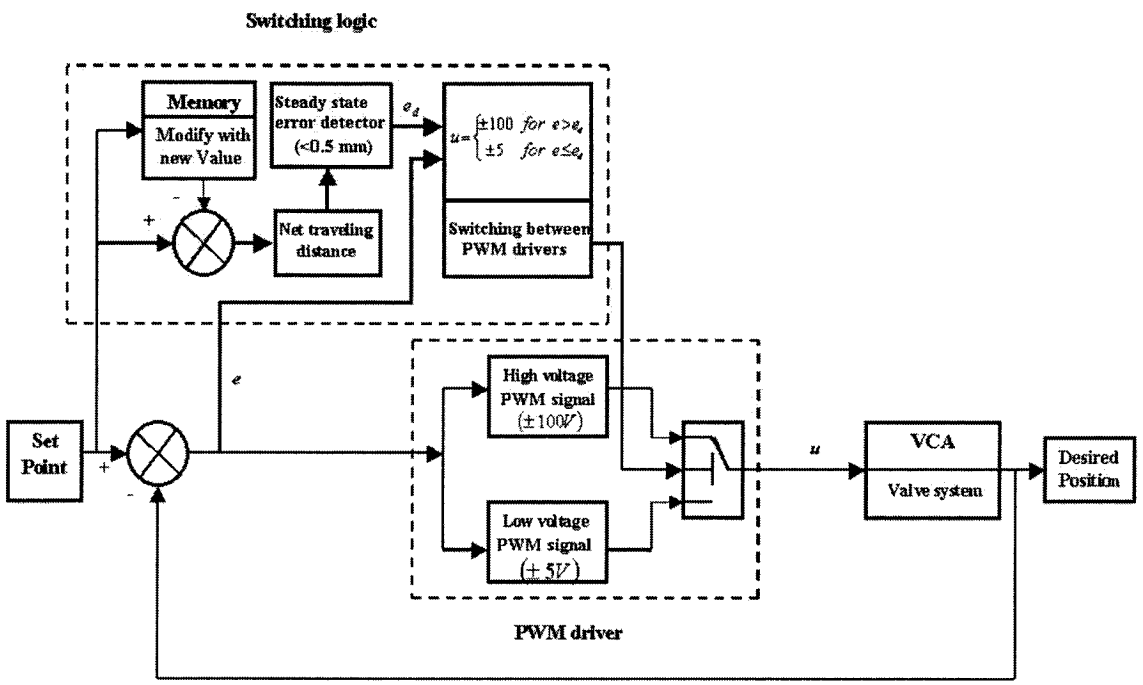

Fig. 3.4 Initial control strategy for the voice coil actuated valve system

As a point-to-point positioning application, the two stages of engine valve actuation can be considered separately. During the transient stage, the VCA requires a high acceleration to overcome the inertia and to achieve very fast valve motion. This is done by applying a higher voltage than the nominal rated voltage for a very short period of time. This PWM voltage signal produces a boost current to accelerate the engine valve. The high voltage PWM driver applies a positive voltage (+100V) pulse to accelerate the VCA for time period 't_1'. After this time, the PWM driver switches its voltage polarity and applies a negative voltage (-100V) pulse to decelerate the actuator for time period 't_2' to achieve low contact velocity. Therefore the total transition time is $t = t_1 + t_2$. The width of the PWM pulse depends on the position error and is determined by the position feedback controller.

At the end of the transient period, the VCA does not need high power to hold the engine valve in the desired position. At this point the high voltage PWM is deactivated and the low voltage PWM driver starts to apply pulses ($\pm 5V$) until the next command. In this phase the PWM control signal is always changing, even in the case where the output signal has reached its steady state [22]. The concept of changing the PWM signal is very useful to reduce the ripple amplitude in steady state. It also reduces the power consumption of the system during the steady state period. The proposed control strategy falls under the framework of switched control [23].

3.4 Pulse Width Modulation (PWM)

The process of creating rapid electronic switched transitions to convert electrical energy from an electrical supply into a series of high frequency voltage or current pulses

is called PWM and is broadly used in various applications. One of the basic reasons for the increased interest in PWM systems is their ability to process large signal power with very high frequency [24]. Many electromechanical actuators are controlled using PWM amplifiers, since the electronic switching leads to amplifiers with reduced size, weight, and power dissipation [25]. More general PWM strategies are described in [22].

A pulse width modulation (PWM) signal is defined as a square wave of fixed frequency with variable width of the '*ON*' time. The amplitude of the signal is also fixed and is equal to the maximum voltage V_{max}. Therefore, at the '*ON*' state, the voltage equals V_{max} for one direction and $-V_{max}$ for the other direction. At the '*OFF*' state it

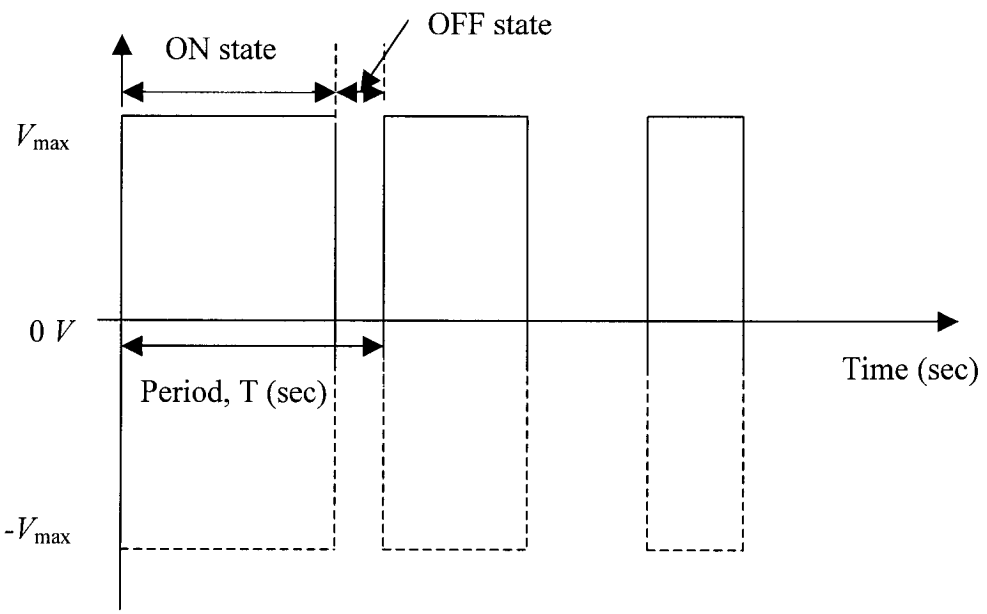

Fig.3.5 Pulse Width Modulation (PWM) signal

equals 0 *V*. As shown in fig.3.5, the portion of time within one time period, *T* (where $T = \frac{1}{f}$ sec and '*f*' is the frequency in *Hz*), during which the signal has the amplitude of $\pm V_{max}$ is called the '*ON state*' and the rest of the time during which the amplitude is 0

(zero) is called the '*OFF state*'. The ratio of the '*ON state*' over the period '*T*' is called the 'duty cycle' (d). The designer can control or modulate the duty cycle.

At a certain voltage V let the current drawn by the plant be $I_{analogue}$. Then the required power input to the system is $P_{analogue} = VI_{analogue}[Watts]$ to reach the desired position. In the PWM system, this energy input per second (or power) is fed to the system in many packets all at the maximum voltage $V_{\max}$. The number of such packets per unit time equals the frequency of the signal used. The amount of energy contained in each packet depends on the duty cycle of the signal. During the '*OFF state*' of the PWM, there is no energy input to the system [59].

So the power input to the system is,

$$P_{PWM} = V_{\max} \times d \times f \times I_{PWM}[Watts]$$

where, $V_{\max}$ = Maximum supply voltage to the system.

f = Frequency (fixed) of the PWM signal

d = Duty cycle (determined by the software position controller)

I_{PWM} = Current drawn by the system.

As long as $P_{PWM} = P_{analogue}$, then the position of the system will be the same. Therefore, the position of the voice coil actuated engine valve system can be controlled using the PWM voltage signal.

The advantage of PWM is that by applying the maximum voltage to the system and by turning off the supply for a certain period of time (as determined by the duty cycle), the control system operates at its maximum efficiency and the energy loss is minimized [60]. This means the PWM control system uses almost full power of its duty

cycle that is transferred to the load whereas a resistive analogue controller consumes more current for transferring the same amount of power to the load as it converts some of the current to heat. Another advantage of PWM is the ability to optimize the amplitude of the actuating signal according to the actuator saturation magnitude while achieving a better control system performance [61].

3.5 The PWM Driver for the Voice Coil Actuated Valve System

Fig.3.6 shows a typical implementation of a PWM controller, where *r(t)* is the input, *u(t)* is the modulator output, and *y(t)* is the controlled variable of the system (output).

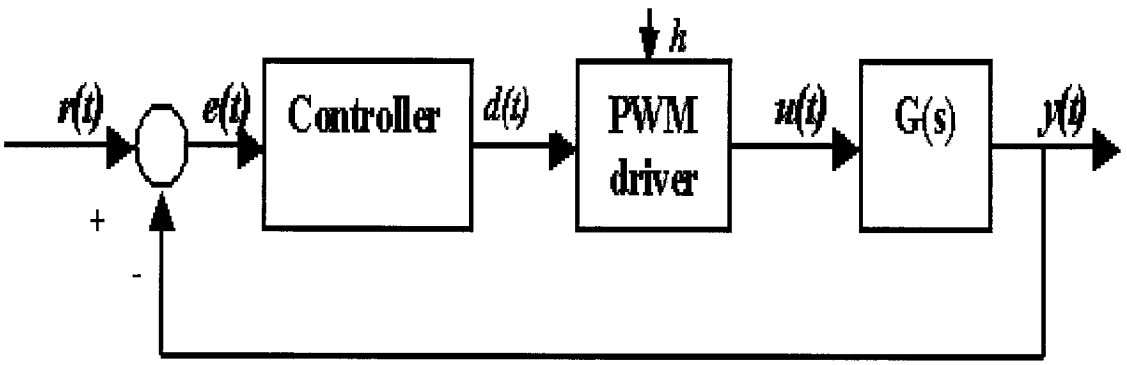

Fig.3.6 Block diagram of a system controlled by PWM

The output of the pulse width modulator is described by:

$$u(t) = \begin{cases} \text{sgn}(e) \times h(e) & for \quad kT \le t < (k + d(e))T \\ 0 & for \quad (k + d(e))T \le t < (k+1)T \end{cases} \tag{3.1}$$

where, T = the period

$d(e)T$ = the pulse width for the $(k+1)th$ period

$h(e)$ = PWM pulse amplitude

e = error for the $(k+1)th$ period

The PWM voltage amplitude h and sign functions for the voice coil actuated valve system are defined by the equations (3.2) and (3.3):

$$h(e) = \begin{cases} 100\,V & for \quad |e| > 0.5\,mm \\ 5V & for \quad |e| \le 0.5\,mm \end{cases} \tag{3.2}$$

$$\text{sgn}\ (e) = \begin{cases} 1 & for \quad e > 0 \\ 0 & for \quad e = 0 \\ -1 & for \quad e < 0 \end{cases} \tag{3.3}$$

The duty ratio of the PWM pulse $d(t)$ depends on the error $e(t)$ as follows:

$$d(e(t)) = \begin{cases} 1 & for \quad e > 1 \\ |e| \times \beta & for \quad -1 \le e \le 1 \\ 1 & for \quad e < -1 \end{cases} \tag{3.4}$$

A typical relation between a sinusoidal input and the corresponding output signal of a PWM driver is shown in fig.3.7. It can be seen that as the input signal (error) increases the duty cycle increases, which results in more power provided to drive the system.

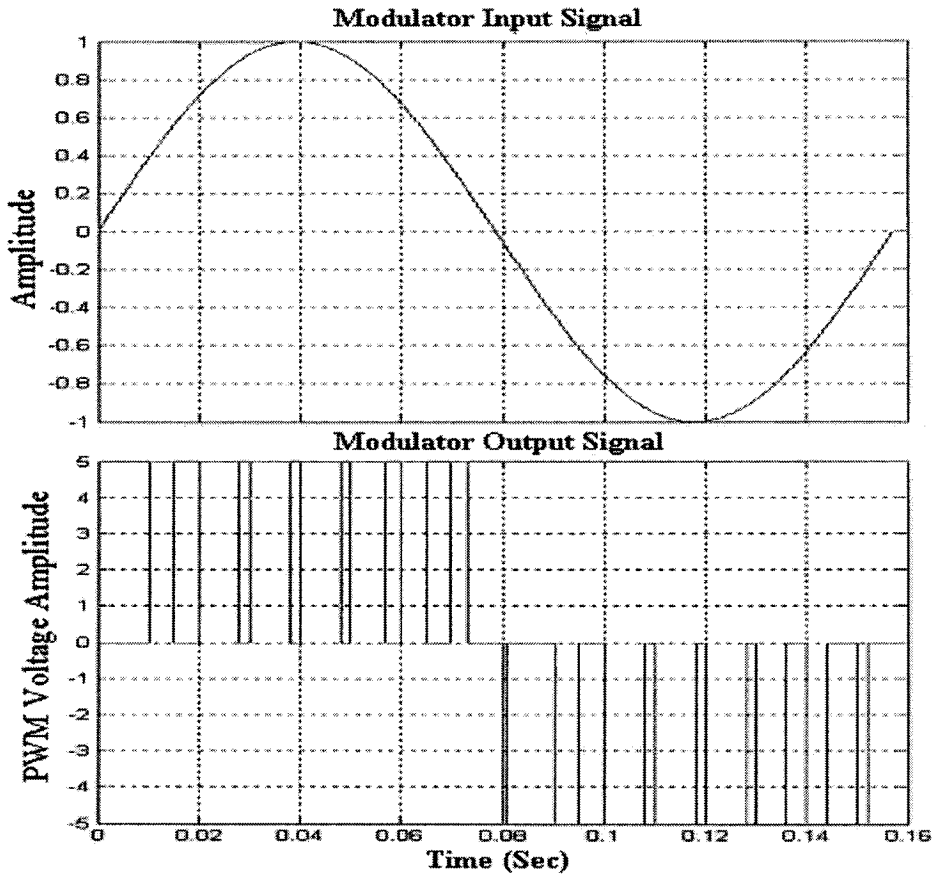

Fig. 3.7 Pulse width modulator input-output relation for sinusoidal error

3.6 Simulation Performance

The voice coil actuated valve system with the control strategy of using two different pulse width modulators (see fig. 3.4) is simulated using SIMULINK. The purpose of the control strategy is to apply a high voltage ($\pm 100V$) PWM signal at the transient period for very fast engine valve response. The control signal changes to a low voltage ($\pm 5V$) PWM signal when the system position error reduces to an absolute value below 0.5mm. As mentioned before, the goal of the control system is to achieve a step

response with an overshoot of less than 5%, a rise time less than 5 ms and a settling time about 5 ms.

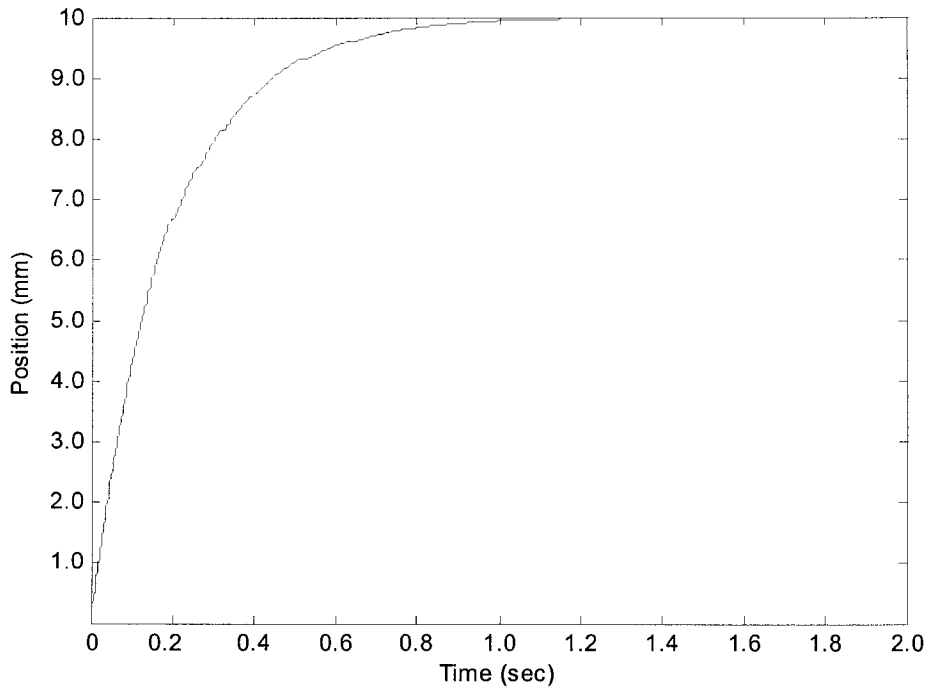

Fig.3.8 Step response of the PWM controlled voice coil actuated valve system

The position response of the PWM controlled voice coil actuated valve system due to a unit step input is shown in fig.3.8. It can be seen that the response of this system provides a rise time of 0.45 sec and a settling time of about 1 sec with no overshoot, which is a significant improvement over the unity feedback control strategy. However, the transient response of this system is still too slow as compared to the desired specification. This implies that the system response does not meet the design criteria and hence requires more development in the control system of the voice coil actuated valve system to achieve the desired performance. One alternative would be to increase the amplitude of the PWM signal. The system would then need a signal with amplitude much higher than 100V for faster response. However, this is not feasible due to actuator

saturation problems and limitations of the power supply unit. The next section will describe the adopted solution to meet all design criteria.

3.6.1 Implementation of a Lead Compensator

The requirements on the rise time, settling time and overshoot of a control system are often conflicting. Thus, designing a control system to meet the transient and the steady state performance together is not as simple as designing one to meet either the transient or the steady state specifications separately. The model of the system addressed in this thesis is linear. Therefore, implementing a lead compensator to meet the desired specifications is an obvious first choice. However, the limitation of a lead compensator for this particular application is the high actuating signal (25000V for the desired response) that is generated, as described at the end of this section. This has motivated a hybrid strategy whereby both a lead compensator and a PWM are used to successfully reach the ultimate goal with reasonable actuating signals. The PWM can limit the amplitude as desired (not exceeding 100V) and the lead compensator makes the VCA system response as fast as desired. This alternative is also advantageous as compared to optimal control design methods that deliver a controller of the same order of the plant (third order in this case). The controller proposed in this thesis will be a cascade of a first order controller and a PWM controller falling into the framework of switched control [23].

The design of the lead compensator can be accomplished in the *s*-plane by the Root Locus method and is explained in detail in Appendix-I. The advantage of the Root Locus method is the ability to specify the location of the dominant roots and therefore the

dominant transient response. The lead compensator that achieves the desired transient performance for the voice coil actuated engine valve system (without the PWM control strategy) is

$$G_c(s) = \frac{2211193\ (s + 800)}{(s + 40863)}$$

The final design of the lead compensator is simulated without the PWM control strategy using SIMULINK and the transient response of the compensated voice coil actuated valve system is obtained as shown in fig.3.9. For a step input using the lead compensator applied to the system, the simulation of the VCA system resulted in an overshoot of 20% instead the specified value of 5%, a rise time of 1.4 ms and a settling time to within 2% of the final value at 5 ms. The difference in the overshoot from the specified value is due to the zero of the lead compensator. Another design iteration to obtain a second compensated system might eliminate the effects of the zero in the closed-loop transfer function. However, one more important constraint must be considered before designing another suitable compensator using a similar approach. This constraint is the saturation of the actuating signal, which is very important in the design of a control system. If an actuator saturates, then the system might not function as designed.

Therefore, in a control system design the actuating signal is often required to be constrained as

$$|u(t)| \leq M \qquad \text{for all} \quad t \geq 0$$

where $u(t)$ is the actuating signal (the amplitude of the voltage signal from the lead compensator) and M is a constant verifying the actuating signal limitation

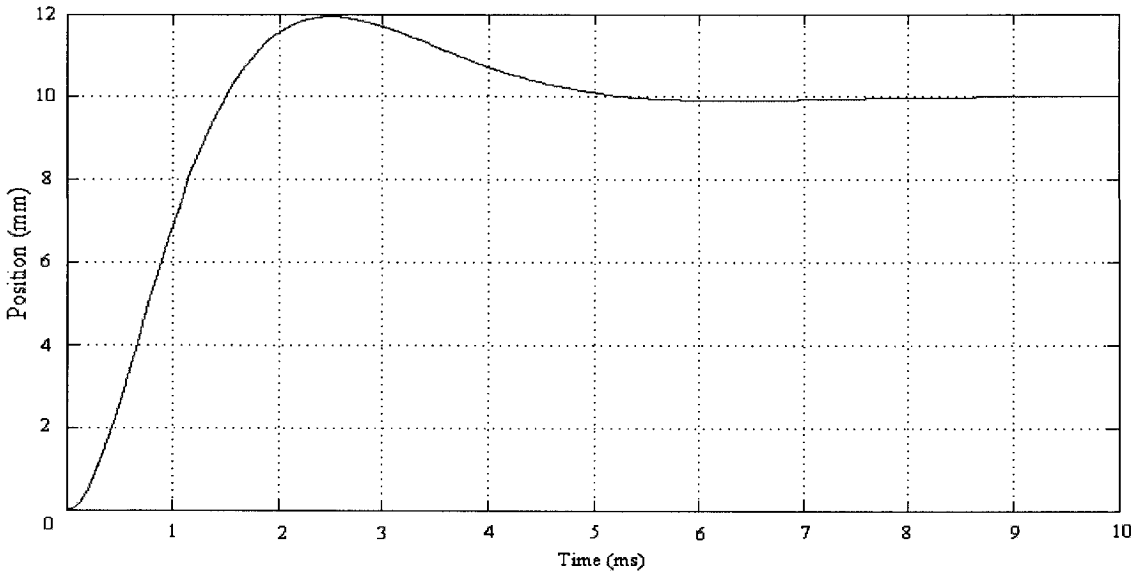

Fig.3.9 Step response of the compensated voice coil actuated valve system

constraint. The response of the actuating signal of the compensated VCA system is plotted in fig. 3.10. The magnitude of the actuating signal is 25000V for the unit step input and this voltage is neither acceptable nor realistic for the voice coil actuated valve system.

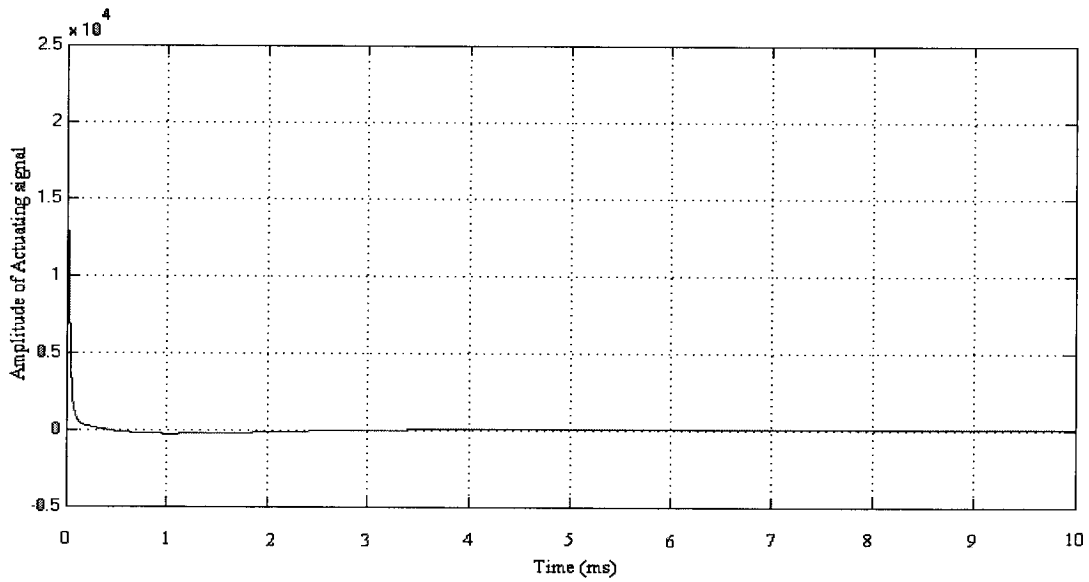

Fig.3.10 Actuating signal response of the compensated voice coil actuated valve system

Preventing that an actuator saturates is not a simple problem. In this thesis it is proposed that the lead compensator is implemented in cascade with a pulse width modulated (PWM) controller to achieve the stringent system performance while maintaining the actuating signal within an acceptable limit range. Limiting the actuating signal is a great advantage of a pulse width modulated (PWM) control strategy. The lead compensator is added just before the PWM controller and the block diagram of this system is shown in fig.3.11. The simulation results are discussed in the next subsection and a proof of stability for a discrete-time model is derived in chapter 4.

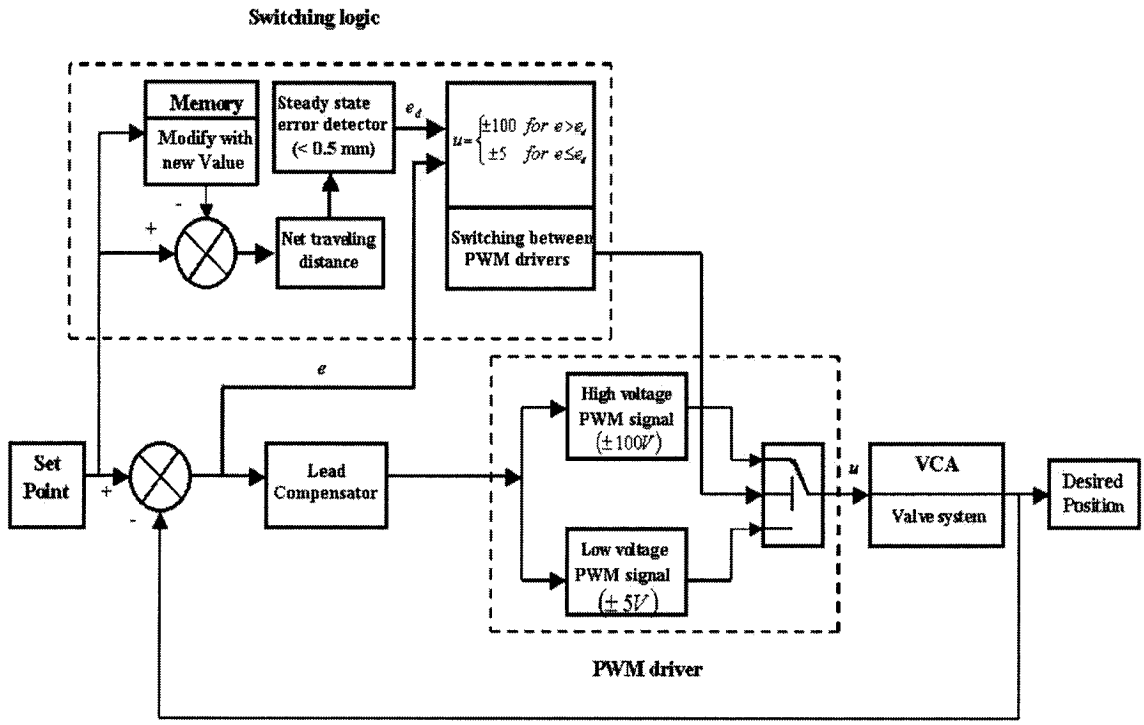

Fig. 3.11 The block diagram of the final PWM control strategy using a lead compensator for the voice coil actuated engine valve system

3.6.2 Simulation of a PWM controlled VCA System with a Lead Compensator

In this subsection, the PWM control strategy with the lead compensator for the voice coil actuated valve control system is simulated in MATLAB / SIMULINK. The controller for the electromagnetic valve (EMV) actuator must achieve stringent performance requirements for fast response and soft landing [26, 27]. At first the VCA valve system is simulated for full open (0 mm) to full closed (10 mm) and then for full closed to full open positions. Fig.3.12 shows the position, velocity, and force responses of the system. From the simulation results it can be seen that the valve opening or closing time is about 5 ms (rise time below 5 ms) and the valve landing velocity is less than 0.02 m/sec, which meet the desired specifications. At the beginning, the engine valve is held in full open position and a high PWM voltage is applied to the VCA to move the valve to the desired full closed position. A low PWM voltage is then applied to hold the valve in that position until the next command.

The maximum force created to accelerate the VCA actuated valve system is 232.7 N and occurs at 0.795 ms. After that moment, the actuating force is gradually decreased. The velocity of the system keeps increasing due to the momentum gained by the system. The maximum velocity of 3.15 m/sec is then achieved and occurs at 3.80 ms. At this point a negative force is applied to the system for deceleration by changing the polarity of the PWM voltage signal. The magnitude of the maximum negative force is 365 N, applied to the VCA for rapid velocity reduction and for ultimately achieving a low contact velocity (soft landing).

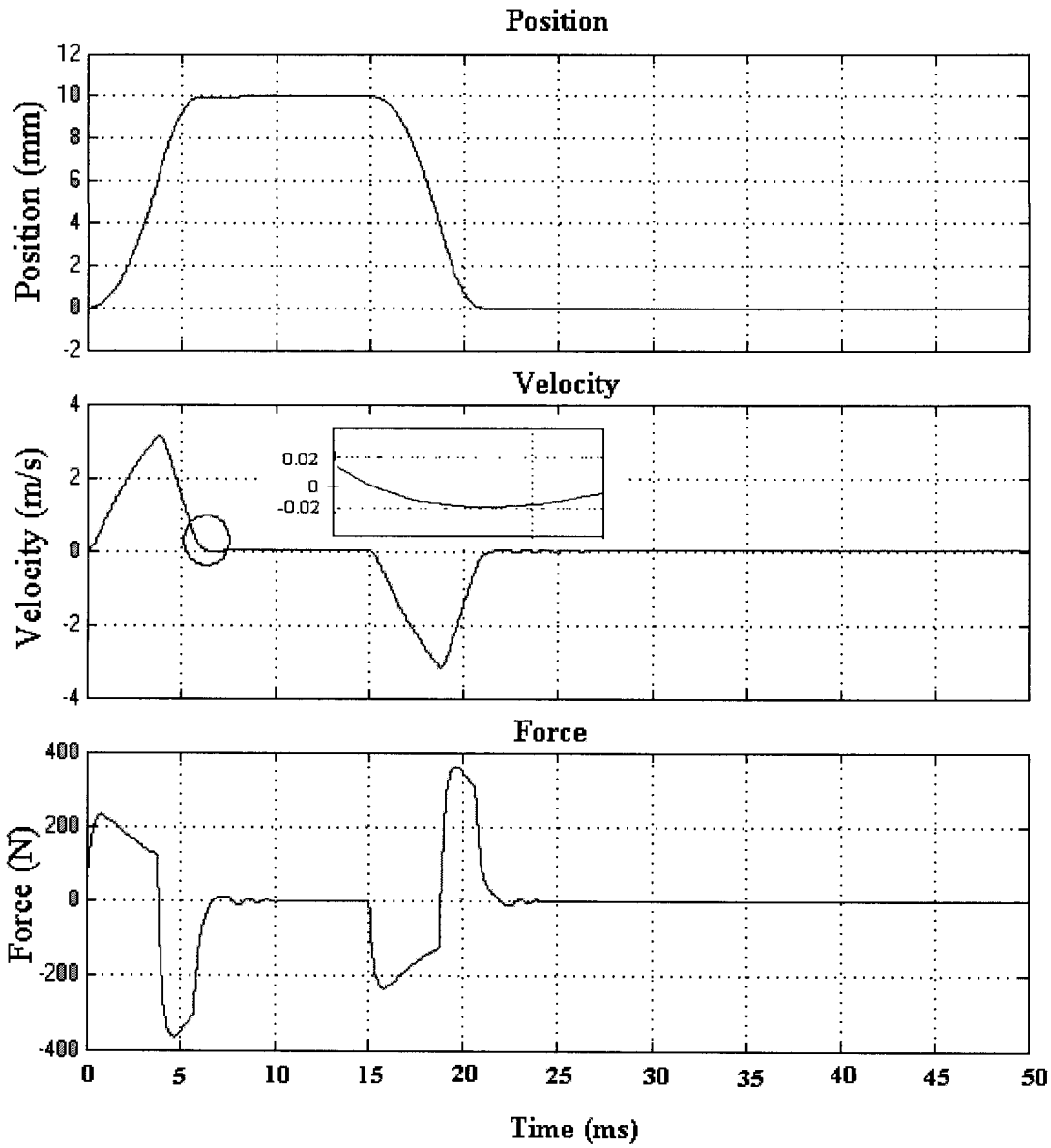

Fig.3.12 Engine valve position, velocity and actuator force

Fig. 3.13 shows the velocity response and the corresponding PWM voltage signal with respect to time. The high voltage PWM signal ($\pm 100V$) is applied at the beginning of the valve movement for fast acceleration against the engine valve inertia. This signal is activated only during the transition period until the position error is reduced to an absolute value of 0.5 mm. At this point the controller starts to apply a low voltage PWM

signal of ($\pm 5V$) (instead of a high voltage signal) to hold the engine valve at the desired position until the next command.

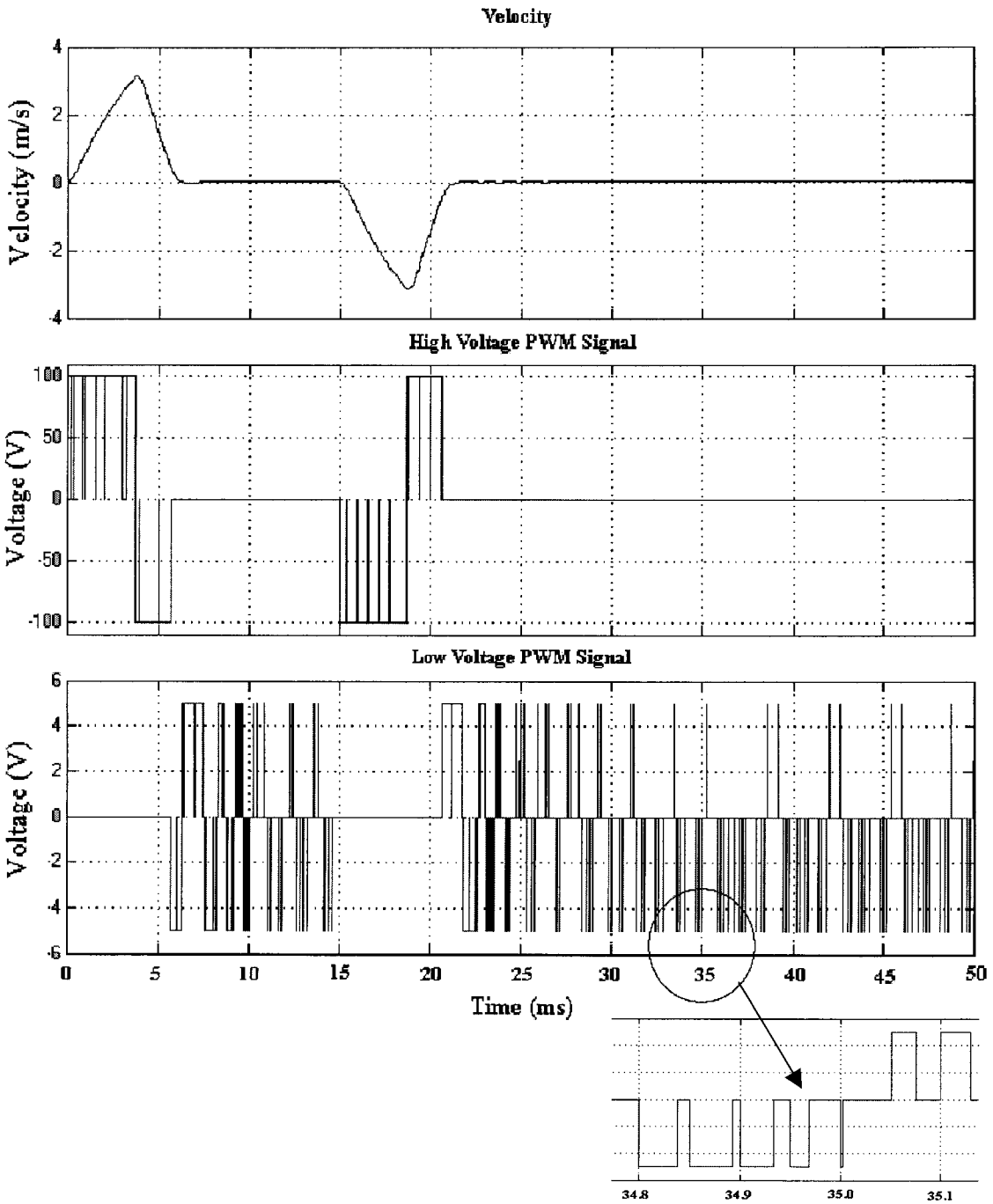

Fig. 3.13 PWM voltage signals and velocity of the valve

From the simulation results it can also be seen that the high voltage PWM signal was activated during the transient period and deactivated in steady state, whereas the low voltage PWM signal is deactivated during the transient time and activated in the steady state period. Also it can be seen in the transition time that the positive voltage (+100V) PWM signal is activated until the valve velocity reaches its peak point (3.15 m/sec for a total of 10 mm movement). Then the controller changes the voltage polarity and a negative voltage (-100V) PWM signal is applied for decelerating the engine valve to achieve soft landing.

Accurate control valve timings can achieve unthrottled load control, good fuel economy and low exhaust emissions [16]. Fig. 3.14 shows the simulation results for unthrottled control of the engine valve. The total valve traveling distance is considered as 10mm and some position commands 2mm, 8mm, 6mm, 10mm and 0mm are used to control the valve for equal durations of 15ms. For each position command the system has taken 5ms to perform the transition and has held the valve at the desired position in steady state for 10ms. The important point to notice is that there is a very small overshoot for any position command of the system response. This implies that it is possible to achieve very low contact velocity of the engine valve for the VVT system using a VCA. It is also possible to stop the engine valve at any position between 0mm~10mm traveling distance that will ensure the unthrottled VVT control of the valve.

The maximum applied force and peak velocity of the system depend on the total relative traveling distance of the engine valve and are controlled by changing the width of

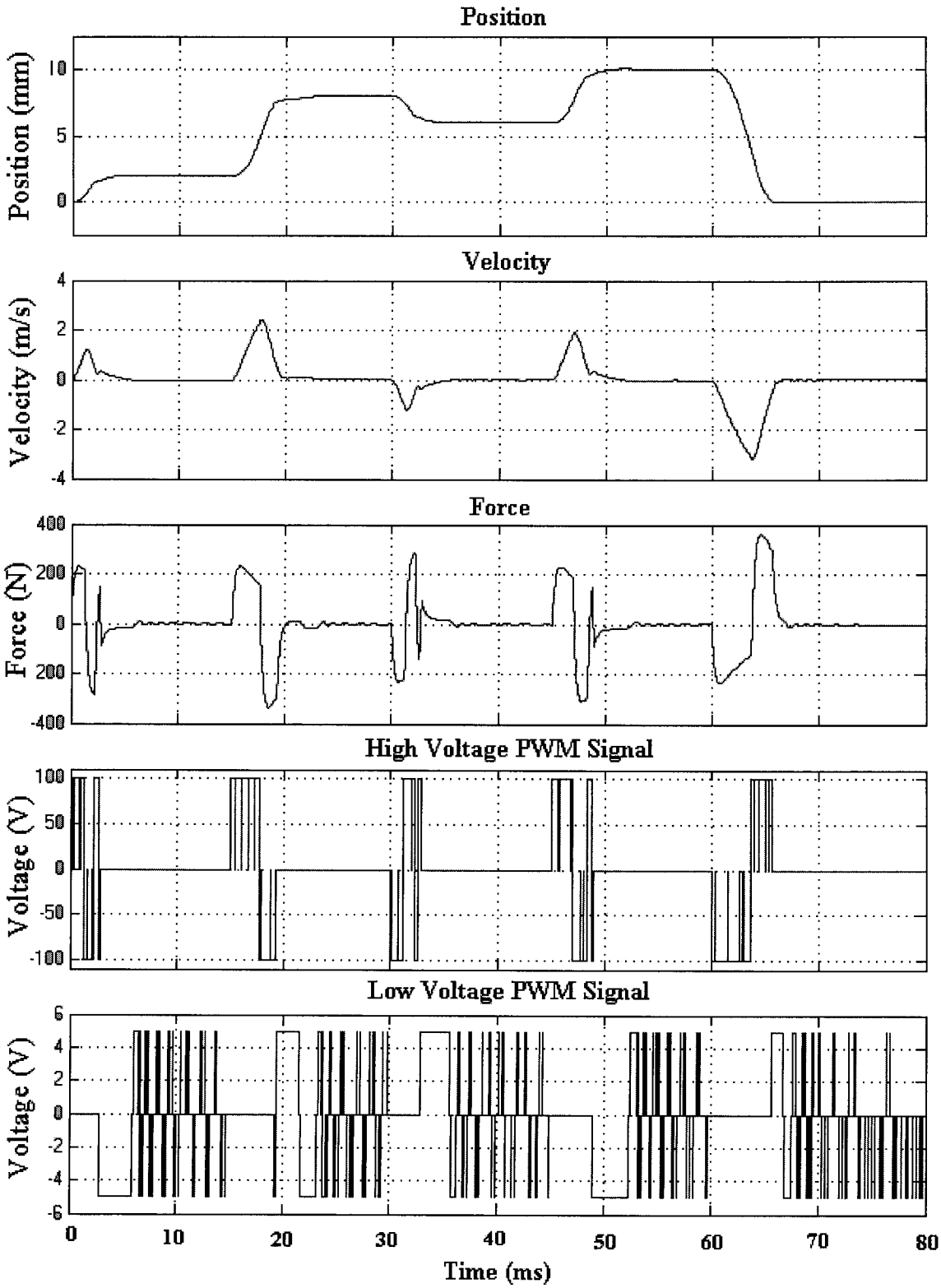

Fig. 3.14 Simulation results of the VCA controlled engine valve for unthrottled operation.

the PWM voltage signal. The relative traveling distance is the difference between the desired position and the current position and is calculated by the controller. Again for each position command the high voltage PWM signal is activated only at the transition period for faster valve movement. The low voltage PWM signal is applied in steady state for holding the engine valve at the desired position until the next command. Table 3.1 summarizes the important conclusions of the simulation results of a voice coil actuated engine valve system.

Table 3.1 Important conclusions of the simulation result

Fig. Number	Achievement showed in simulation
3.12	Soft landing (impact velocity 0.02 m/s). Fast transition time (about 5 ms)
3.13	The control strategy of two different PWM voltages for transient and steady state performance.
3.14	The valve position control at any point between 0mm~10mm for unthrottled operation in the VVT system using a VCA.

3.6.3 Controller Methodology for the PWM and Lead Compensator

Fig. 3.15 is a flow chart showing the logic decision of how the +100V or -100V PWM signal is chosen to drive the VCA plant, and the function of the lead compensator. First, with the input given as the desired length of travel, this is compared to the feedback signal from the actual VCA travel distance. The lead compensator manipulates the error signal according to the system performance requirements and the output signal of the lead

compensator (together with the design specifications of PWM sampling time) is used to determine the width of the PWM signal for the PWM controller. Essentially, the function of the pulse width generator is to produce longer duty cycles for larger errors, and to gradually produce smaller duty cycles as the error reduces. The S-function for PWM signal generator used in a SIMULINK block is given in Appendix-II. The amplitude of the control signal from the lead compensator alone would not be realistic to drive the plant; this limitation was already explained in detail in Section 3.6.1 with respect to fig. 3.10. Therefore, the lead compensator is only used for duty cycle control while the PWM generator has its amplitudes limited to ±100V.

Initially, the VCA system is at rest with zero initial velocity. The objective is to initiate the VCA travel with a fast acceleration, and then to decelerate it for soft landing. For example, initially the PWM width is large because the positional error is large, and the +100V is applied for acceleration. With reference to fig. 3.15, the PWM controller is programmed in such a way that at the present simulation iteration, it calculates and stores the velocity of the moving coil, and other state variables for later use. During the VCA transients, its position depends on the applied force, which is a function of the duty cycle (or positional error), and on its inertia. At the next iteration, the velocity is compared to the velocity of the previous iteration. If the current velocity is greater than the velocity of the previous iteration, the simulation continues because the VCA is still accelerating. Otherwise, if the velocity is less or equal to the previous iteration value, the polarity of the PWM amplitude is reversed because it is now time to decelerate the VCA system to ensure soft landing. The present iteration is discarded and is restarted with the saved state

variables as the initial conditions, and the simulation continues with the PWM amplitude reversed to decelerate the VCA system dynamics.

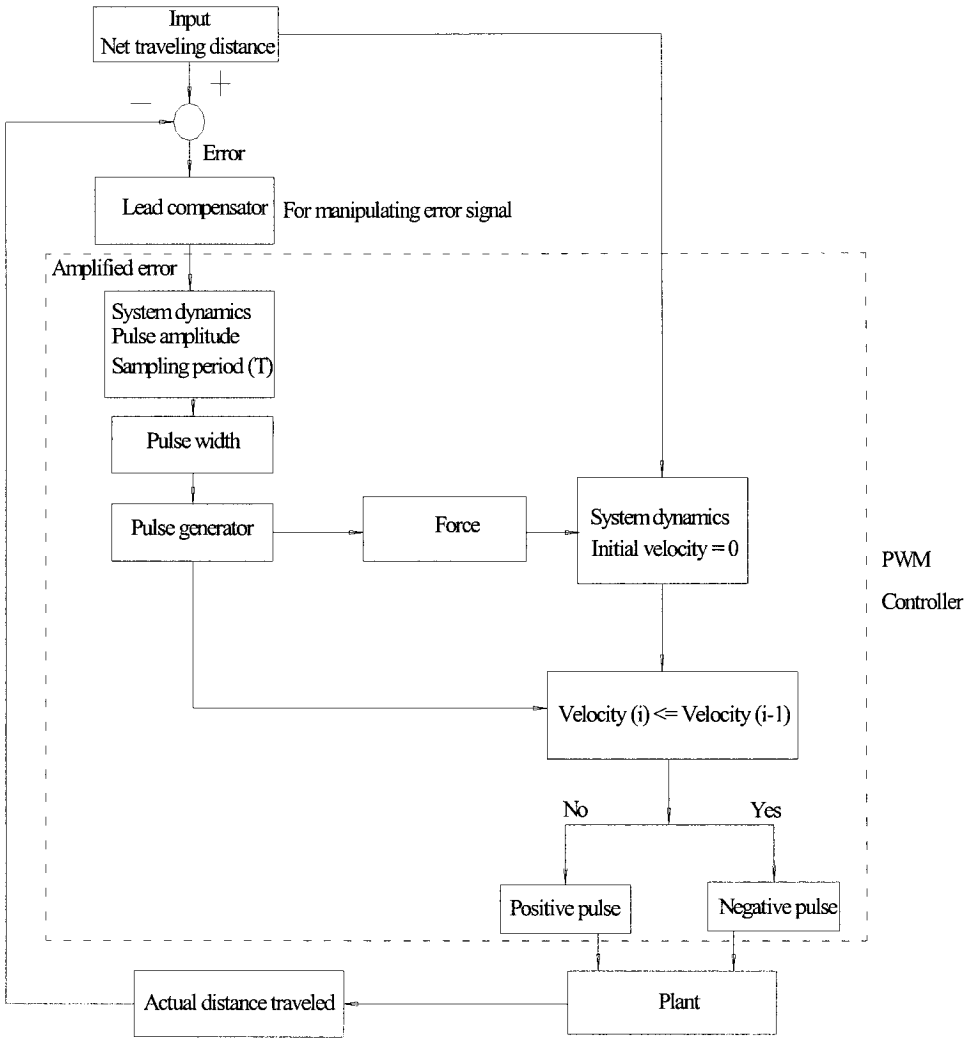

Fig. 3.15 Flow diagram for the programming concept of the PWM controller

The forces developed in the VCA engine valve system for the acceleration and the deceleration phases are different because of the system dynamics. The developed positive force (232.7N for 10mm traveling distance) to accelerate the engine valve is less than the

negative force (365N for 10mm traveling distance) developed for deceleration. This is due to the fact that the back electromotive force (bemf) acts in the opposite direction of the force developed in the VCA during acceleration and acts in the same direction during deceleration. For the same reason the time required to reach maximum velocity during acceleration is longer than the time required during deceleration (Fig. 3.12).

CHAPTER 4

LYAPUNOV-BASED STABILITY ANALYSIS OF A DISCRETE-TIME MODEL OF THE VCA OPERATED ENGINE VALVE SYSTEM

4.1 Introduction

In this chapter a Lyapunov stability result is derived for a discrete-time model of the proposed pulse width modulated (PWM) feedback system with the linear voice coil actuated valve plant. A digital control methodology is used to describe the PWM closed-loop system. The digital implementation has some advantages over the more common analog technique in that it is more reliable and less sensitive to aging and parameter variation [45]. The discrete-time approximate model of the closed-loop system is obtained by ignoring higher order terms in the pulse period. Using this approximation, it is shown that a PWM system can be described as a discrete-time piecewise-affine (PWA) system. The obtained PWA system is defined by partitioning the error space into a finite number of polyhedral regions and associating to each region a different affine dynamic model [46]. At first, the system is represented in state space form and a corresponding discrete-time model is developed approximating the derivative operator by a finite difference. Next, the error space is partitioned using the structure of the feedback control. Finally, a parameterized Lyapunov function is proposed whose parameters can be obtained by the solution of a set of Linear Matrix Inequalities (LMIs).

Checking the stability of a PWA system with polyhedral regions is in general a complex problem. Furthermore, nothing can be concluded for the stability/instability of a PWA system from the stability/instability of its component subsystems [47]. The use of

piecewise-quadratic Lyapunov functions was proposed to test stability for discrete-time PWA systems in [46] by exploiting the switching structure and using relaxation procedures. Various stability tests for discrete-time PWA systems are used in this chapter, such as stability analysis using a common quadratic Lyapunov function and also using a piecewise-quadratic Lyapunov function whose parameters are computed by solving Linear Matrix Inequalities (LMIs). The system is asymptotically stable if the LMIs have a solution, but nothing can be concluded if no solution is found. Finally, a test with LMIs involving a relaxation strategy described in [45] is used for the stability analysis of the approximate discrete-time model of the system in this thesis. The following section will introduce the necessary background material for the stability method used in this chapter.

4.2 Basic Notions

Linear Matrix Inequality (LMI)

A linear Matrix Inequality (LMI) has the form [52,57]

$$F(x) = F_0 + \sum_{i=1}^{n} x_i F_i > 0$$

where x_i are the decision variables and the symmetric matrices $F_i = F_i^T$ are known.

The first LMIs appeared around 1890 when Lyapunov showed that a given linear system with differential equation

$$\dot{x} = Ax \qquad\qquad x \in \Re^n$$

is asymptotically stable in the sense of Lyapunov if and only if there exists a quadratic energy-like positive definite function (Lyapunov function) $V(x(t)) = x^T Px$, such that,

$$V(x(t)) > 0,\ \dot{V}(x(t)) < 0$$

along system trajectories. These conditions can be rewritten as the following set of matrix inequalities in the unknown matrix P,

$$P = P^T > 0$$

$$A^T P + PA < 0$$

Similarly, a discrete-time linear time invariant (LTI) system

$$x_{k+1} = Ax_k$$

is asymptotically stable if there exists a quadratic Lyapunov function $V(x) = x^T Px$, such that,

$$V(x_k) > 0$$

$$V(x_{k+1}) - V(x_k) < 0$$

along system trajectories. Equivalently, this can be expressed as the LMIs,

$$P = P^T > 0$$

$$A^T PA - P < 0$$

Polyhedron

A convex region in space is a set for which the line segment connecting any two of its points is fully contained in the set. A convex polyhedron in n-dimensional space is defined as the region corresponding to the intersection of a finite number of half-spaces. A polytope is a bounded polyhedron (fig. 4.1) [53].

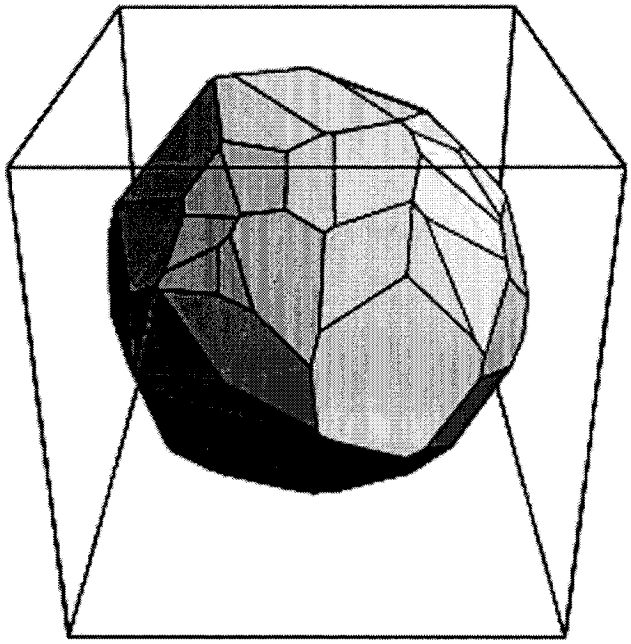

Fig.4.1 Polytope [53]

A convex polyhedron can be formally defined as the set of solutions to a system of linear inequalities

$$Ax \leq b$$

where $A \in \Re^{m \times n}$, $x \in \Re^{n}$ and $b \in \Re^{m}$

Consider as an example of a convex polyhedron the one defined by

$$A = \begin{bmatrix} 1 & 1 \\ -1 & 1 \end{bmatrix} \qquad \text{and} \qquad b = \begin{bmatrix} 2 \\ 0 \end{bmatrix}$$

Then the inequality equations can be written as,

$$x_1 + x_2 \leq 2$$

$$-x_1 + x_2 \leq 0$$

The convex polyhedron of this example is shown in fig.4.2.

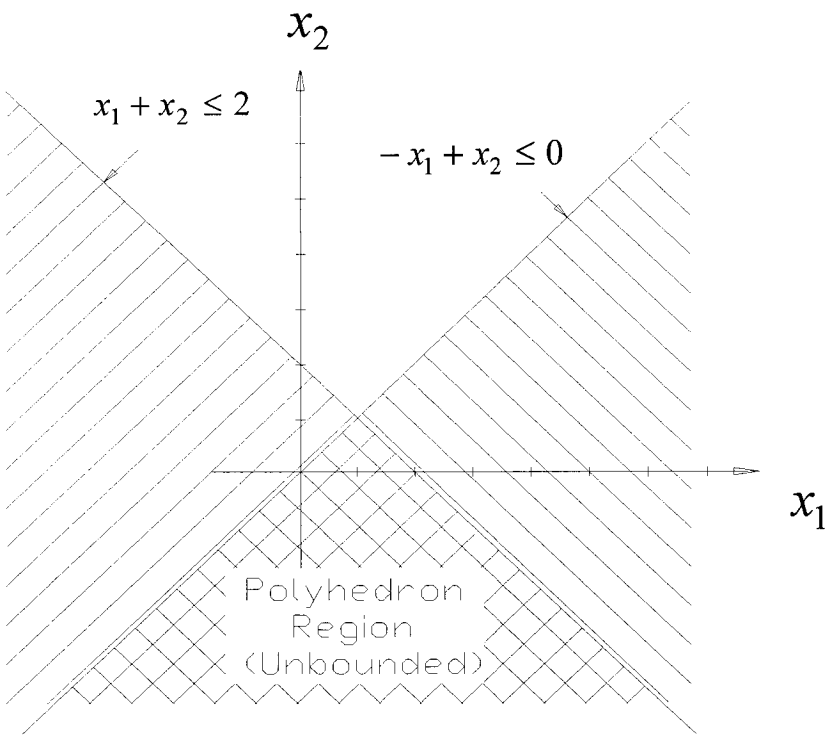

Fig. 4.2 Convex polyhedron

Affine function

$f : \Re^n \to \Re$; is an affine function of x , if it can be written in the form $f(x) = C^T x + b$ where $C \in \Re^{n\times 1}$ and $b \in \Re$.

Piecewise-affine (PWA) System

A piecewise-affine (PWA) dynamical system is a nonlinear system [52,54]

$$\dot{x} = f(x,u)$$

$$y = g(x,u)$$

whose right hand side is a piecewise-affine function of its arguments. Piecewise-affine indicates that the state space can be partitioned into a set of regions $\Re_i$, such that the dynamics within each region are affine, i.e, they can be written as

$$\dot{x} = A_i x + a_i + B_i u \qquad \text{for } x \in \Re_i$$

$$y = C_i x + c_i + D_i u$$

It has two important components:

1. The partition $\{\Re_i\}_{i=1,\ldots,n}$ of the state space into regions.
2. The affine ordinary differential equations (ODEs) describing the dynamics within each region.

4.3 Discretized State Space Model

The forward path of the voice coil actuated valve system with a lead compensator is a linear time invariant (LTI) and strictly proper system. The state space model realization of the VCA valve system with the lead compensator can be derived from the transfer function given in Appendix-I as follows:

$$\dot{x}(t) = Ax(t) + Bu(t)$$

$$y(t) = Cx(t) \tag{4.1}$$

where $x(t) \in R^n$ is the state of the system, $u(t)$ is the input, $y(t)$ is the output,

$$A = \begin{bmatrix} -4.48\times10^4 & -4952 & -158.8 & -28.06 \\ 3.277\times10^4 & 0 & 0 & 0 \\ 0 & 3.277\times10^4 & 0 & 0 \\ 0 & 0 & 4096 & 0 \end{bmatrix}, \qquad B = \begin{bmatrix} 16 \\ 0 \\ 0 \\ 0 \end{bmatrix},$$

$$C = \begin{bmatrix} 0 & 0 & 8.979 & 1.754 \end{bmatrix}.$$

For each period T, the output of a pulse width modulator can be described by

$$u(t)=\begin{cases} U\alpha(kT); & for \quad kT \le t < (k+d_k)T \\ 0; & for \quad (k+d_k)T \le t < (k+1)T \end{cases} \tag{4.2}$$

where U is a constant and for simplicity, stability will be analyzed only for one value of U.

$$\alpha(kT)=\begin{cases} +1; & for \quad r(kT)-y(kT)>0 \\ 0; & for \quad r(kT)-y(kT)=0 \\ -1; & for \quad r(kT)-y(kT)<0 \end{cases} \tag{4.3}$$

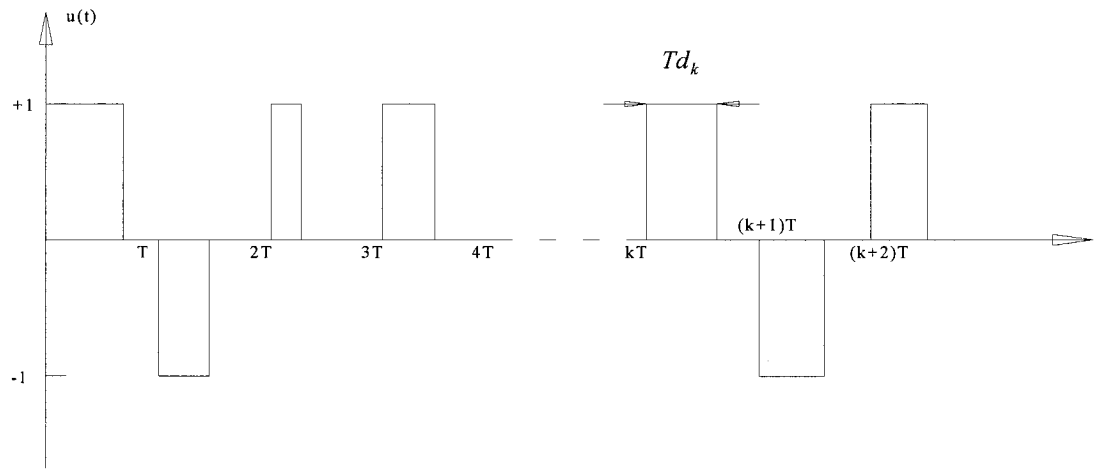

Fig.4 .3 PWM signal for the voice coil actuated engine valve system

and $d_k \in [0, \quad 1]$ is the duty ratio and is determined for each time interval $[kT, \quad (k+1)T]$

$$d_k=\begin{cases} 1 & if \quad r(kT)-y(kT)>1 \\ |r(kT)-y(kT)|\times\beta & if \quad -1\le r(kT)-y(kT)\le 1 \\ 1 & if \quad r(kT)-y(kT)<-1 \end{cases} \tag{4.4}$$

where $r(kT)$ is the reference signal, and β is a control gain. The duty ratio d_k determines the portion of the time the modulator is on.

The pulse width modulator yields a piecewise-continuous output, as illustrated in fig. 4.3. The amplitude of the pulses is fixed while their width varies, depending on the magnitude of the error signal $e(kT) = r(kT) - y(kT)$.

A discrete-time model of the pulse–width-modulated VCA system can be obtained from an approximation of the derivative as the finite difference

$$\dot{x}(t_0) \approx \frac{x(t_0 + \delta) - x(t_0)}{\delta}$$

If we substitute $t = t_0$ into the state equation (4.1) yields

$$x(t_0 + \delta) - x(t_0) \cong \delta[Ax(t_0) + Bu(t_0)]$$

$$\Rightarrow x(t_0 + \delta) \cong Ix(t_0) + \delta Ax(t_0) + \delta Bu(t_0)$$

$$\therefore x(t_0 + \delta) \cong (I + \delta A)x(t_0) + \delta Bu(t_0)$$

where δ is called the integration step size. This difference equation holds in particular, for the time instants kT, $(k+d_k)T$, *and* $(k+1)T$.

Now for $t_0 = kT$ and $\delta = d_k T$ ($T = 100\mu s$ in this thesis)

$$x[(k + d_k)T] = (I + d_k TA)x(kT) + d_k TBU\alpha(kT)$$

For $t_0 = (k + d_k)T$ and $\delta = (1 - d_k)T$,

$$x[(k + d_k + 1 - d_k)T] = \{I + (1 - d_k)TA\}x[(k + d_k)T]$$

$$\Rightarrow x[(k+1)T] = \{I + (1 - d_k)TA\}(I + d_k TA)x(kT) + \{I + (1 - d_k)TA\}d_k TBU\alpha(kT)$$

$$= \{I + d_k TA + TA - d_k TA + (1 - d_k)d_k T^2 A^2\}x(kT) + \{d_k TI + (1 - d_k)d_k T^2 A\}BU\alpha(kT)$$

Neglecting the higher order terms on T ($T = 100\mu s$ in this thesis) yields

$$x[(k+1)T] = (I + TA)x(kT) + d_k TBU\alpha(kT)$$

$$y(kT) = Cx(kT) \tag{4.5}$$

Since equation (4.5) depends on the duty ratio, different dynamics will be obtained for different values of the position error. The regions associated to the different dynamics, as a function of the position error in a voice coil actuated valve system, can be seen in Fig.4.4. The error space is therefore partitioned into four regions based on the duty ratio d_k and the PWM sign detector $\alpha(kT)$. A different set of LMIs will be determined next for each regions of the partition to verify the stability of the system. For simplicity, the reference input $r(kT)$ is considered zero and thus $e(kT) = -y(kT)$.

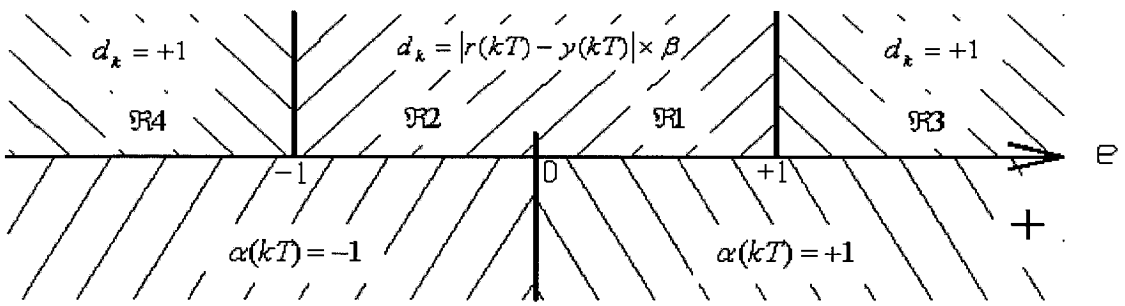

Fig.4.4. Visualization of the values of the duty ratio d_k and the PWM sign detector $\alpha(kT)$ with respect to the error signal $e(kT)$.

Region 1: **Error** $0 < e \leq +1$; $d_k = |0 - y(kT)| \times \beta$ **and** $\alpha(kT) = +1$

In this region the discretized state space model can be simplified as follows:

$$d_k = |y(kT)| \times \beta = |Cx(kT)| \times \beta$$

$$\therefore x[(k+1)T] = (I + TA)x(kT) + |Cx(kT)|\beta TBU$$

$$= (I + TA)x(kT) - \beta TUBCx(kT) \quad \because Cx(kT) \text{ is a negative scalar.}$$

$$= (I + TA)x(kT) + Gx(kT) \qquad \text{where } G = -\beta TUBC \in R^{n \times n}$$

$$\therefore x[(k+1)T] = (I + TA + G)x(kT)$$

$$y(kT) = Cx(kT) \tag{4.6}$$

This is a linear and homogeneous model of the system.

Region 2: Error $-1 \le e < 0$; $d_k = |r(kT) - y(kT)| \times \beta$ and $\alpha(kT) = -1$

Similarly in region 2 the discretized state space model can also be simplified as

$$\therefore x(k+1)T = (I + TA + G)x(kT)$$

$$y(kT) = Cx(kT) \tag{4.7}$$

This is the same linear and homogeneous model of the system as in region 1.

Region 3: Error $e > +1$; $d_k = +1$ and $\alpha(kT) = +1$

The discretized state space PWM model of the voice coil actuated system in region 3 can be calculated as:

$$\therefore x(k+1)T = (I + TA)x(kT) + TBU$$

$$y(kT) = Cx(kT) \tag{4.8}$$

The system equation is affine in region 3.

Region 4: Error $e < -1$; $d_k = +1$ and $\alpha(kT) = -1$

Similar to region 3, the discretized state space PWM model of the voice coil actuated system in region 4 is determined as

$$\therefore x(k+1)T = (I + TA)x(kT) - TBU$$

$$y(kT) = Cx(kT) \tag{4.9}$$

The system equation is also affine in region 4.

In the next section, discrete-time Lyapunov theory is used to obtain the sufficient conditions for the discretized closed-loop system to be asymptotically stable.

4.4 Lyapunov Stability

4.4.1 Quadratic Lyapunov Function

The asymptotic stability of the piecewise-affine discretized system

$$x[(k+1)T] = A_i x(kT) + b_i \Leftrightarrow \bar{x}[(k+1)T] = \bar{A}_i \bar{x}(kT)$$

where $\bar{x}(kT) = \begin{bmatrix} x(kT) \\ 1 \end{bmatrix}$, $\bar{A}_i = \begin{bmatrix} A_i & b_i \\ 0 & 1 \end{bmatrix}$

can be checked with a quadratic Lyapunov function.

$$V[x(kT)] = \bar{x}^T(kT)\bar{P}\bar{x}(kT)$$

Sufficient conditions on P for asymptotic stability are given by the LMIs:

$$\bar{P} > 0$$

$$\bar{A}_i^T \bar{P} \bar{A}_i - \bar{P} < 0 \qquad \forall i \in I \qquad (4.10)$$

If a feasible solution exists for the above LMIs, the piecewise-affine system is termed as quadratically stable and the function $V[x(kT)]$ is called a common Lyapunov function for the matrices $\bar{A}_1, \bar{A}_2, \bar{A}_3, \bar{A}_4$.

4.4.2 Piecewise-quadratic Lyapunov Function

A piecewise-quadratic (PWQ) Lyapunov function for the discretized system can be defined as

$$V[x(kT)] = \bar{x}^T(kT)\bar{P}_i\bar{x}(kT)$$

The continuity of $V[x(kT)]$ is not required to prove the stability, as long as the number of cells is finite [47]. According to [46], for stability, $V[x(kT)]$ must be positive definite in a neighborhood of the origin. The LMIs for this case are,

$$\overline{P}_i > 0 \qquad \forall i \in I$$

$$\overline{A}_j^T \overline{P}_i \overline{A}_j - \overline{P}_j < 0 \qquad \forall (j,i) \in I \times I \tag{4.11}$$

If a feasible solution exists for the above LMIs, the piecewise-affine system is termed as piecewise-quadratically (PWQ) stable.

4.4.3 Piecewise-quadratic Lyapunov Function with Relaxations

In this subsection another method is used to relax the conservativeness of the stability analysis via PWQ Lyapunov functions. The relaxation is considered as follows. Assume a Lyapunov Function of the PWA system described by

$$V[x(kT)] = x^T P x + x^T q + q^T x + r > 0$$

$$\Rightarrow \begin{bmatrix} x \\ 1 \end{bmatrix}^T \begin{bmatrix} P & q \\ q^T & r \end{bmatrix} \begin{bmatrix} x \\ 1 \end{bmatrix} > 0$$

$$\Rightarrow \bar{x}^T \overline{P} \bar{x} > 0 \qquad i.e. \qquad \overline{P} > 0$$

Region 1: Error, $0 < e \le 1$ where, $e = [r(kT) - y(kT)]$

$$\therefore \; 0 \; < \; -y \; < \; 1 \quad \Rightarrow \quad 0 \; > \; y \; > \; -1 \qquad [\because r(kT) = 0]$$

$$\Rightarrow \; 0 \; > \; Cx \; > \; -1 \quad [\because \; y \; = \; Cx \;]$$

i.e. $\quad Cx + 1 > 0 \quad and \quad -Cx > 0$

$$\Rightarrow \begin{bmatrix} C \\ -C \end{bmatrix} x + \begin{bmatrix} 1 \\ 0 \end{bmatrix} > 0$$

Now the above equation can be written as,

$$H_1 x + g_1 > 0 \quad \text{where, } H_1 = \begin{bmatrix} C \\ -C \end{bmatrix} \quad \text{and} \quad g_1 = \begin{bmatrix} 1 \\ 0 \end{bmatrix}$$

$$\Rightarrow \begin{bmatrix} H_1 & g_1 \end{bmatrix} \begin{bmatrix} x \\ 1 \end{bmatrix} > 0$$

$$\Rightarrow \overline{H}_1 \bar{x} > 0$$

$$i.e. \qquad \left(\overline{H}_1 \bar{x}\right)^T W_1 \left(\overline{H}_1 \bar{x}\right) > 0 \quad \text{where, } W_1 > 0$$

$$\Rightarrow \bar{x}^T \left(\overline{H}_1^T W_1 \overline{H}_1\right) \bar{x} > 0 \qquad \Rightarrow \overline{H}_1^T W_1 \overline{H}_1 > 0$$

Using this matrix, the following relaxed conditions for stability can be formulated. They offer less conservative constraints because they ensure that the positive definiteness and negative definiteness Lyapunov constraints only occur inside the respective region instead of globally (as before)

$$\overline{P}_1 - \overline{H}_1^T W_1 \overline{H}_1 > 0$$

and

$$\begin{cases} \overline{A}_2^T \overline{P}_1 \overline{A}_2 - \overline{P}_2 + \overline{H}_1^T W_1 \overline{H}_1 < 0 \\ \overline{A}_3^T \overline{P}_1 \overline{A}_3 - \overline{P}_3 + \overline{H}_1^T W_1 \overline{H}_1 < 0 \end{cases} \tag{4.12}$$

Region 2: Error $-1 \le e < 0$ where, $e = \left[r(kT) - y(kT)\right]$

Similar to region 1, one can find,

$$\bar{x}^T \left(\overline{H}_2^T W_2 \overline{H}_2\right) \bar{x} > 0 \qquad \Rightarrow \overline{H}_2^T W_2 \overline{H}_2 > 0 \qquad \text{where, } W_2 > 0$$

Therefore, $\overline{P}_2 - \overline{H}_2^T W_2 \overline{H}_2 > 0$ where, $\overline{H}_2 = \begin{bmatrix} H_2 & g_2 \end{bmatrix}$,

$$H_2 = \begin{bmatrix} -C \\ C \end{bmatrix}; \quad g_2 = \begin{bmatrix} 1 \\ 0 \end{bmatrix}$$

and
$$\begin{cases} \overline{A}_1^T \overline{P}_2 \overline{A}_1 - \overline{P}_1 + \overline{H}_2^T W_2 \overline{H}_2 < 0 \\ \overline{A}_4^T \overline{P}_2 \overline{A}_4 - \overline{P}_1 + \overline{H}_2^T W_2 \overline{H}_2 < 0 \end{cases} \tag{4.13}$$

Region 3: Error $e > 1$ where, $e = [r(kT) - y(kT)]$

i.e. $-y > 1 \quad \Rightarrow -Cx > 1 \quad \Rightarrow -Cx - 1 > 0$

$\therefore H_3 x + g_3 > 0$ where, $H_3 = [-C]$ *and* $g_3 = [-1]$

$\Rightarrow \overline{H}_3 \bar{x} > 0$ where, $\overline{H}_3 = [H_3 \quad g_3]$

Using this matrix the following relaxed conditions for stability can be formulated,

$$\overline{P}_3 - \overline{H}_3^T W_3 \overline{H}_3 > 0$$

$$\overline{A}_1^T \overline{P}_3 \overline{A}_1 - \overline{P}_1 + \overline{H}_3^T W_3 \overline{H}_3 < 0 \tag{4.14}$$

Region 4: Error $e < -1$ where, $e = [r(kT) - y(kT)]$

Similarly, the following LMIs can be formulated for region 4,

$$\overline{P}_4 - \overline{H}_4^T W_4 \overline{H}_4 > 0$$

$$\overline{A}_2^T \overline{P}_4 \overline{A}_2 - \overline{P}_2 + \overline{H}_4^T W_4 \overline{H}_4 < 0 \tag{4.15}$$

where, $\overline{H}_4 = [H_4 \quad g_4]$ and $H_4 = [C]$; $g_4 = [-1]$

Each method for stability analysis for the pulse–width-modulated VCA system is tested using YALMIP [55] and SeDuMi [56] in MATLAB to find a feasible Lyapunov function. The program for stability analysis is given in Appendix-III. The stability analysis gave conclusive results only when looking for a piecewise-quadratic Lyapunov function with relaxation. All other methods did not give any feasible results. However, the plots of the Lyapunov functions with respect to the error for the different methods look all similar to a globally quadratic function (fig. 4.5). The possible reason of this

similarity is that the magnitudes of the negative residuals found in the stability analysis are very small (considerably near zero), which might indicate a strictly infeasibility problem. The primary residual values for different stability test are given as follows:

Residual values found for quadratic Lyapunov function test

ID	Constraint	Type	Primal residual
#1	P_bar>0	LMI	**-2.1213e-012**
#2	A1d_bar'*P_bar*A1d_bar - P_bar < 0	LMI	**-4.8495e-012**
#3	A2d_bar'*P_bar*A2d_bar - P_bar < 0	LMI	**-4.8495e-012**
#4	A3d_bar'*P_bar*A3d_bar - P_bar < 0	LMI	**-5.5422e-012**
#5	A4d_bar'*P_bar*A4d_bar - P_bar < 0	LMI	**-5.5422e-012**

Residual values found for piecewise-quadratic Lyapunov function test

ID	Constraint	Type	Primal residual
#1	P1_bar>0	LMI	1.6555e-015
#2	P2_bar>0	LMI	1.6064e-015
#3	P3_bar>0	LMI	6.9423e-015
#4	P4_bar>0	LMI	6.9383e-015
#5	A2d_bar'*P1_bar*A2d_bar-P2_bar <0	LMI	**-6.9315e-015**
#6	A3d_bar'*P1_bar*A3d_bar-P3_bar <0	LMI	**-7.1308e-015**
#7	A1d_bar'*P2_bar*A1d_bar-P1_bar <0	LMI	**-6.5058e-015**
#8	A4d_bar'*P2_bar*A4d_bar-P4_bar <0	LMI	**-7.1909e-015**
#9	A1d_bar'*P3_bar*A1d_bar-P1_bar <0	LMI	**-7.4349e-015**
#10	A2d_bar'*P4_bar*A2d_bar-P2_bar <0	LMI	**-7.4815e-015**

Residuals found for piecewise-quadratic Lyapunov function with relaxation test

ID	Constraint	Type	Primal residual
#1	P1_bar>0	LMI	0.48657
#2	P2_bar >0	LMI	0.48657
#3	P3_bar >0	LMI	0.57724
#4	P4_bar >0	LMI	0.57724
#5	W1>0	LMI	0.0022818
#6	W2>0	LMI	0.0022818
#7	W3>0	Element-wise	0.0055371
#8	W4>0	Element-wise	0.0055371
#9	P1_bar-H1_bar'*W1*H1_bar>0	LMI	0.26912
#10	A2d_bar'*P1_bar*A2d_bar-P2_bar+H1_bar'*W1*H1_bar<0	LMI	0.022902
#11	A3d_bar'*P1_bar*A3d_bar-P3_bar+H1_bar'*W1*H1_bar<0	LMI	0.023079
#12	P2_bar-H2_bar'*W2*H2_bar>0	LMI	0.26912
#13	A1d_bar'*P2_bar*A1d_bar-P1_bar+H2_bar'*W2*H2_bar<0	LMI	0.022902
#14	A4d_bar'*P2_bar*A4d_bar-P4_bar+H2_bar'*W2*H2_bar<0	LMI	0.023079
#15	P3_bar-H3_bar'*W3*H3_bar>0	LMI	0.34913
#16	A1d_bar'*P3_bar*A1d_bar-P1_bar+H3_bar'*W3*H3_bar<0	LMI	0.023313
#17	P4_bar-H4_bar'*W4*H4_bar>0	LMI	0.34913
#18	A2d_bar'*P4_bar*A2d_bar-P2_bar+H4_bar'*W4*H4_bar<0	LMI	0.023313

The positive definite matrices P_i found for the four regions have the following eigenvalues:

P1_bar =	0.4866	P2_bar =	0.4866	P3_bar =	0.5772	P4_bar =	0.5772
	1.2308		1.2308		0.8641		0.8641
	1.4895		1.4895		1.2065		1.2065
	1.6438		1.6438		1.6358		1.6358
	2.2355		2.2355		2.2085		2.2085

The plot of the Lyapunov function versus the position error with other functions found from other stability analysis methods is shown in fig.4.5.

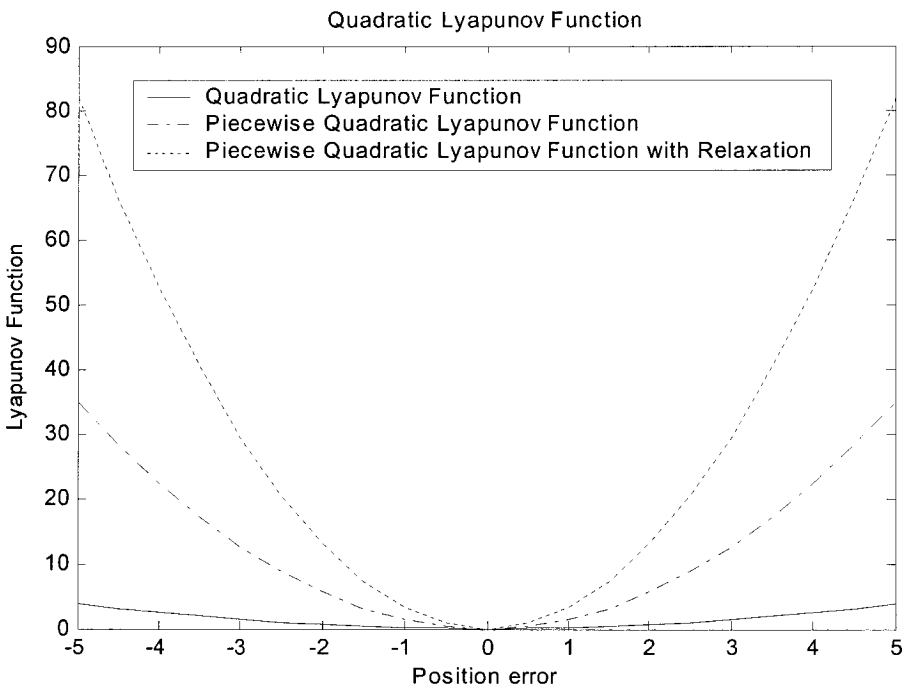

Fig. 4.5 Lyapunov functions versus system position error.

CHAPTER 5

EXPERIMENTAL VALIDATION OF STATIC FORCE AND CURRENT CHARACTERISTICS OF A VOICE COIL ACTUATOR

This chapter presents the experimental work that includes the experimental setup, experimental data analysis and comparison of the data with the simulation performance. The performed experiment determines how the VCA static force is related to the current and it validates the theoretical predictions.

5.1 Experimental Setup

The experimental setup to measure the voice coil actuator force and current response characteristics at various coil positions is shown in fig. 5.1. The test platform consist of a housing of square shaped aluminum stand, a brass made fixture to hold the voice coil actuator, a piezoelectric load cell transducer for measuring the force due to the applied current, and two threaded rods which are used to hold the fixture and the load cell to the main frame body. The voice coil actuator is held in the lower part of the fixture and a hollow top cover is screwed together with the lower part to ensure the actuator shell cannot move freely. The actuator coil can freely pass through the hole of the top cover of the fixture to measure the developed force due to the applied current.

One threaded rod is used to hold the fixture to the middle plate of the main frame. It can move in and out through the threaded holes in the middle plate and in the bottom of the fixture. An adjustable non-ferromagnetic brass plate is placed in the inside groove of the lower fixture part and connected by the threaded rod to ensure that the voice coil

actuator is held rigidly in the fixture during the experiment. Another threaded rod is used to hold the piezoelectric load cell transducer on top of the moving coil of the actuator. The detail assembly and parts drawings of the experimental setup are given

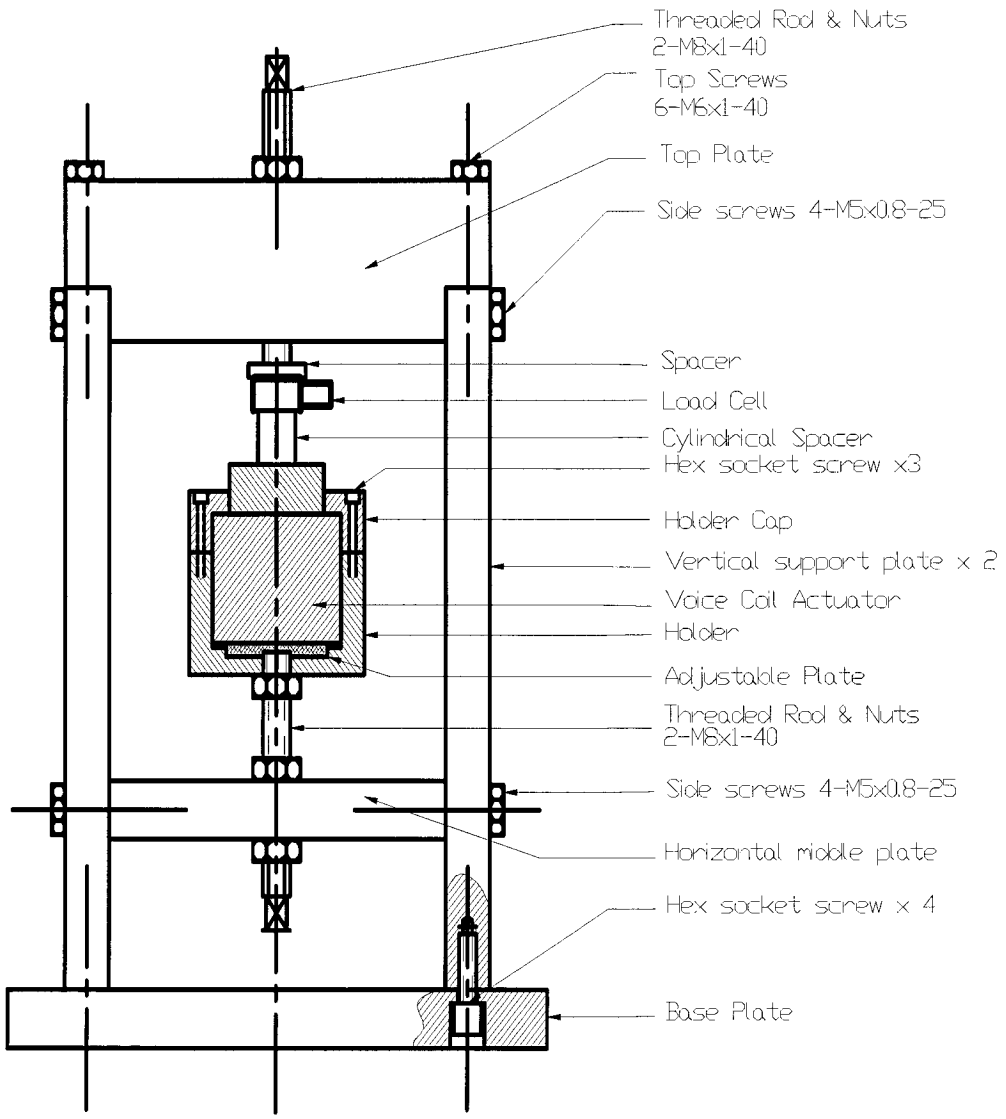

Fig. 5.1. Schematics of experimental fixture

in Appendix-IV. A cylindrical brass spacer is added between the moving coil and the transducer to prevent the magnetic flux from affecting the transducer because the force

transducer is made of a magnetic material. Some donut shaped brass discs with different thickness of 2mm, 4mm, 5mm, 6mm, 8mm and 10mm are used inside the moving coil holder for different coil positions in its traveling path. As a result, the developed force due to the applied current can be measured at different coil positions.

A pre-load is applied using the threaded rod on the force transducer to hold the moving coil rigidly at the proper position in the fixture. When the current is applied it produces an induced force that acts on the moving coil. Since the moving coil is fixed, the force is transmitted to the load cell transducer, and thus data of the induced force due to the applied current can be measured in the oscilloscope. The piezoelectric transducer can be used to measure the developed force in both directions by applying a pre-load on it during the experiment. This means that the piezoelectric transducer can be used to measure the pushing force when the developed force acts in the direction of the pre-load. It can also be used to measure the pulling force when the developed force acts in the opposite direction of the pre-load. Therefore, when the pre-load is set properly, both the pushing force and the pulling force due to the applied current can be obtained by altering the coil current direction.

A piezoelectric load cell was used to measure the developed force in both directions during the experiment. Fig. 5.2 shows the calibration curve for the load cell. In the calibration of the force transducer, dead weights were gradually applied from 0 to 78.50N to load the cell under compression, and the electrical output from the cell was recorded using an oscilloscope.

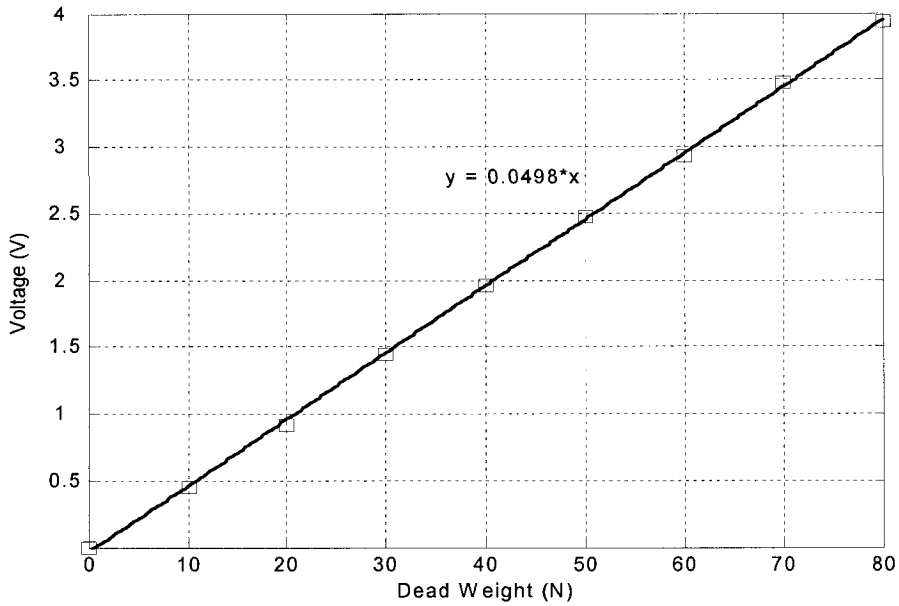

Fig.5.2 Piezoelectric load cell transducer calibration curve [43]

The switching circuit used in the experiment to apply a step input is shown in Figure 5.3. A variable power supply is connected to one terminal of the voice coil actuator, while the other terminal is connected to an N-channel power MOSFET, which is used as a switch to control the current through the voice coil actuator. The source voltage V is applied to the voice coil actuator and a square voltage signal is applied to the gate of the MOSFET to turn the transistor on and off. The MOSFET transistors require a positive 6 V gate-to-source voltage to turn ON and zero voltage to turn OFF. However a ±20 V (higher and lower) was used to speed up the transistor turn ON and OFF. The current will pass through the voice coil L when the MOSFET is ON due to the high voltage control signal and the voice coil current is cut off when the MOSEFT is off due to the low voltage control signal. The fly-back diode D is used in the circuit to provide a path for the coil current to decay during the OFF time of the transistor and the capacitor is used to prevent that the supply voltage V drops when the circuit is ON.

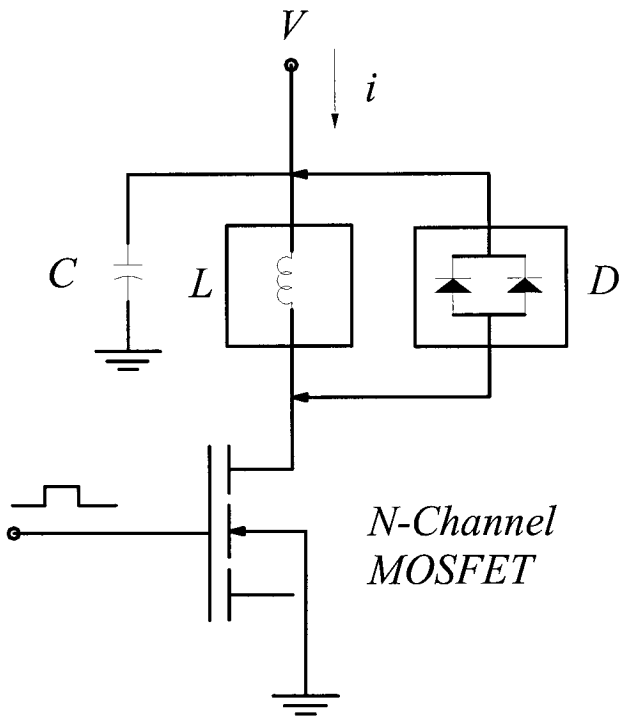

Fig.5.3 Switching circuit to apply a step input voltage to the voice coil actuator

The developed force due to the applied current is measured with the load cell transducer. The output of the load cell transducer is connected to the data acquisition port of the oscilloscope. A clamp-on meter around the voice coil actuator terminal wire is used to measure the current applied to the coil. A block diagram of the data acquisition system of the experiment is shown in fig. 5.4. After recording the experimental data using a data acquisition software (WAVESTAR for the oscilloscope), the data file is imported into MATLAB and over plotted with the simulation result. Contrary to the case of a solenoid the force in a voice coil is also developed in the reverse direction due to the opposite polarity of the applied current. Therefore, the developed forces in both directions, acting on the coil holder due to the applied current can be measured.

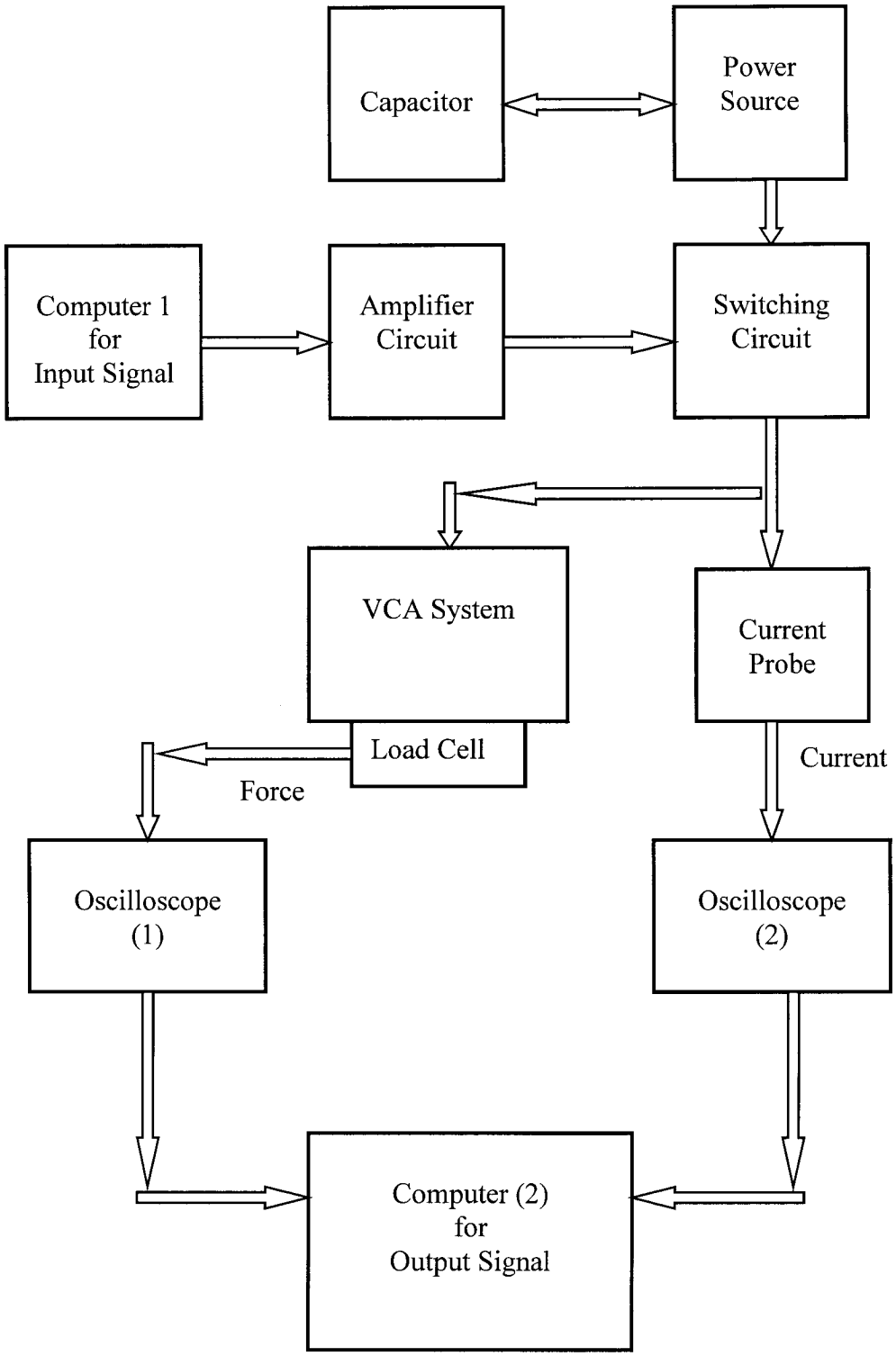

Fig.5.4 Block diagram of the data acquisition system of the experiment

5.2 Equations of Force and Current Response of VCA for Simulation

The force produced in the VCA is proportional to the applied current and is described by equation (2.1) in Chapter 2, repeated here for convenience,

$$F(t) = K_1 Blin \tag{5.1}$$

where the design constant K_1, the magnetic flux density B, the conductor length l and the number of wire turns n are all constant. The force $F(t)$ can thus be expressed as:

$$F(t) = K_F i(t)$$

where $K_F = K_1 Bln$ is the force sensitivity constant.

In the Laplace domain,

$$I(s) = \frac{1}{K_F} F(s) \tag{5.2}$$

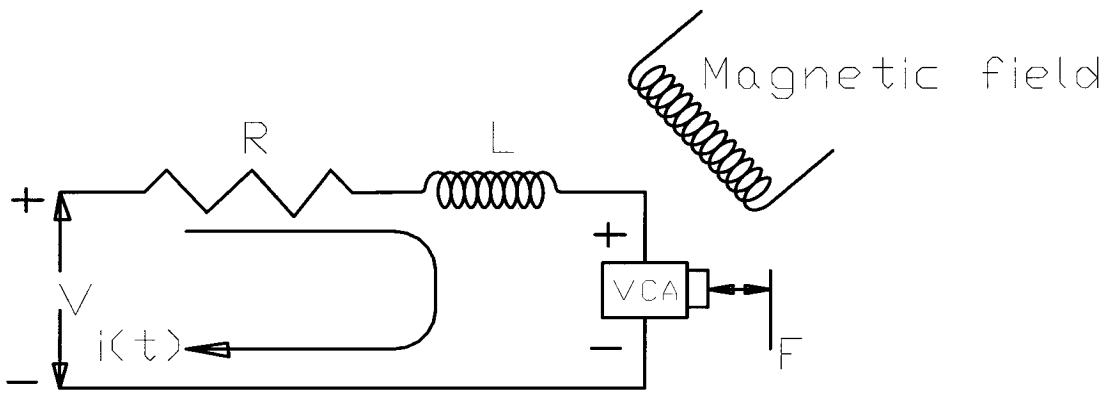

Fig. 5.5 Loop diagram of VCA for static force measurement

In the experiments, the coil is maintained steady while measuring the force. In that case, there is no back electromotive force and the relationship between the current *I(s)* and the applied voltage *V(s)* is written from the circuit loop equation as (fig. 5.5)

$$V(s) = RI(s) + LsI(s) \tag{5.3}$$

where R and L are the resistance and inductance of the system, respectively. Equations (5.2), and (5.3) yield the force and current equations:

$$V(s) = R\frac{1}{K_F}F(s) + Ls\frac{1}{K_F}F(s)$$

$$F(s) = \left(\frac{1}{R+Ls}\right) \times K_F \times V(s) \tag{5.4}$$

$$I(s) = \left(\frac{1}{R+Ls}\right) \times V(s) \tag{5.5}$$

Therefore the open loop block diagram for the force and current response of the VCA can be drawn as follows:

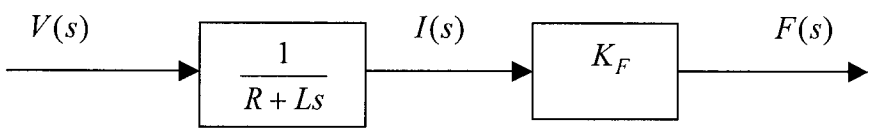

Fig. 5.6 Open loop block diagram for the static (mechanical) force and current response

5.3 Test and Simulation Results of Force and Current at Various Applied Voltages and Traveling Positions

The applied current and the corresponding force are measured for the voice coil actuator at different coil-traveling positions from 0 mm to 10 mm with 2 mm increments and at a center position of 5mm. At each traveling point, there are four different voltages applied to the voice coil actuator: 12.3V, 24.4V, 36.7V and 49.1V. The test results are presented in Figures 5.6 to 5.33.

The transient current response of the voice coil actuator follows an exponential path due to the coil inductance and at steady state the current reaches its maximum value. The figures show that the transient and steady state responses of the current are essentially the same at different traveling points for the same supply voltage. This proves the fact that the current response of the VCA is only dependent on the resistance and inductance of the coil and does not depend on the coil traveling positions. This is a very important feature of an actuator to control the engine valve perfectly during operation. As compared to a solenoid, which is more complicated, the force is a nonlinear function of the core travel (*ie*: air gap). The experimental force plots at different traveling positions for equal supply voltage are also the same and the profiles are similar to that of the current profiles, since force is directly proportional to the current of the VCA.

The figures also show that at low supply voltages, the experimental pushing and pulling forces have very little fluctuation during steady-state. However in the case of high voltages, the force fluctuation is more distinct at steady state. The reasons for this behavior are twofold. First the experimental setup is not stiff enough for large forces and

the components of the VCA holder could vibrate due to elasticity, but in the case of low voltages there is not enough force developed to affect the experimental structure. Second, the contact surfaces between the load cell transducer, the spacers, the moving coil and the disc are not perfectly flat. Therefore, force fluctuations could occur due to bouncing at the contact surfaces.

The pushing and pulling forces were measured by changing the current direction of the voice coil actuator. It can be seen from the experimental results that the pushing and pulling force responses have the same transients and magnitude with opposite direction for the given traveling point and supply voltage. These experimental results prove that, contrary to the case of a solenoid, the voice coil actuator can develop equal forces in reverse direction by changing the polarity of the applied voltage. This is one of the most important characteristics of the voice coil actuator.

Since the parameters of the voice coil actuator system are available in the manufacturer specification, the static force and current equations (5.4) and (5.5) are computer simulated and plotted on the same graphs of the experimental data in Figures 5.7 to 5.34, for direct comparison. The MATLAB program for computer simulation and experimental data plot at 5mm traveling distance is given in Appendix-V. The comparison shows that the simulation results and the experimental results match very well and hence validate the mathematical model of the force and current response of the voice coil actuator. The deviation between the experimental results and the simulation is the force fluctuation at steady state for high voltages already discussed in the previous paragraph. Improving the stiffness of the experimental setup, by creating a perfect

alignment among the VCA holder parts and increasing the precision of the contact surfaces can remarkably reduce the force fluctuation at steady state [42].

As discussed, the force developed in the voice coil actuator due to the applied current does not vary too much with respect to the coil position while the supply voltage is constant. Therefore, the experimental average steady-state data (experimental data from 1ms to 2.25ms is considered as steady state value) of the forces at different traveling positions for each supply voltage are calculated and plotted in fig.5.35. It can be seen from the figure that the maximum average force curve with respect to the coil position is almost flat. The degradation of the force at the two travel extremes with respect to the mid-stroke force for 12.3V, 24.4V, 36.7V and 49.1V is less than 16%, 9%, 8.3% and 7.5% respectively. The average steady-state force values of each coil position for four different supply voltages are listed in Table 5.1.

Table 5.1 Experimental Results of maximum average force

Supply Voltage	Coil Position (mm)						
(*V*)	0	2	4	5	6	8	10
12.3	16.8000	17.9200	18.4320	19.2000	18.7200	17.4240	6.1280
24.4	34.7200	36.4000	37.1000	37.5000	36.5400	35.8400	34.2200
36.7	49.0000	51.8000	54.0000	54.0160	53.9070	51.0400	49.5000
49.1	67.0240	69.9600	70.8000	71.0400	70.8492	70.3800	66.4000

5.4 Summary

In this chapter the performed experiments were discussed. The experiments measured the force and current characteristics of the voice coil actuator. These results were overplotted with the computer simulation results for comparison. The forces and currents were measured at seven different coil positions for four different supply voltages. The major deviation between the simulated and experimental results is due to force fluctuation at steady state for a high voltage supply. This force fluctuation can be remarkably reduced by improving the experimental setup.

The experimental results of the voice coil actuator match well with the simulation results and validate the mathematical model of the voice coil actuator for the case of force and current relationship. The maximum step voltage applied in the experiment was 49.1V, which is much higher than the rated voltage (26.2V) of the VCA. It should be noted that the experiment proved the bi-directional motion ability of the voice coil actuator. Experiments also confirmed that the voice coil actuator can produce equal pulling and pushing forces for the same supply voltage with opposite polarity and the developed force does not vary too much with coil displacement.

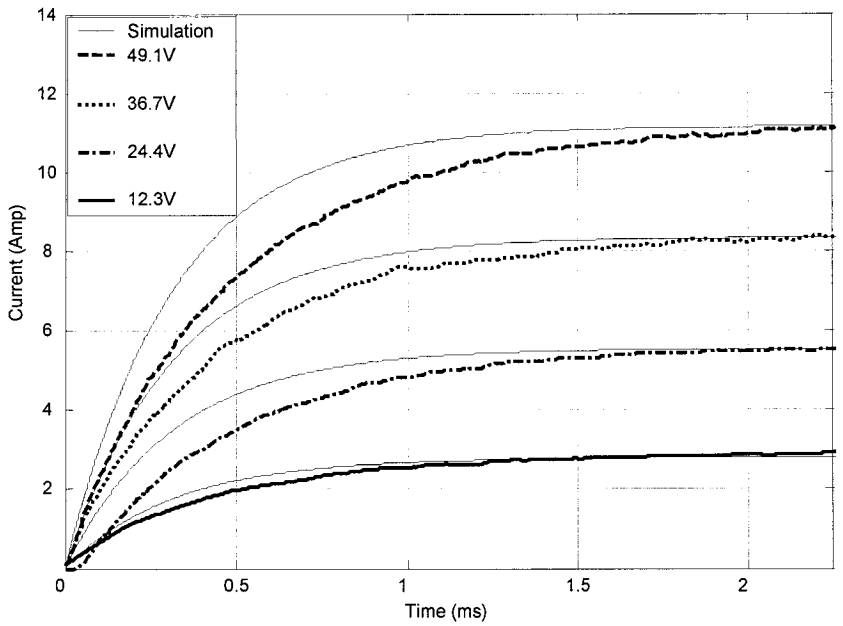

Fig.5.7 Experimental vs. simulation results of Current response

(Traveling position 0mm)

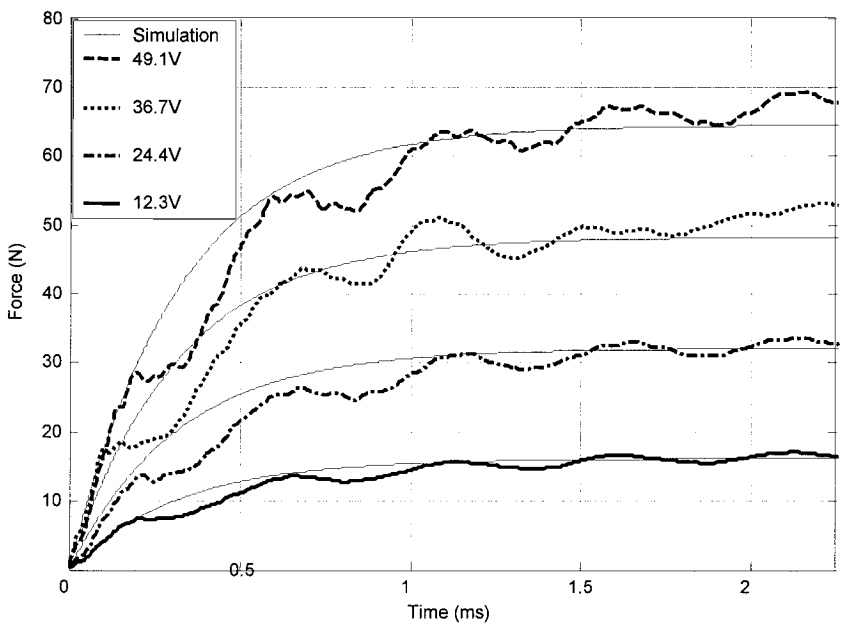

Fig.5.8 Experimental vs. simulation results of Force response

(Traveling position 0mm)

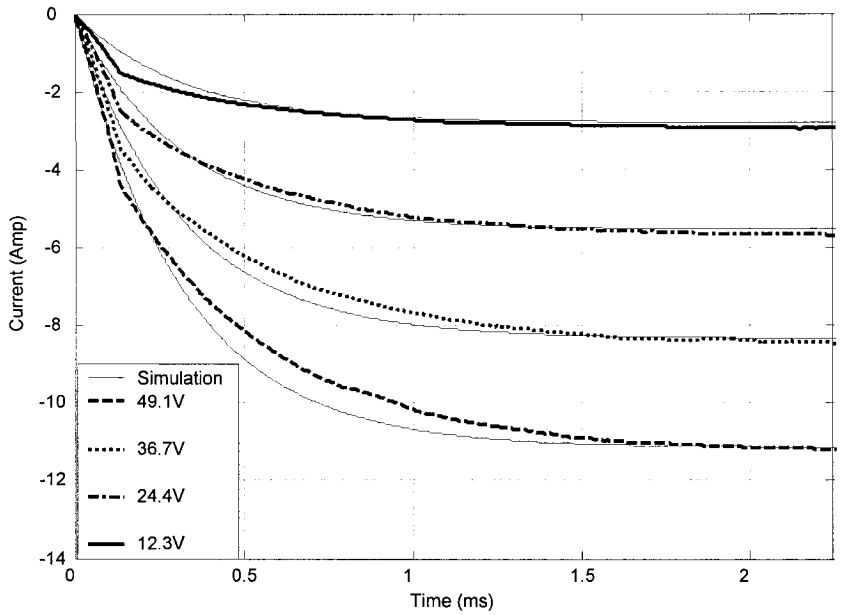

Fig.5.9 Experimental vs. simulation results of Current response in opposite direction (Traveling position 0mm)

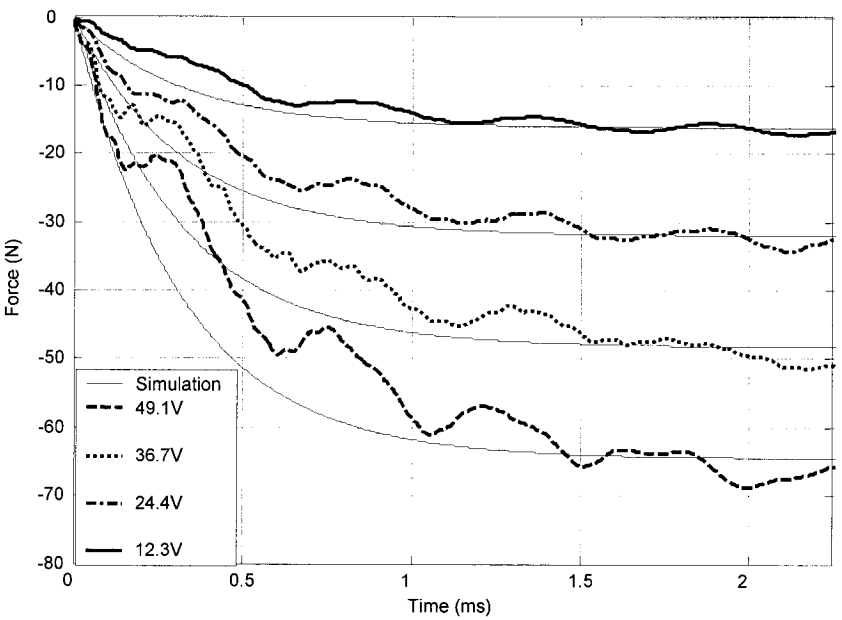

Fig.5.10 Experimental vs. simulation results of Force response in opposite direction (Traveling position 0mm)

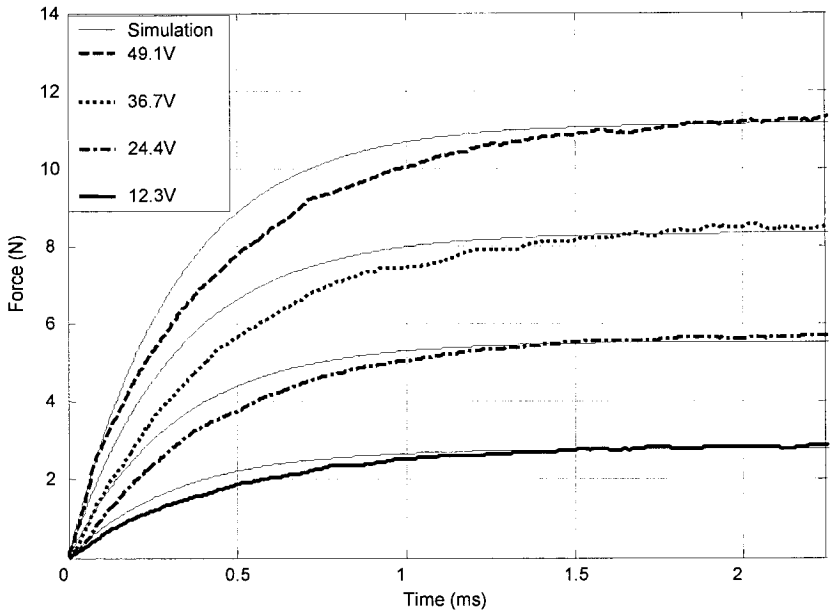

Fig.5.11 Experimental vs. simulation results of Current response

(Traveling position 2mm)

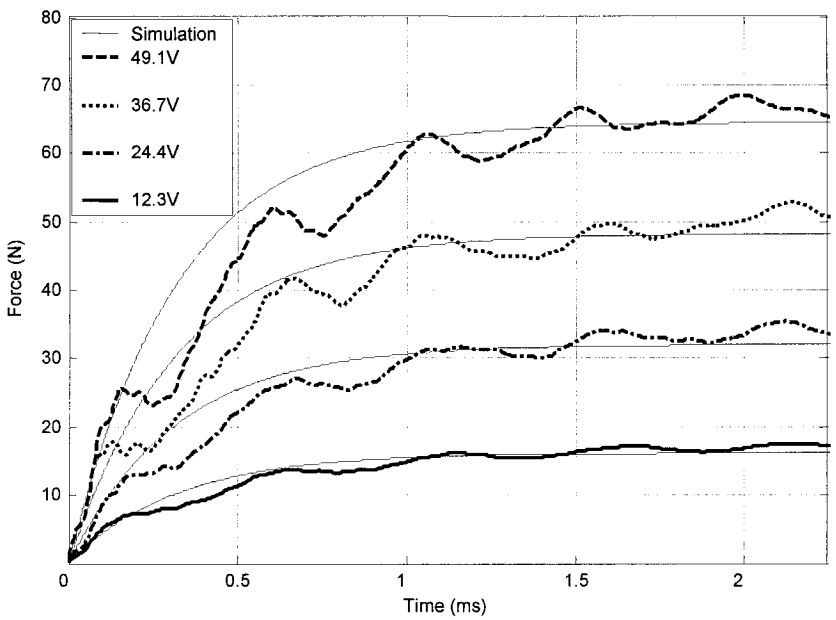

Fig.5.12 Experimental vs. simulation results of Force response

(Traveling position 2mm)

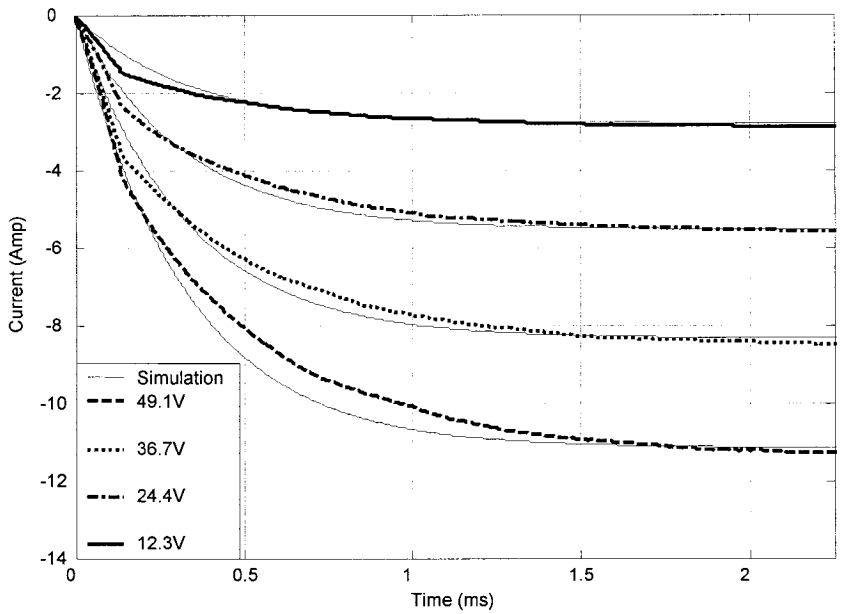

Fig.5.13 Experimental vs. simulation results of Current response in opposite direction (Traveling position 2mm)

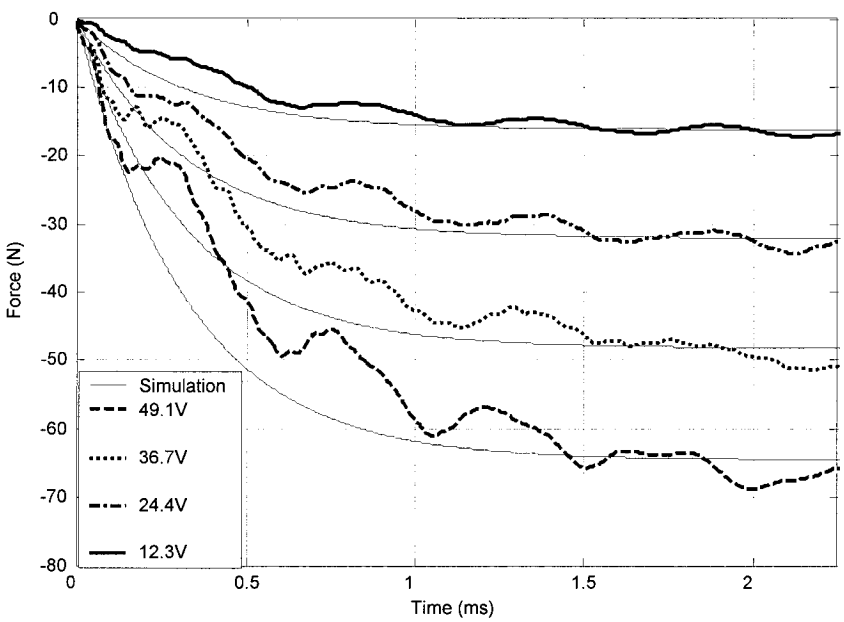

Fig.5.14 Experimental vs. simulation results of Force response in opposite direction (Traveling position 2mm)

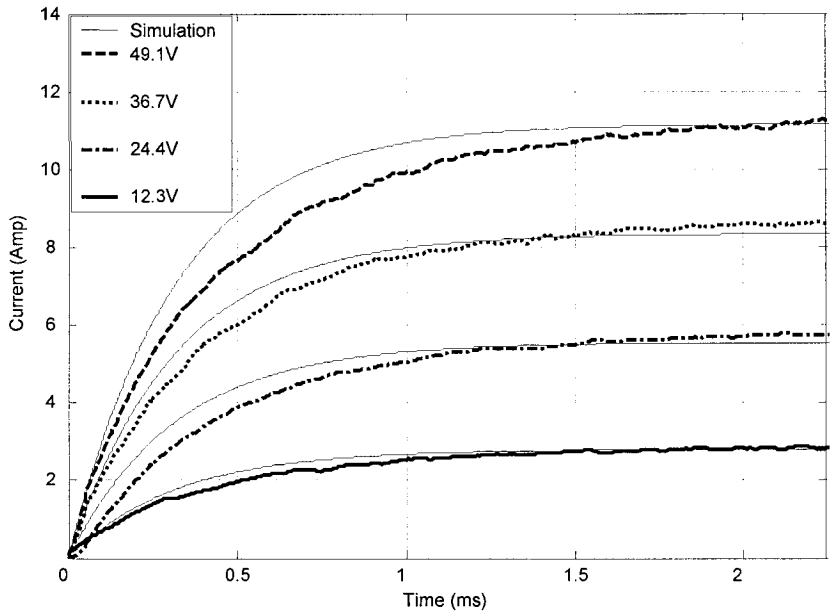

Fig.5.15 Experimental vs. simulation results of Current response

(Traveling position 4mm)

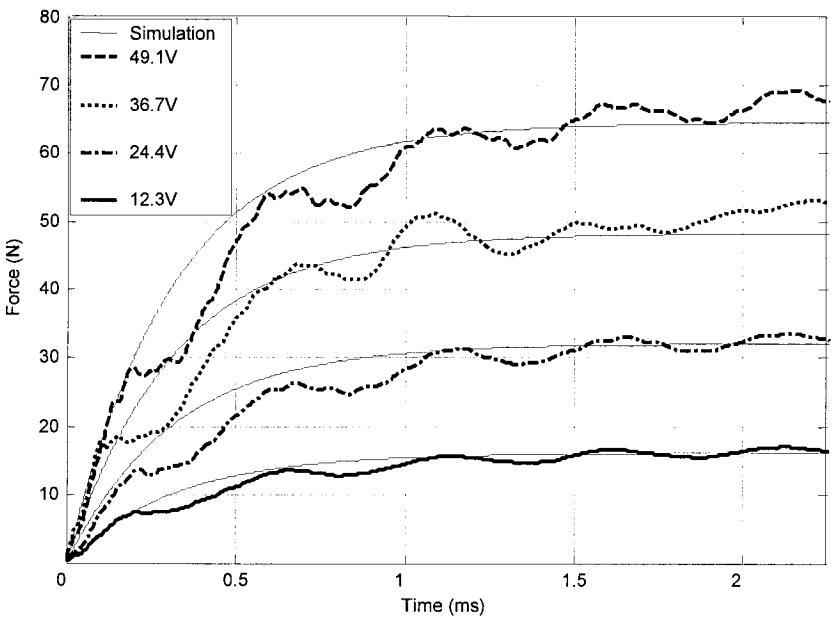

Fig.5.16 Experimental vs. simulation results of Force response

(Traveling position 4mm)

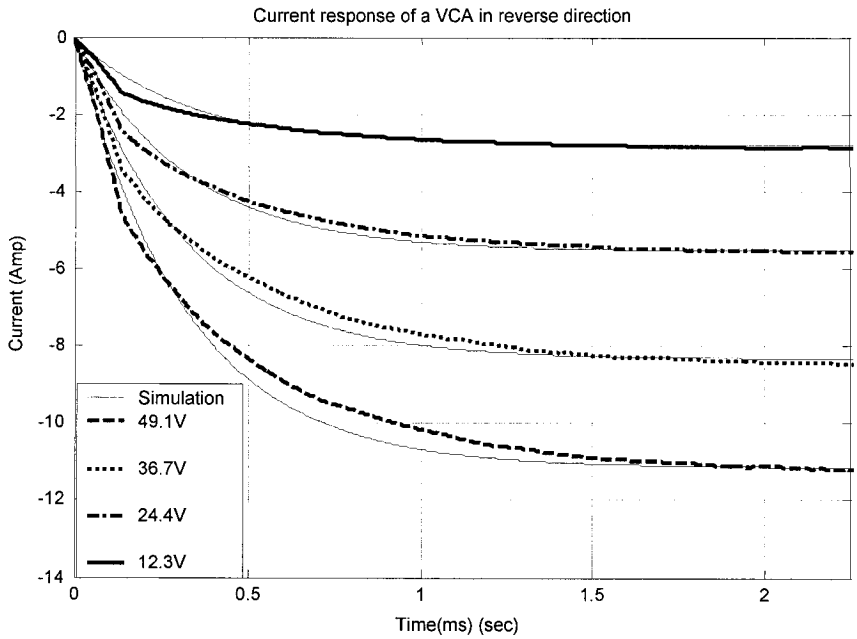

Fig.5.17 Experimental vs. simulation results of Current response in opposite direction (Traveling position 4mm)

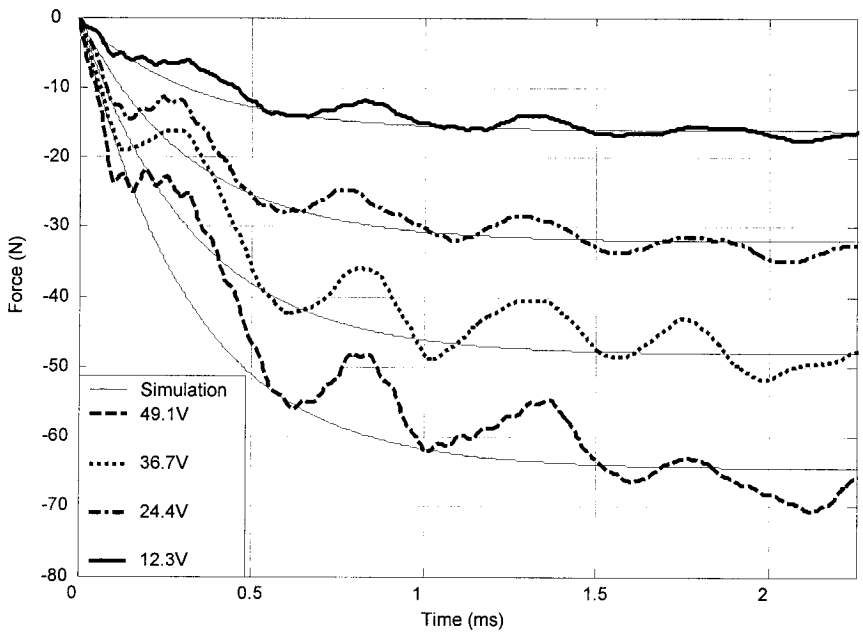

Fig.5.18 Experimental vs. simulation results of Force response in opposite direction (Traveling position 4mm)

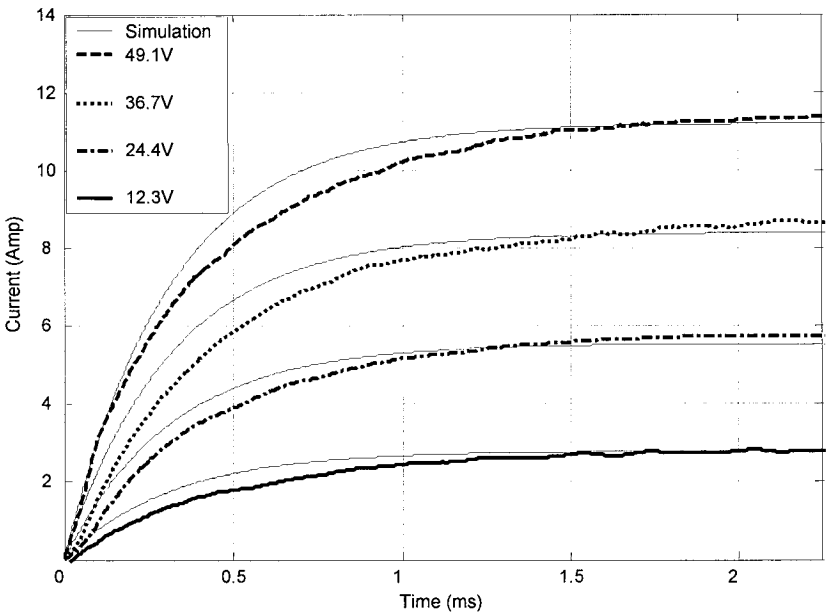

Fig.5.19 Experimental vs. simulation results of Current response

(Traveling position 5mm)

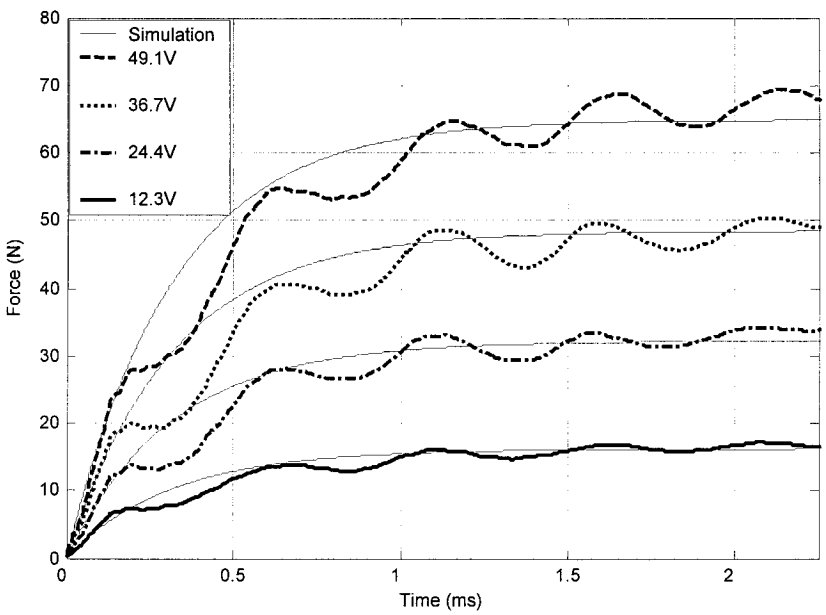

Fig.5.20 Experimental vs. simulation results of Force response

(Traveling position 5mm)

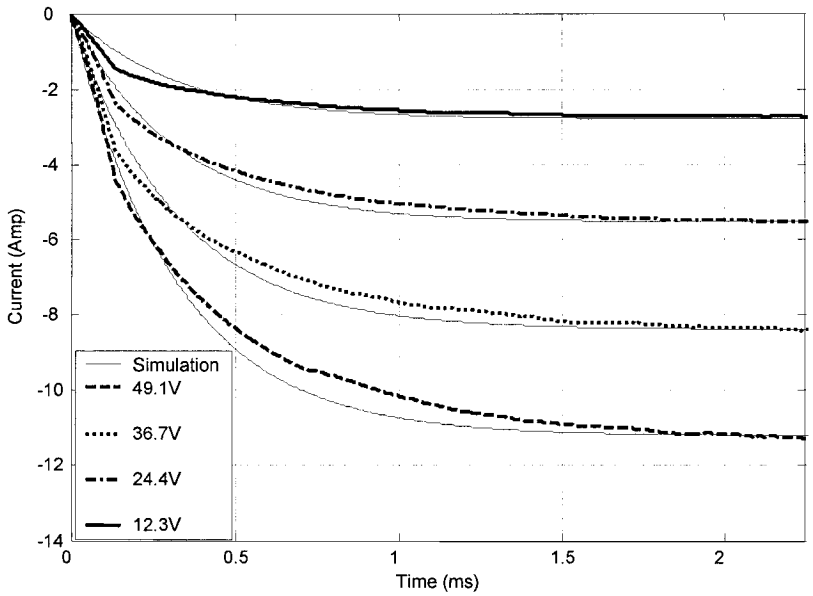

Fig.5.21 Experimental vs. simulation results of Current response in opposite direction (Traveling position 5mm)

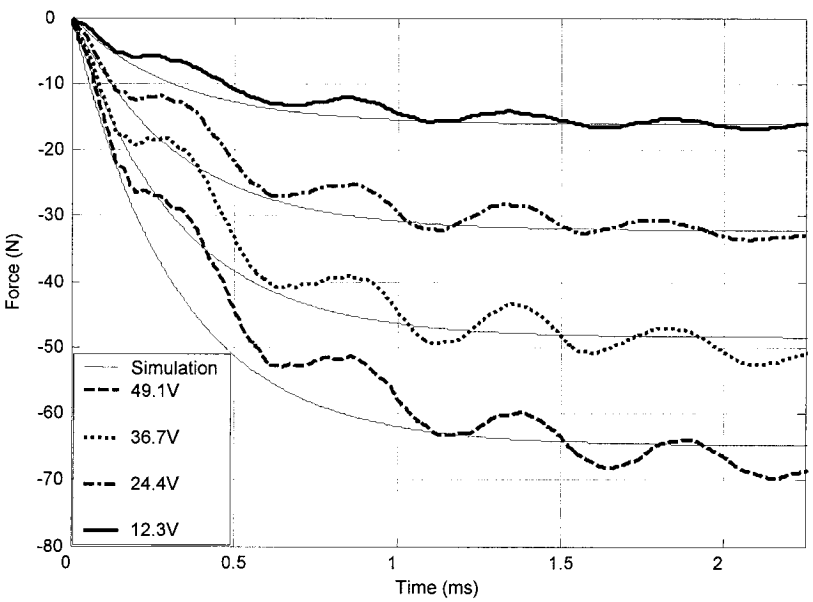

Fig.5.22 Experimental vs. simulation results of Force response in opposite direction (Traveling position 5mm)

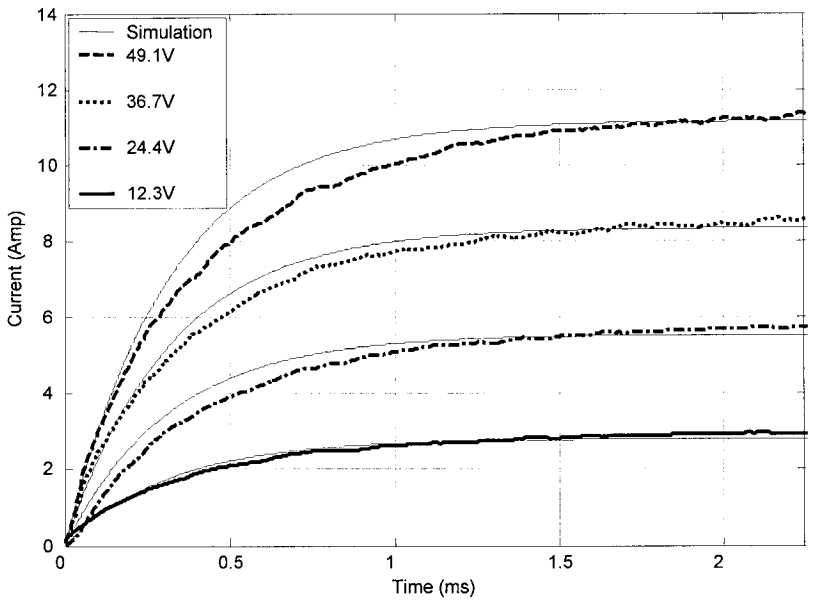

Fig.5.23 Experimental vs. simulation results of Current response

(Traveling position 6mm)

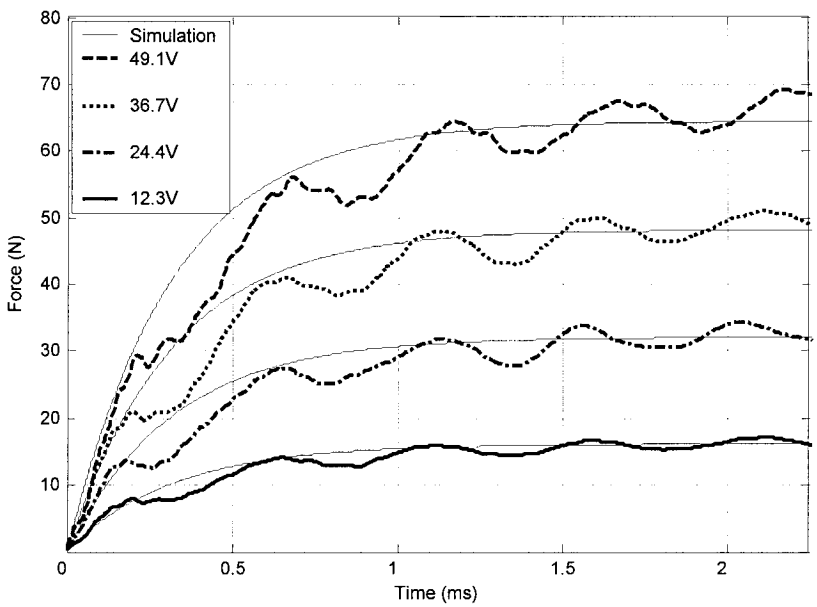

Fig.5.24 Experimental vs. simulation results of Force response

(Traveling position 6mm)

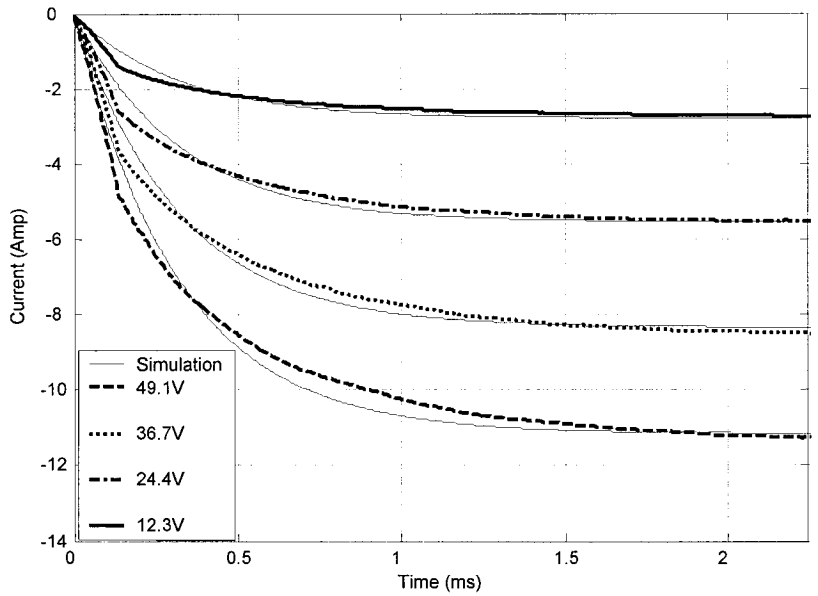

Fig.5.25 Experimental vs. simulation results of Current response in opposite direction (Traveling position 6mm)

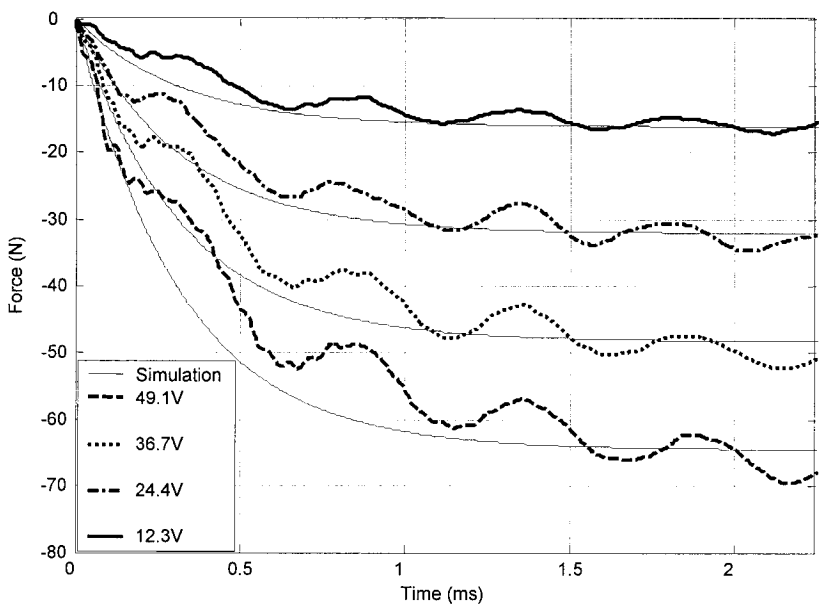

Fig.5.26 Experimental vs. simulation results of Force response in opposite direction (Traveling position 6mm)

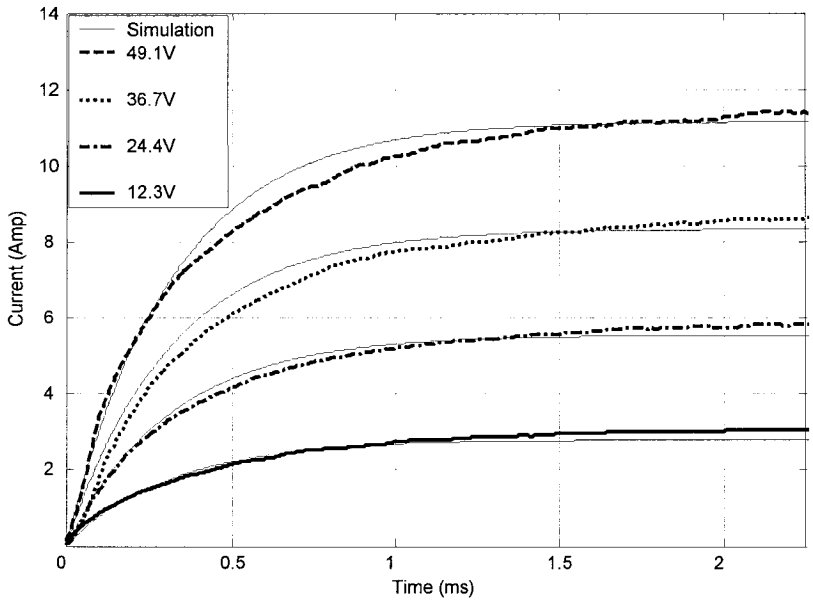

Fig.5.27 Experimental vs. simulation results of Current response

(Traveling position 8mm)

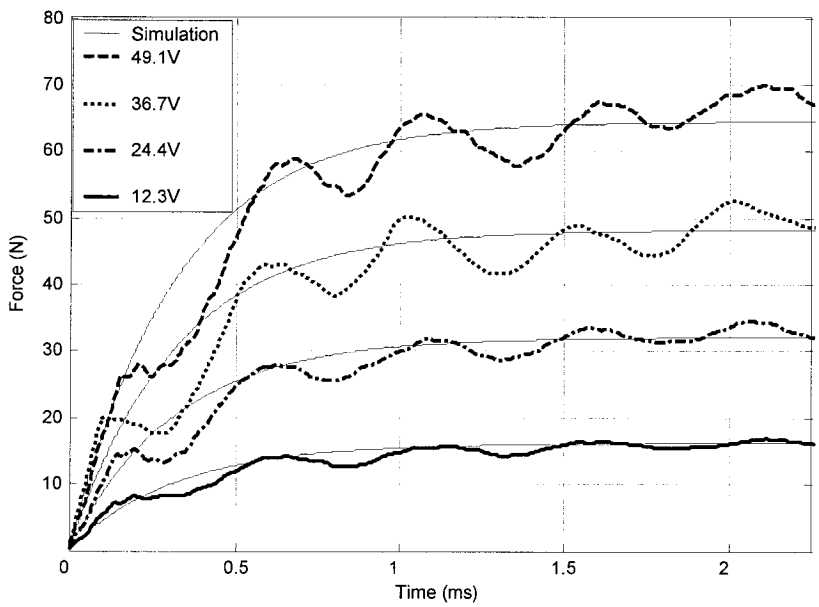

Fig.5.28 Experimental vs. simulation results of Force response

(Traveling position 8mm)

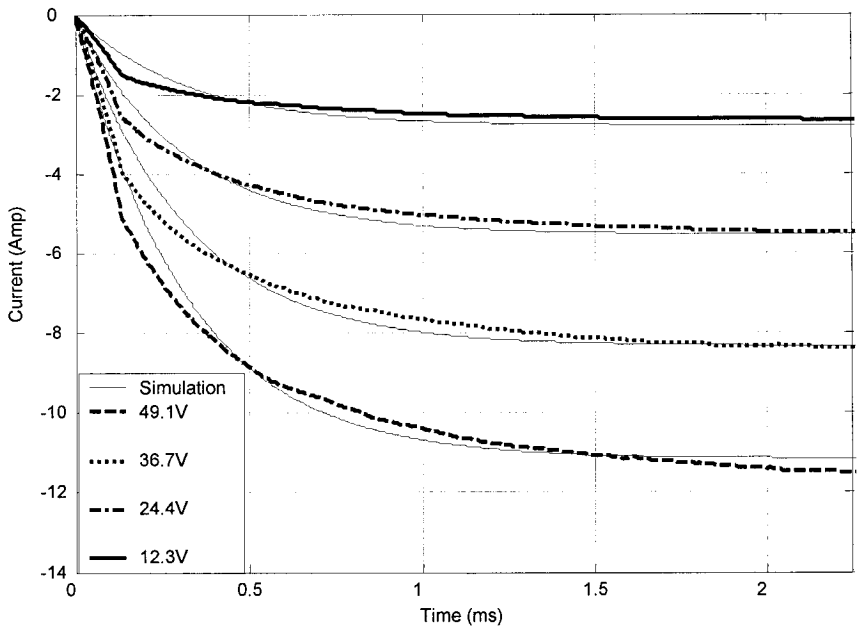

Fig.5.29 Experimental vs. simulation results of Current response in opposite direction (Traveling position 8mm)

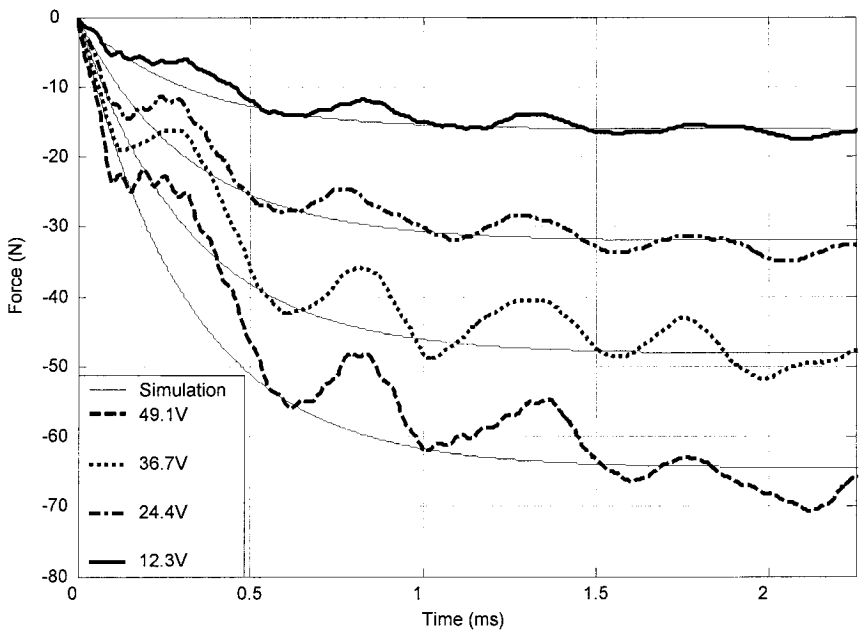

Fig.5.30 Experimental vs. simulation results of Force response in opposite direction (Traveling position 8mm)

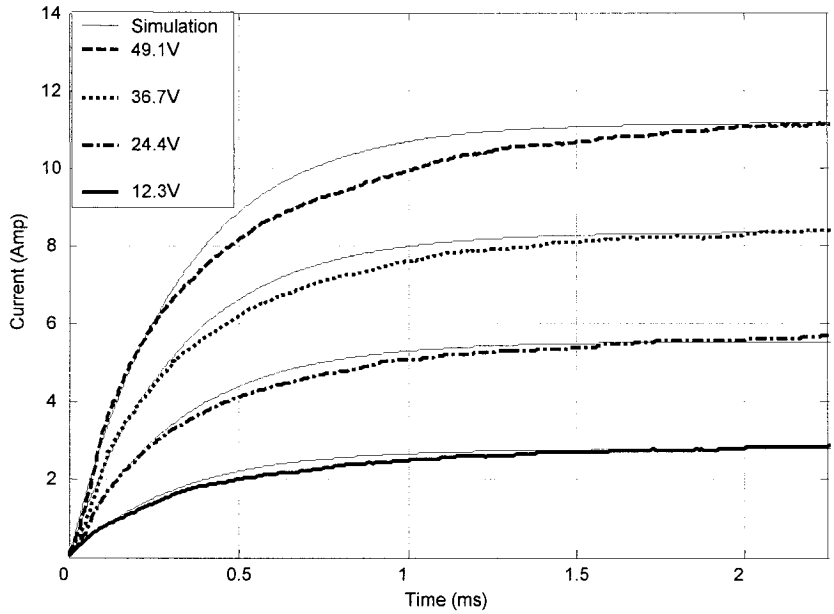

Fig.5.31 Experimental vs. simulation results of Current response

(Traveling position 10mm)

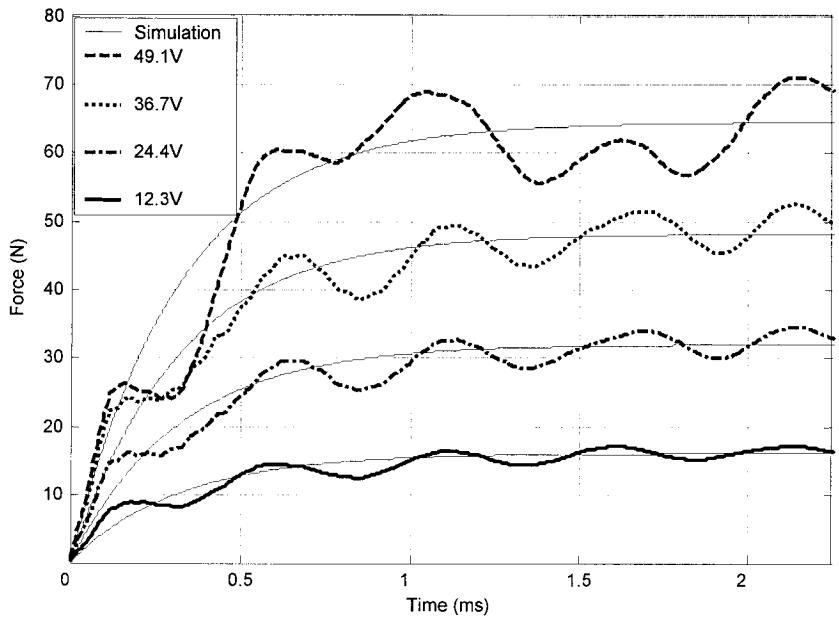

Fig.5.32 Experimental vs. simulation results of Force response

(Traveling position 10mm)

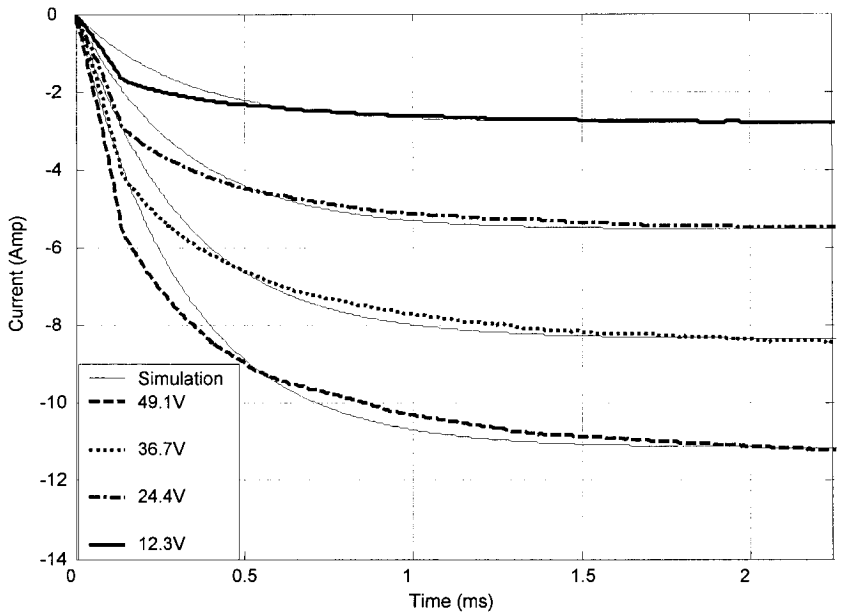

Fig.5.33 Experimental vs. simulation results of Current response in opposite direction (Traveling position 10mm)

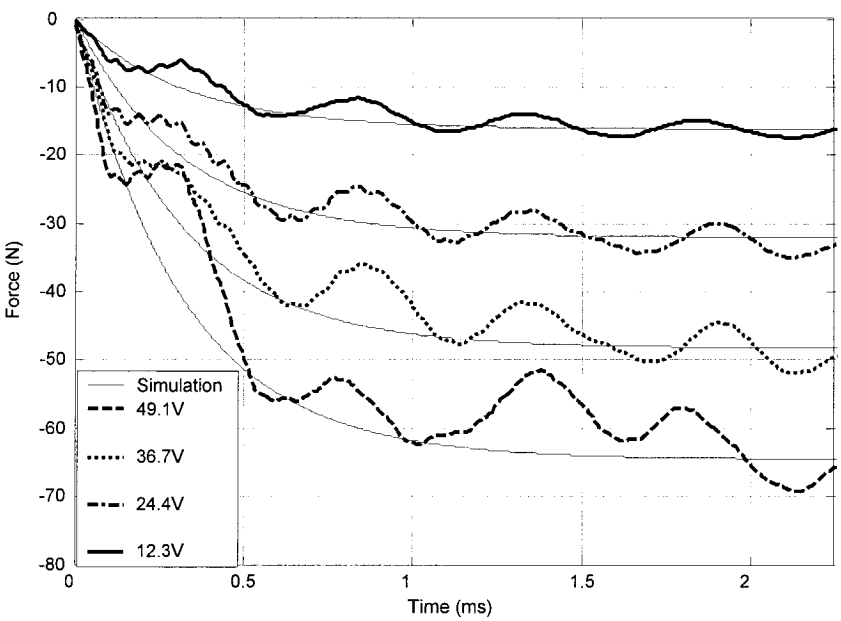

Fig.5.34 Experimental vs. simulation results of Force response in opposite direction (Traveling position 10mm)

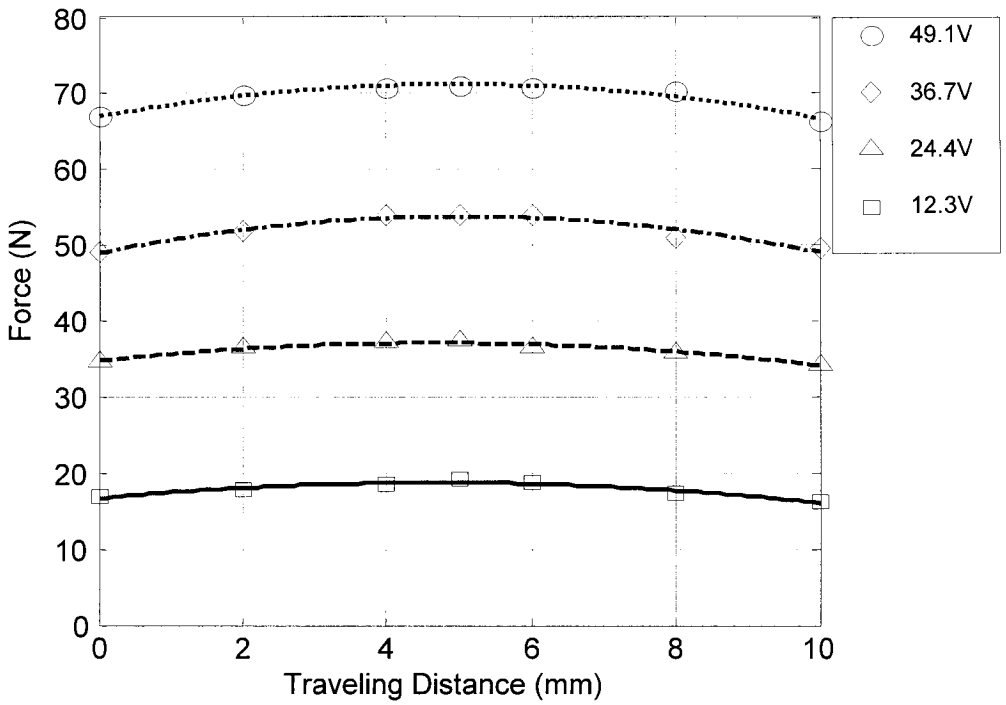

Fig.5.35 Experimental average steady state force vs. traveling distance

CHAPTER 6

CONCLUSIONS AND RECOMMENDATIONS

6.1 Conclusions

A mathematical model of a voice coil actuator (VCA), a switched pulse width modulated (PWM) controller, and the closed-loop stability analysis of a discrete-time model of a VCA spark ignition (SI) engine valve system have been developed in this thesis. This research work has shown that a VCA is an ideal electromechanical device to control the intake and exhaust valves of a camless SI engine. To achieve a faster VCA transient response, the theoretical current and force response characteristics of a VCA for applied voltages above the nominal value must be obtained and these were validated by experiments. The theoretical predictions of the ability to generate bi-directional forces and of the very small force degradation at the extreme traveling ends of a VCA are also validated by the experiments. The literature review has shown that a bi-directional actuator, such as the one described in this thesis, had not been previously used to control the inlet and exhaust valves of an SI engine.

Furthermore, a mathematical model was developed for a VCA valve system with a feedback closed-loop controller to achieve stringent performance requirements for small contact velocity with very fast transient response. A lead compensator can be designed to achieve the desired transient performance of a VCA valve system. However, the magnitude of the output control signal from the lead compensator was 25000V, which is neither feasible nor acceptable in a practical application. Therefore, in this thesis a

novel switched PWM controller preceded by a lead compensator was proposed to control the VCA valve system that can achieve the desired performance requirements while maintaining the amplitude of the control signal output within an acceptable range. In the proposed control strategy the lead compensator is used to improve the system transient response and the PWM controller is used to maintain the control signal output within the desired bounds. The proposed PWM controller consists of two different PWM signal generators that can be activated independently for transient and steady-state response. A 100V PWM signal is used to create high acceleration for fast system transient whereas a 5V PWM signal is used to reduce and keep the contact velocity between the valve and valve seat within an acceptable range. The 5V PWM signal also reduces the power consumption and ripple amplitude in steady-state. The fact that the VCA system does not require much power to hold the engine valve in a certain position is taken in to consideration in the design of this low amplitude PWM signal. The system achieved a simulation performance of contact velocity equal to 0.02 m/sec with a transition time of 5 ms. The simulation results also show that unthrottled camless operation is possible using a VCA in a variable valve timing (VVT) system.

Various control schemes of the electromechanical valve actuator have been proposed in previous research, however stability is often neglected due to the bounded motion of the actuator. In this thesis, the Lyapunov direct method was applied to establish a stability result for a discrete-time model of the PWM feedback system with a linear VCA plant based on PWA control theory. By application of the stability analysis method used in this thesis, one can obtain a sufficient condition for the stability of the discrete-time model of the PWM feedback VCA system. The stability analysis of the discrete-time

model of the PWM VCA system is proved using a relaxation method together with piecewise-quadratic Lyapunov functions whose parameters were computed as the solution of a set of linear matrix inequalities (LMIs).

The mathematical model of the VCA has been simulated and overplotted with the experimental results to determine its current and force characteristics at various travel positions. A prototype experimental setup has been designed and built to measure the current and force response of the VCA. Experiments performed on the prototype confirmed the theoretical current and force characteristics and the capability of the bi-directional motion of the VCA. The major deviation between test and simulation results occurs during steady-state caused by the force fluctuation for the high voltage input signal. A high voltage PWM signal, above the specified nominal value of the VCA, is used in the control system design to achieve a very fast transient response. The experiments proved that the high voltage spike applied for a very short duration does not burn the VCA but results in a much higher force generated as compared to the rated maximum force of the VCA at the nominal applied voltage.

In reality, the effects of VVT on an engine are very much dependent on the type of actuator used. Mechanical valve mechanisms are very complicated in design and true variable valve timing has not been achieved by this technique. Electromechanical valve actuation is the proper solution to achieve this goal. The development of true variable valve timing by electromechanical valve actuation will give unique opportunities to get maximum benefits from VVT on an actual engine and to confirm an unthrottled VVT engine for further engine advancement and development.

With the implementation of proper design and control techniques, it can be expected that the proposed VCA valve actuating mechanism can achieve near-zero pumping losses, maximum volumetric efficiency, and reduced exhaust pollutions from an unthrottled VVT engine.

6.2 Recommendations for Future Work

The results of this thesis can be extended and enhanced in several ways. These include:

Improvements of the Mathematical Model

Forces acting on the valve due to the gases should be considered and included in the mathematical model. Hysteresis should also be included.

Improvements of the Experimental setup

1) Analysis of the hysteresis of a VCA.

The hysteresis was not considered in the mathematical modeling of this research because the hysteresis was considered as negligible for a VCA (as stated from the specifications of the manufacturer). However, the hysteresis characteristics should be validated so as to determine an optimal controller for position control if necessary, if such a hysteresis phenomenon is of significance. To study the hysteresis phenomenon, therefore, a bi-directional electric driving circuit is required to be built to activate the VCA.

2) Experimental validation for pulse width modulated voltage of 100V amplitude.

A ±100V PWM driving circuit is required to be built to implement the novel control strategy of the voice coil actuated engine valve system. An excessive voltage input will generate more heat and reduce performance of the voice coil actuator, or it may even burn the coil of the VCA. A high voltage step input with 49.1V was already applied without any problem in the experiment of this thesis and the experimental result was well matched with the theory. However, further experiments are necessary to verify that applying a 100V PWM input to the present voice coil actuated engine valve system is feasible; otherwise another VCA size may need to be selected.

In addition, experiments should be performed with PWM voltages beyond 100V because the present controller design is for a SI engine operating at 3000 rpm. This is because some SI engines can operate beyond the red-line to 6000 rpm.

3) Power supply design for the high voltage PWM circuit.

Several batteries are used in series to generate the different voltages applied in the experiment. A suitable power supply unit with variable output should be used in the experiment for a high voltage PWM input so as to have the experiments more standardized with minimal effects from the voltage source (such as possible power supply voltage drop due to load).

4) Prototype for the voice coil actuated valve system.

A voice coil actuated engine valve prototype should be designed and manufactured for a benchmark experiment to confirm the expected results and adjust

design parameters. A new electronic circuit driven by a computer program should be designed to implement the PWM feedback controller.

5) Validation of the PWM control strategy in a voice coil actuated valve system.

Further experiments are necessary to validate the theory of the novel control strategy with two different PWM voltages for a voice coil actuated engine valve system. The experiments including a load cell should validate the simulation achievement of soft landing and very fast transient response of the voice coil actuated valve system.

6) Integrate the methods in the VCA system to be used with an engine.

The crankshaft angular position should be considered to confirm and to validate the desired position of the engine valve. The engine speed must be taken in consideration to calculate the desired overlap period between the intake and exhaust valves.

REFERENCES

1. Khandaker, M. F., Hong, H. and Rodrigues, L., " Modeling and Controller Design for a Voice Coil Actuated Engine Valve", *Proceedings of 2005 IEEE Conference on Control Application*, pp. 1234 - 1239, 28 – 31 August 2005.

2. Wang, Y. Stefanopoulou A., Haghgooie, M., Kolmanovsky, I. and Hammoud, M., "Modeling of an Electromechanical Valve Actuator for a Camless Engine", *5th International Symposium on Advanced Vehicle Control*, Ann Arbor, Michigan USA, 2000.

3. Parvate-Patil, G. B., Hong, H. and Gordon, B. W., " An Assessment of Intake and Exhaust Valve Strategies for Variable Valve Timing", 2003-32-0078, SAE Transactions, Journal of Engines, Sec.3, Vol. 112, pp.2174-2190, 2003.

4. Pierik, R. J. and Burkhard, J. F., "Design and Development of a Mechanical Variable Valve Actuation System", SAE 2000 World Congress, Detroit, Michigan, SAE paper no. 2000-01-1221, March 6-9, 2000.

5. Peterson, K.S., Stefanopoulou, A.G., Megli, T. and Haghgooie, M., "Output Observer Based Feedback for Soft Landing of Electromechanical Camless Valvetrain Actuator", *Proceedings of 2002 American Control Conference*, pp. 1413-1418, May 2002.

6. http://www.keveney.com/otto.html, "Animated four stroke (Otto) engine".

7. Peterson, K.S. and Stefanopoulou, A.G., "Rendering the Electromechanical Valve

Actuator Globally Asymptotically Stable", Proceedings of *IEEE Conference on Decision and Control*, 2003.

8. H. Hong., "Optimum Performance of Solenoid Injectors for Direct Injection of Gaseous Fuels in IC Engine", Ph.D. Thesis, Concordia University, 1995.

9. Peterson, K.S., Wang, Y., Stefanopoulou A. and Megli, T., "Virtual Lash Adjuster for an Electromechanical Valve Actuator Through Iterative Learning Control" *Proceedings of 2002 ASME International Mechanical Engineering Congress"*, IMECE2003-41270, November 15-21, 2003.

10. Tuttle, J.H., "Controlling Engine Load by Means of Late Intake-Valve Closing", SAE paper no. 800794, 1980.

11. Sunders, R.J. and Abdual-Wahab, E.A., "Variable Valve Closure Timing for Load Control and the Otto Atkinson Cycle Engine", *SAE paper* no. 890677, 1989.

12. Blakey, S.C., Foss, P.W., Basset, M.D. and Yates, P.W., "Improved Automotive Part Load Fuel Economy Through Late Intake Valve Closing", *XIV proceedings of Internal Combustion Engine and Combustion,* India, 1995.

13. Tuttle, J.H., "Controlling Engine Load by Means of Early Intake-Valve Closing", *SAE* paper no. 820408, 1982.

14. Hong, H., Parvate-Patil and Gordon, B. W., "Review and Analysis of Variable Valve Timing Strategies- Eight Ways to Approach", *IMechE*, Journal of Automobile Engineering, Part D, Vol. 218, No. 10, pp. 1179-1200, 2004.

15. Stubbs, A., "*Modeling and Controller Design of an Electromagnetic Engine Valve*", M.S. Thesis, University of Illinois at Urbana-Champaign, 2000.

16. Wang, Y., Stefanopoulou, A., Peterson, K., Megli, T. and Haghgooie, M., "Modeling and Control of Electromechanical Valve Actuator", *SAE Paper* No. 2002-01-1106, 2002.

17. Butzmann, S., Melbert, J. and Koch, A., "Sensorless Control of Electromagnetic Actuators for Variable Valve Train," *SAE Paper* No. 2000-01-1225, 2000.

18. Chun, T., and Tsao, T., "Quiet Seating Control Design of an Electromagnetic Engine Valve Actuator", *ASME International Mechanical Engineering Congress and Exposition*, Paper No. IMECF 2001/DSC-24520, 2001.

19. Morcos, A., "Voice Coil Actuators For Use in Motion Control Systems", *Motion Magazine*, Fall 1998.

20. "Voice Coil Actuators", *Application Guide, BEI Kimco Magnetics Division*, BEI Technologies, Inc.

21. "Electromechanical Actuators", *Design Manual, Densitron Technologies* plc.

22. Nuez, I. and Feliu, V., "On the Voltage Pulse-Width Modulation Control of L-C Filters", *IEEE Transactions on Circuits and Systems*, Vol. 47, No. 3, March 2000.

23. Liberzon, D. and Morse. A.S., "Basic Problems in Stability and Design of Switched Systems", *IEEE Control Systems Magazine*, Vol.19, No. 5, pp 59-70, 1999.

24. Skoog, R., "On the Stability of Pulse-Width-Modulated Feedback Systems", *IEEE Transactions on Automatic Control*, Vol. AC-13, No. 5, pp. 532–538, October 1968.

25. Taylor D., "Pulse Width Modulated Control of Electromechanical Systems", *IEEE Transactions on Automatic Control*, Vol. 37, No. 4, pp. 524–528, April 1992.

26. Peterson, K., Stefanopoulou, A., Wang, Y. and Haghgooie, M., "Nonlinear Self-Tuning Control for Soft Landing of an Electromechanical Valve Actuator", *IFAC Mechatronics Conference*, pp. 207-212, Nov. 2002.

27. Hoffmann, W., Peterson, S. and Stefanopoulou, A., "Iterative Learning Control of Electromechanical Camless Valve Actuator in Camless Engine," *IEEE Transactions on Control System Technology*, Vol. 11, No. 2, pp. 174-184, March 2003.

28. Chun, T., and Tsao, T., "Control of an Electromechanical Actuator for Camless Engines", *Proceedings of the American Control Conference, Denver, Colorado, June 4-6, 2003.*

29. http://auto.howstuffworks.com/question229.htm, "What does the VTEC system in a Honda engine do?"

30. http://auto.howstuffworks.com/camshaft6.htm, "Variable Valve Timing."

31. Badami, M., Marzano, M.R. and Nuccio, P., "Influence of Late Intake-Valve

Opening on the S.I. Engine-Performance in Idle Condition", *SAE* paper no. 960586, 1996.

32. Siewert, R.M., "How Individual Valve Timing Events Affect Exhaust Emissions", *SAE* paper no. 710609, 1971.

33. Hara, S., Nakajima, Y. and Naguma, S., "Effects of Intake-Valve Closing Timing on Spark-Ignition Engine Combustion", *SAE* paper no. 850074, 1985.

34. Law, D., Kemp, D., Allen, J., Kirkpatrick. G. and Copland, T., "Controlled Combustion in an IC-Engine with a Fully Variable Valve Train", *SAE* paper no 2000-01-0251, 2000.

35. Asmus, T.W., "Valve Events and Engine Operation", SAE paper no. 820749, 1982.

36. Stein, R.A., Galietti, K.M., and Leone, T.G., "Dual Equal VCT- A Variable Camshaft Timing Strategy for Improved Fuel economy and Emissions", *SAE* paper no. 950975, 1995.

37. Wang, Y., Stefanopoulou, A. and Smith, R. "Inherent Limitations and Control Design for Camless Engine Idle Speed Dynamics", International Journal of Robust and Nonlinear Control, Vol. 11, pp. 1023-1042, 2001.

38. Parker, P. H., "The VVT Mechanism for the Rover K16 Engine, Part 2: Application to the Engine and the Performance Obtained", *IMechE, Journal of Automobile Engineering*, Part D, Vol. 214, No. 2, pp. 207-216, February 21, 2000.

39. Stefanopoulou, A., Freudenberg, J. - S. and Grizzle, J. W., "Variable Camshaft Timing Engine Control", IEEE Transaction on Control Systems Technology, Vol. 8, No. 1, January 2000.

40. Chladny, R., Koch, C. R. and Lynch, A. F., "Modeling Automotive Gas-Exchange Solenoid Valve Actuators", IEEE transactions on Magnetics, Vol. 41, No. 3, March 2005.

41. Genc, A. U., Glover, K. and Ford, R., "Nonlinear Control of Hydraulic Camshaft Actuators in Variable Cam Timing Engines", International workshop on Modeling, Emissions and Control in Automotive Engines, MECA '01, University of Salerno, Italy, September 9-10, 2001.

42. He, D., "Permanent Magnet Plunger Bi-Directional Solenoid Actuator for Direct Alternative Fuel Injector" M.A.Sc. thesis, Concordia University at Montreal, Quebec 2005.

43. Patil, G. P., "Solenoid Operated Variable Valve Timing for Internal Combustion Engines" M.A.Sc. thesis, Concordia University at Montreal, Quebec 2005.

44. Hong, H., Krepec, T., and Cheng, R. - M. - H., "Transient Response of Fast Acting Solenoid in Automotive Applications", Journal of Circuits, Systems, and Computers, Vol.4, No. 4, pp. 415-428, 1994.

45. Johansson, M. and Rantzer, A., "Computation of Piecewise Quadratic Lyapunov Functions for Hybrid Systems.", *IEEE Transactions on Automatic Control,* Vol. 43 No. 4, pp. 555-559, April 1998.

46. Almer, S., Jonsson, U., Kao, C-Y., and Mari, J., "Global Stability Analysis of DC-DC Converters Using Sampled-Data Modeling", *Proceedings of the 2004 American Control Conference, Boston, Massachusetts, June 30 – July 2, 2004.*

47. Branicky, M. S., "Multiple Lyapunov Functions and other Analysis Tools for Switched and Hybrid Systems.", *IEEE Transactions on Automatic Control,* Vol. 43, No. 4, pp. 475-482, April 1998.

48. Qiu, Y. H., Parlikar, T. A., Chang, W. S., Seeman, M. D., Keim, T. A., Perreault, D. J. and Kassakian, J. G., "Design and Experimental Evaluation of An Electromechanical Engine Valve Drive", *Proceedings of 2004 35th Annual IEEE Power Electronics Specialists Conference,* Aachen, Germany, 2004, pp. 4838-4843.

49. Tai, C., Stubbs, A. and Tsao, T. C., "Modeling and Controller Design of an Electromagnetic Engine Valve", *Proceedings of 2001 IEEE American Control Conference,* USA, June 25-27, 2001, pp. 2890-2894.

50. Shaver, G. M., Gerdes, J. C., Jain, P., Caton, P. A. and Edwards, C. F., "Modeling for Control of HCCI Engines", *Proceedings of the American Control Conference, Denver, Colorado, June 4-6, 2003, pp.749-754.*

51. Henry, R. R., "Single-Cylinder Engine Tests of a Motor-Driven, Variable-Valve Actuator", *SAE paper no. 2001-01-0241, SAE 2001 World Congress, Detroit, Michigan, March 5-8, 2001.*

52. Rodrigues, L., "Dynamic Output Feedback Controller Synthesis For Piecewise-

Affine Systems". Ph.D. thesis, Stanford University, 2002.

53. http://mathworld.wolfram.com/Polyhedron.html, "Polyhedron".

54. Johansson, M., "Piecewise Linear Control Systems", Springer, Verlag, 2003.

55. http://control.ee.ethz.ch/~joloef/yalmip.php.

56. http://sedumi.mcmaster.ca/.

57. Boyd, E. F. S., Ghaoui, L. E. and Balakrishnan, V., "Linear Matrix Inequalities in System and Control Theory (Studies in Applied Mathematics). Philadelphia: SIAM 1994.

58. Palit, S., "Principles of Electricity and Magnetism" Harrow, Middlesex: Alpha Science International, c2005, ISBN 1842652052.

59. Pande, M., "Voltage Controlled Pulse Width Modulation Pattern Generators for Static Power Converters", M.A.Sc. Thesis, Dept. of Electrical and Computer Engineering, Concordia University, 1993.

60. Mangat, S., "A Modified Asymmetrical Pulse-width Modulated Series Resonant DC/DC Converter", M.A.Sc. Thesis, Dept. of Electrical and Computer Engineering, Concordia University, 2000.

61. Delfeld, F.R. and Murphy, G., "Analysis of Pulse-width-modulated Control Systems", *IRE Trans. Automatic Control,* vol. AC-6, pp. 283-292, September 1961.

APPENDIX-I

Design of a Lead compensator for voice coil actuated valve system.

The desired overall system performance is required to meet the specifications:

4. Rise time < 5 ms
5. Settling time ≤ 5 ms
6. Overshoot ≤ 5%

The open loop uncompensated transfer function of the VCA system is,

$$G(s)H(s) = \frac{69765}{s(s^2 + 3941s + 1240416)} = \frac{69765}{s(s+345)(s+3596)}$$

The specifications of the system are

Percent Overshoot, $\text{P.O.} = 100 \times e^{\frac{-\pi\xi}{\sqrt{1-\xi^2}}} < 5\%$

$$\therefore -\frac{\pi\xi}{\sqrt{1-\xi^2}} = \ln\frac{5}{100} = -2.996 \qquad \therefore \xi > 0.6901 \approx 0.70$$

The settling time, T_s = 5 ms = 0.005 sec. Therefore, $\xi\omega_n = \frac{4}{T_s} = \frac{4}{0.005} = 800$

So the required system phase margin is, $\varphi_m = \frac{\xi}{0.01} = \frac{0.70}{0.01} = 70^0$

The Root Locus of the uncompensated system is shown in fig.A-I.1.

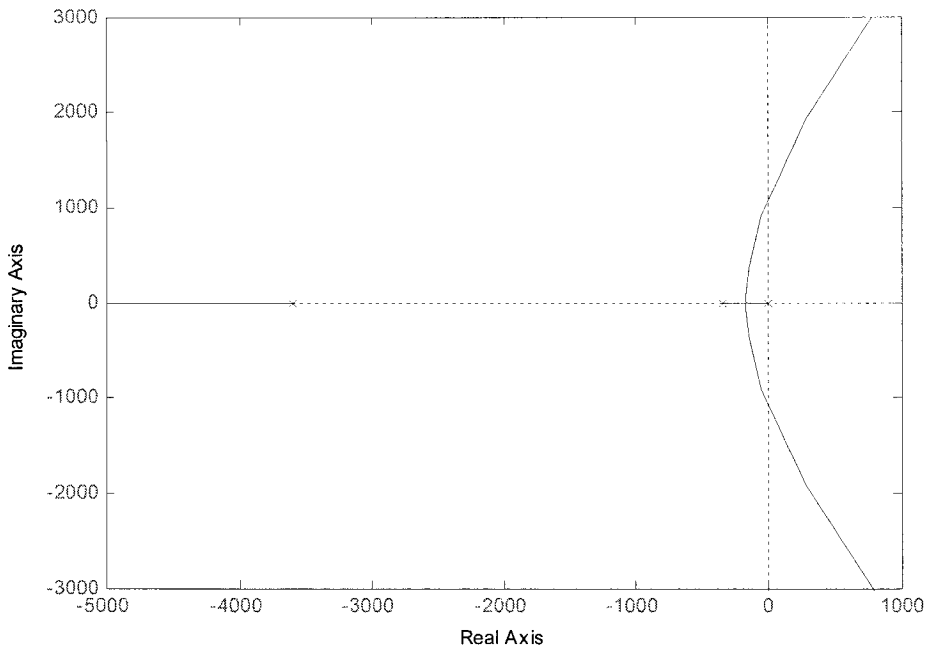

Fig.A-I.1 Root locus of the uncompensated VCA system

To achieve the rapid settling time, select the real part of the desired roots as $\xi\omega_n = 800$.

$\therefore$ The natural frequency $\omega_n = \dfrac{800}{0.70} = 1142.86$ i.e. $\omega_d = \omega_n\sqrt{1-\xi^2} = 816$

and $\cos\theta = 54.5^0$

Now place the zero of the compensator at $s = -800$, directly below the desired root location.

So the desired compensator for VCA system is $G_C(s) = \dfrac{K(s+800)}{(s+p)}$

The compensated transfer function for the system is

$$\therefore G(s)G_C(s) = \frac{69765}{s(s+345)(s+3596)} \times \frac{K(s+800)}{(s+p)}$$

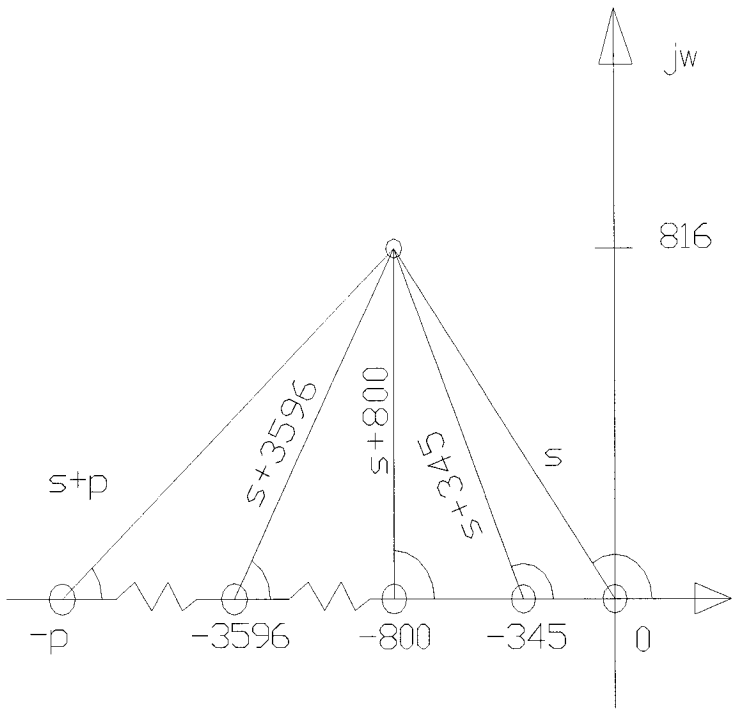

Fig.A-I.2 Lead compensator design of the voice coil actuated valve system

From fig.A-I.2, using the angle requirement determines the desired root location as,

$$90^0 - [180 - \tan^{-1}(\frac{816}{800})] - [180 - \tan^{-1}(\frac{816}{800-345}) - \tan^{-1}(\frac{816}{3596-800}) - \theta_p = 180^0$$

$$\Rightarrow 90^0 - 134.4^0 - 119^0 - 15.4^0 - \theta_p = 180^0 \quad \Rightarrow \theta_p = -358.84^0 = 1.16^0$$

Therefore, to achieve a total of 180^0 at the desired root the angle from the undetermined pole, $\theta_p = 1.16^0$

Therefore, the pole location is, $p = \frac{816}{\tan 1.16^0} + 800 = 40863$

Thus the lead compensator and the compensated transfer function for the system are

$$\therefore G_c(s) = \frac{K(s+800)}{(s+40863)} \quad \text{and} \quad G(s)G_c(s) = \frac{69765K(s+400)}{s(s+345)(s+3596)(s+40863)}$$

From the magnitude requirement, the gain K is evaluated by measuring the vector lengths from the poles and zeros to the root location. Hence

$$| G(s)G_c(s) |_{s=-800+816j} = 1$$

$$\Rightarrow \left| \frac{69765K(s+800)}{s(s+345)(s+3596)(s+40863)} \right|_{s=-800+816j} = 1$$

$$K = \frac{1142.8 \times (941.7) \times (2919) \times (40072)}{(69765) \times (816)} = 2211193$$

Therefore the cascade lead compensator is

$$G_c(s) = \frac{2211193\ (s+800)}{(s+40863)}$$

The overall system transfer function for the feedback VCA system is

$$G_0(s) = \frac{G(s)C(s)}{1+G(s)C(s)} = \frac{\frac{69765}{s(s+345)(s+3596)} \times \frac{2211193(s+800)}{(s+40863)}}{1+\frac{69765}{s(s+345)(s+3596)} \times \frac{2211193(s+800)}{(s+40863)}}$$

$$= \frac{69765 \times 2211193(s+800)}{s(s+345)(s+3596)(s+40863) + 69765 \times 2211193(s+800)}$$

$$\therefore G_o(s) = \frac{69765 \times 2211193 \quad (s + 800)}{s^4 + 44804 \quad s^3 + 162281703 \quad s^2 + p \times s + q}$$

Where, p=(146943348×345+69765×2211193) and q=69765×2211193×800

The Root Locus of the compensated system is shown in fig.A-I.2.

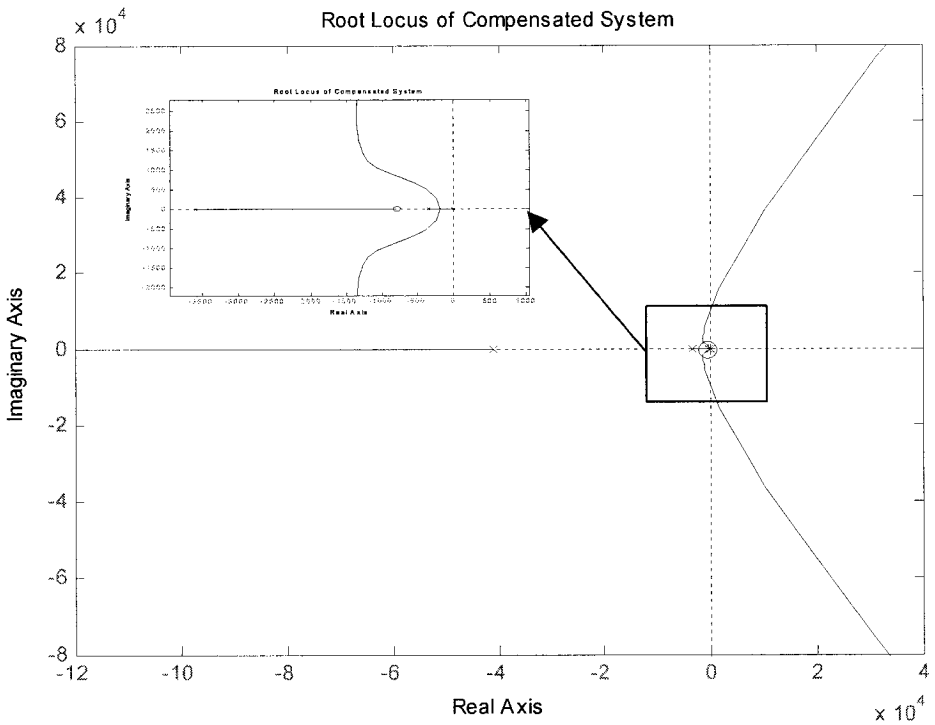

Fig.A-I.3 Root locus of the compensated VCA system

APPENDIX-II

S – function used in PWM Controller

```
% Below is the M-file code for the SfunPWM.m S-function.
function [sys,x0,str,ts] = sfunpwm(t,x,u,flag)
% Dispatch the flag. The switch function controls the calls to
% S-function routines at each simulation stage.
switch flag,
  case 0
    [sys,x0,str,ts] = mdlInitializeSizes; % Initialization
  case 3
    sys = mdlOutputs(t,x,u); % Calculate outputs
  case { 1, 2, 4, 9 }
    sys = []; % Unused flags
  otherwise
    error(['Unhandled flag = ',num2str(flag)]); % Error handling
end;
% End of function sfunpwm.

%Below are the S-function subroutines that sfunpwm.m calls.
%=============================================================
% Function mdlInitializeSizes initializes the states, sample
% times, state ordering strings (str), and sizes structure.
%=============================================================
```

```
function [sys,x0,str,ts] = mdlInitializeSizes

% Call function simsizes to create the sizes structure.

sizes = simsizes;

% Load the sizes structure with the initialization information.

sizes.NumContStates= 0;

sizes.NumDiscStates= 0;

sizes.NumOutputs=    1;

sizes.NumInputs=     1;

sizes.DirFeedthrough=1;

sizes.NumSampleTimes=1;

% Load the sys vector with the sizes information.

sys = simsizes(sizes);

x0 = []; % No continuous states

str = []; % No state ordering

ts = [0.00004 0]; % Inherited sample time

% End of mdlInitializeSizes.

%=============================================================================

% Function mdlOutputs performs the calculations.

%=============================================================================

function sys = mdlOutputs(t,x,u)

period1 = 0.0001;

period=0.001;

dutycyclemax=(period1/100)*95;
```

```
dutycycle=(period/100)*95*abs(u)*100;

if (dutycycle > period)
      dutycycle = period;
   elseif (dutycycle <= period)
      dutycycle = dutycycle;
end
if (dutycyclemax > 0.95*period1)
     dutycyclemax = 0.95*period1;
   elseif (dutycyclemax <= 0.95*period1)
      dutycyclemax = dutycyclemax;
end
ymax =100;
y=20;
for m=0:period1:0.5
if (t>=(0+m) & t<=(dutycyclemax+m))
   if (u >0)
         sys = ymax;
      elseif (u < 0)
         sys = -ymax;
      else
         sys=0;
      end
   elseif (t>(dutycyclemax+m) & t<(period1+m))
```

```
   sys=0;
   end
end

for a=0.0064:period:10
        if ((t >=(0+a)) & (t<=(dutycycle+a)))
      if (u >0)
         sys = y;
      elseif (u < 0)
         sys = -y;
      else
         sys=0;
      end
      elseif   ((t>(dutycycle+a)) & (t<(period+a)))
      sys = 0;
      end
end
```

APPENDIX-III

The MATLAB program for stability analysis using YALMIP and SeDuMi is given as follows:

```
%Piece Wise Quadratic Lyapunov Function With Relaxations
clc;
clear all;
A = [-4.48e+004 -4952 -158.8 -28.06; 3.277e+004 0 0 0; 0 3.277e+004 0 0; 0 0 4096 0];
B = [16; 0; 0; 0];
C=[0 0 8.979 1.754]; D = 0;
T = 0.00001;
U = 100;
beta = 1;
G = beta*T*U*B*C;
Ad = eye(4)+A*T; %Linearization using Taylor series

%For Region 1
A1d = (Ad+G); b1 = [0; 0; 0; 0];
A1d_bar = [A1d b1; zeros(1,4) 1];

%For Region 2
A2d = (Ad+G); b2 = [0; 0; 0; 0];
A2d_bar = [A2d b2; zeros(1,4) 1];
```

```
%For Region 3

A3d = Ad; b3 = T*U*B;

A3d_bar = [A3d b3; zeros(1,4) 1];

%For Region 4

A4d = Ad; b4 = -T*U*B;

A4d_bar = [A4d b4; zeros(1,4) 1];

% Create symmetric matrix (full syntax)

P1 = sdpvar(4,4,'symmetric');

P2 = sdpvar(4,4,'symmetric');

P3 = sdpvar(4,4,'symmetric');

P4 = sdpvar(4,4,'symmetric');

q1 = sdpvar(4,1); r1 = sdpvar(1,1);

q2 = sdpvar(4,1); r2 = sdpvar(1,1);

q3 = sdpvar(4,1); r3 = sdpvar(1,1);

q4 = sdpvar(4,1); r4 = sdpvar(1,1);

P1_bar = [P1 q1; q1' r1];

P2_bar = [P2 q2; q2' r2];

P3_bar = [P3 q3; q3' r3];

P4_bar = [P4 q4; q4' r4];

W1 = sdpvar(2,2,'symmetric');

W2 = sdpvar(2,2,'symmetric');
```

```
W3 = sdpvar(1,1,'symmetric');

W4 = sdpvar(1,1,'symmetric');

H1 = [C; -C];

g1 = [1; 0];

H1_bar = [H1 g1];

H2 = [-C; C];

g2 = [1; 0];

H2_bar = [H2 g2];

H3 = [-C];

g3 = [-1];

H3_bar = [H3 g3];

H4 = [C];

g4 = [-1];

H4_bar = [H4 g4];

F = set('P1_bar>0')+set('P2_bar>0')+set('P3_bar>0')+set('P4_bar>0')

F = F+set('W1>0')+set('W2>0')+set('W3>0')+set('W4>0')

F = F+set('P1_bar-H1_bar"*W1*H1_bar>0')

F = F+set('A2d_bar"*P1_bar*A2d_bar-P2_bar+H1_bar"*W1*H1_bar<0')

F = F+set('A3d_bar"*P1_bar*A3d_bar-P3_bar+H1_bar"*W1*H1_bar<0')
```

```
F = F+set('P2_bar-H2_bar"*W2*H2_bar>0')

F = F+set('A1d_bar"*P2_bar*A1d_bar-P1_bar+H2_bar"*W2*H2_bar<0')

F = F+set('A4d_bar"*P2_bar*A4d_bar-P4_bar+H2_bar"*W2*H2_bar<0')

F = F+set('P3_bar-H3_bar"*W3*H3_bar>0')

F = F+set('A1d_bar"*P3_bar*A1d_bar-P1_bar+H3_bar"*W3*H3_bar<0')

F = F+set('P4_bar-H4_bar"*W4*H4_bar>0')

F = F+set('A2d_bar"*P4_bar*A2d_bar-P2_bar+H4_bar"*W4*H4_bar<0')

solution = solvesdp(F);

P1_feasible = double(P1);

P2_feasible = double(P2);

P3_feasible = double(P3);

P4_feasible = double(P4);

q1_feasible = double(q1);

q2_feasible = double(q2);

q3_feasible = double(q3);

q4_feasible = double(q4);

r1_feasible = double(r1);

r2_feasible = double(r2);

r3_feasible = double(r3);

r4_feasible = double(r4);
```

```
P1_bar_feasible = double(P1_bar);

P2_bar_feasible = double(P2_bar);

P3_bar_feasible = double(P3_bar);

P4_bar_feasible = double(P4_bar);

W1_feasible = double(W1);

W2_feasible = double(W2);

W3_feasible = double(W3);

W4_feasible = double(W4);

P1_bar = eig(P1_bar_feasible)

P2_bar = eig(P2_bar_feasible)

P3_bar = eig(P3_bar_feasible)

P4_bar = eig(P4_bar_feasible)

Eig_09 = eig(P1_bar_feasible-H1_bar'*W1_feasible*H1_bar)

Eig_12 = eig(P2_bar_feasible-H2_bar'*W2_feasible*H2_bar)

Eig_15 = eig(P3_bar_feasible-H3_bar'*W3_feasible*H3_bar)

Eig_17 = eig(P4_bar_feasible-H4_bar'*W4_feasible*H4_bar)

Eig_10=eig(A2d_bar'*P1_bar_feasible*A2d_bar-
                        P2_bar_feasible+H1_bar'*W1_feasible*H1_bar)
Eig_11=eig(A3d_bar'*P1_bar_feasible*A3d_bar-
                        P3_bar_feasible+H1_bar'*W1_feasible*H1_bar)
```

```
Eig_13=eig(A1d_bar'*P2_bar_feasible*A1d_bar-
                    P1_bar_feasible+H2_bar'*W2_feasible*H2_bar)
Eig_14=eig(A4d_bar'*P2_bar_feasible*A4d_bar-
                    P4_bar_feasible+H2_bar'*W2_feasible*H2_bar)

Eig_16=eig(A1d_bar'*P3_bar_feasible*A1d_bar-
                    P1_bar_feasible+H3_bar'*W3_feasible*H3_bar)

Eig_18=eig(A2d_bar'*P4_bar_feasible*A2d_bar-
                    P2_bar_feasible+H4_bar'*W4_feasible*H4_bar)

checkset(F);

% Plot Lyapunov Function

X1 = -5:0.5:5;

Lyap = [];
for i = 1:size(X1,1),
   for j = 1:size(X1,2),
      if X1(i,j)<=-1,
      Lyap(i,j) = [X1(i,j) 0 0 0 0]*P4_bar_feasible*[X1(i,j); 0; 0; 0; 0];
      elseif X1(i,j) > -1 & X1(i,j) < 0,
      Lyap(i,j) = [X1(i,j) 0 0 0 0]*P2_bar_feasible*[X1(i,j); 0; 0; 0; 0];
      elseif X1(i,j) > 0 & X1(i,j) < 1,
      Lyap(i,j) = [X1(i,j) 0 0 0 0]*P1_bar_feasible*[X1(i,j); 0; 0; 0; 0];
```

```
        else  X1(i,j) >= 1,
        Lyap(i,j) = [X1(i,j) 0 0 0 0]*P3_bar_feasible*[X1(i,j); 0; 0; 0; 0];
        end
    end
end

figure(10)
plot(X1,Lyap);

title('Quadratic Lyapunov Function');
xlabel('Position error'); ylabel('Lyapunov Function');
```

APPENDIX-IV

The experimental setup for static force analysis of a VCA is designed using AutoCAD. Total eight parts are designed separately and then assembled all together in a new assembly drawing. All drawings are given from fig.A-IV.1 to fig.A-IV.9.

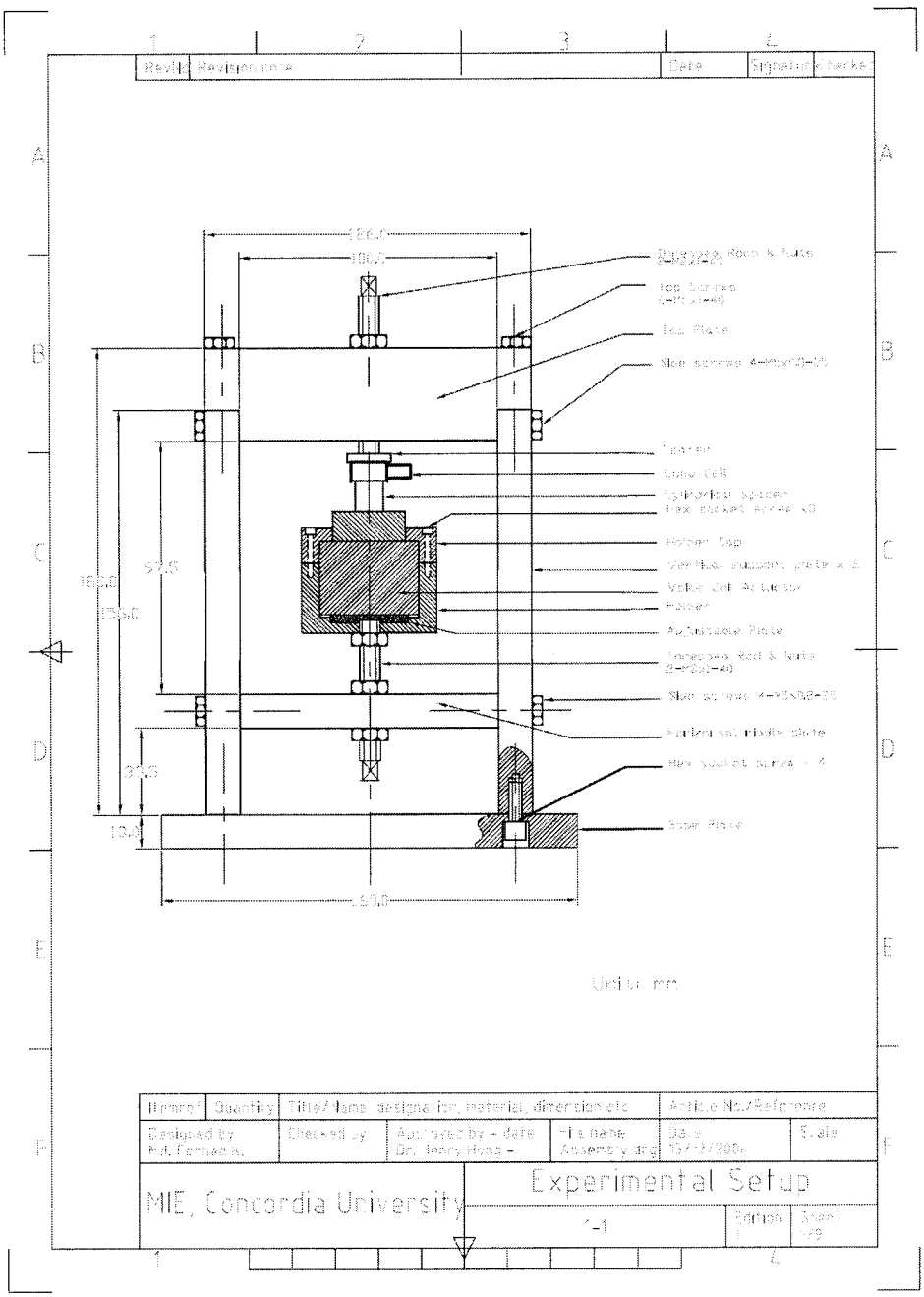

Fig.A-IV.1 Assembly Drawing of the experimental setup

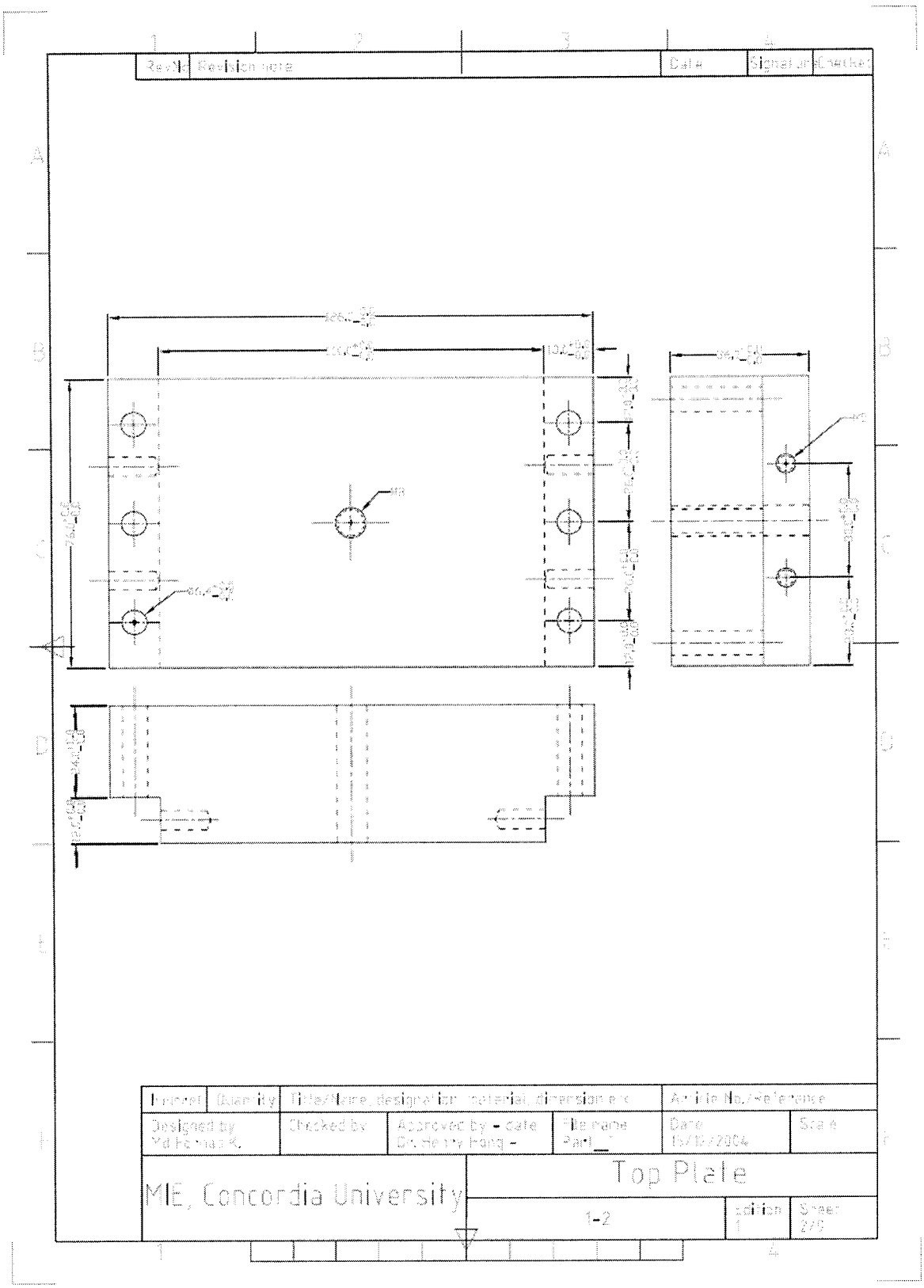

Fig.A-IV.2 Top Plate (Part-1)

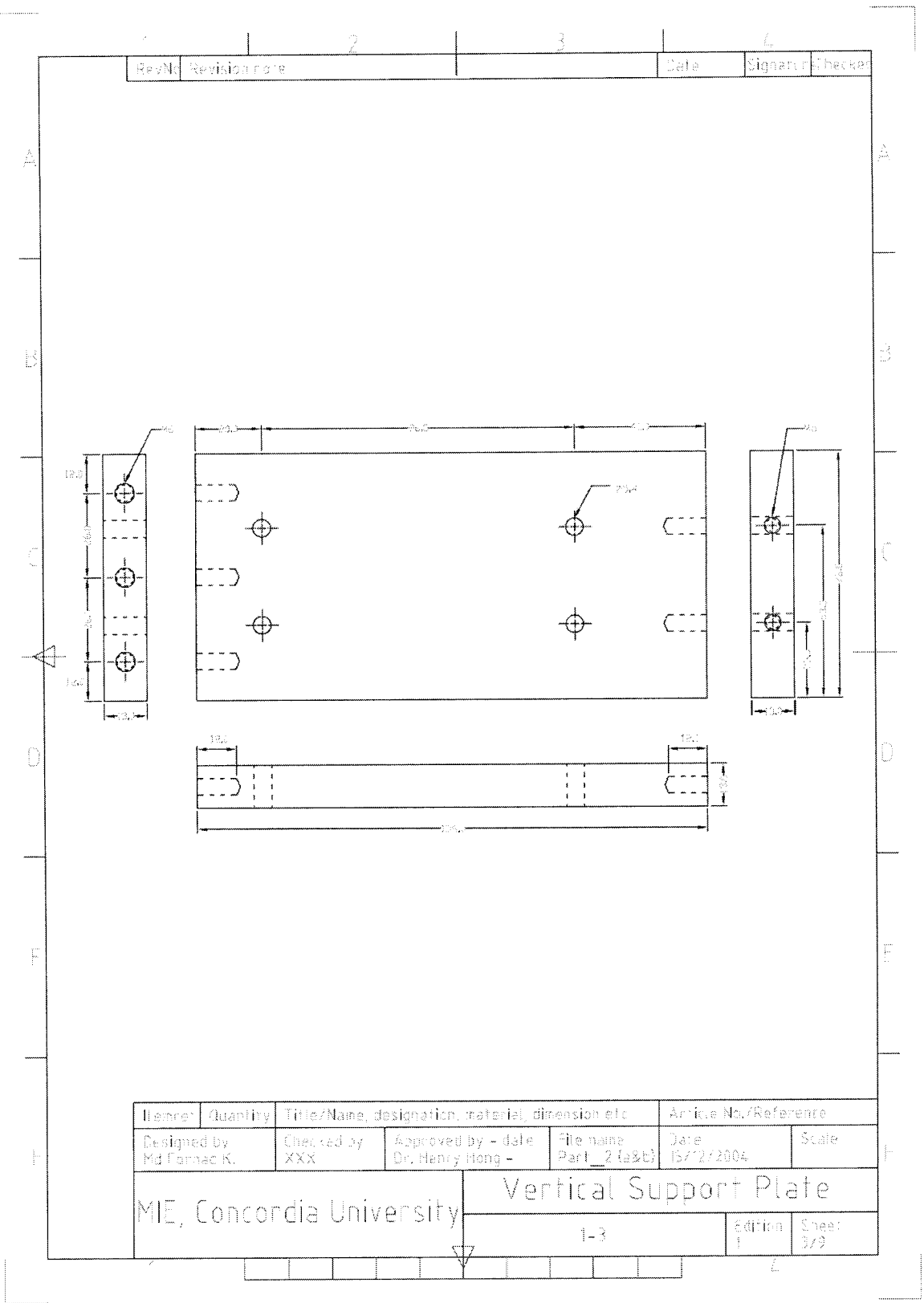

Fig.A-IV.3 Vertical Support Plate (Part-2)

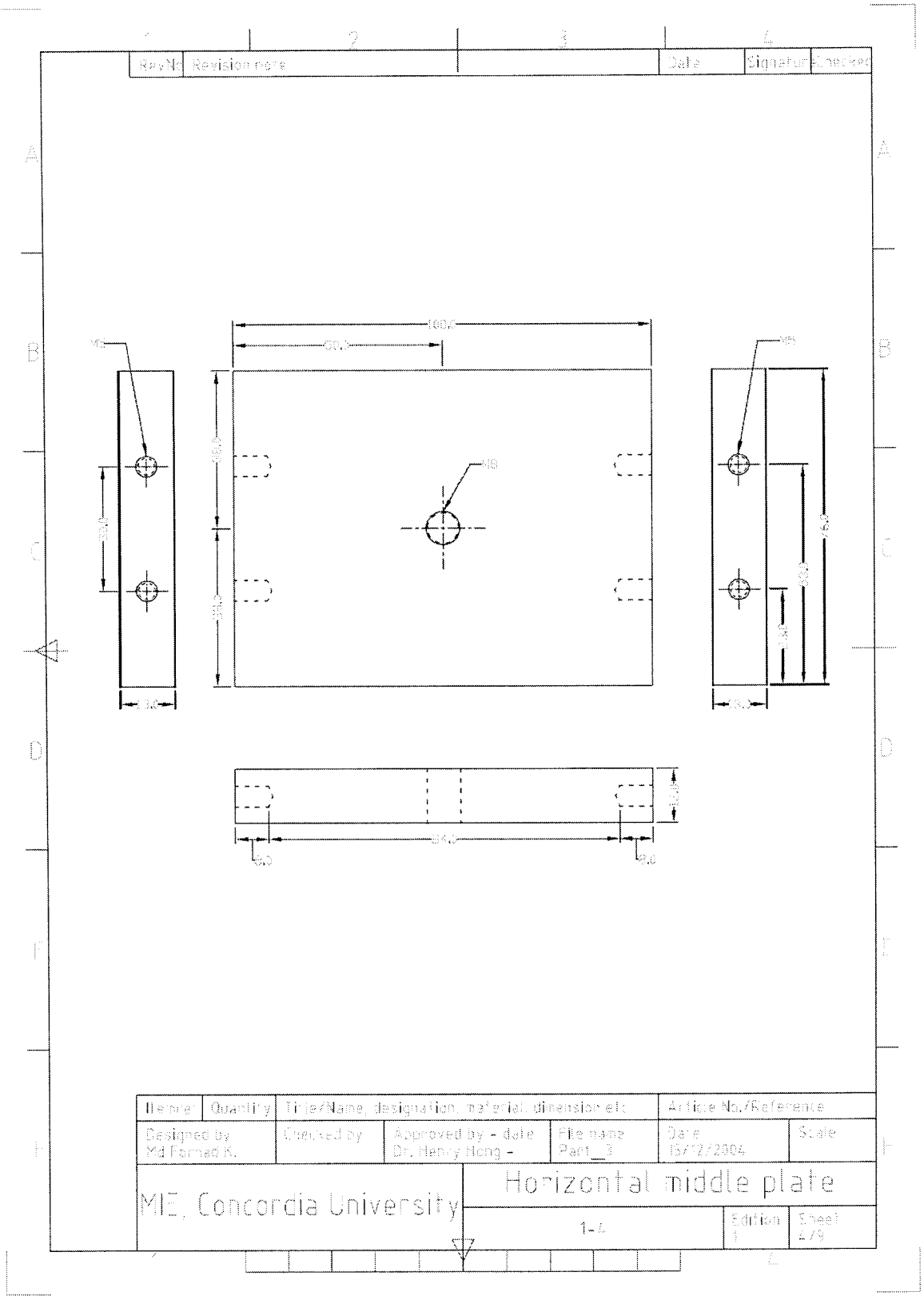

Fig.A-IV.4 Horizontal middle Plate (Part-3)

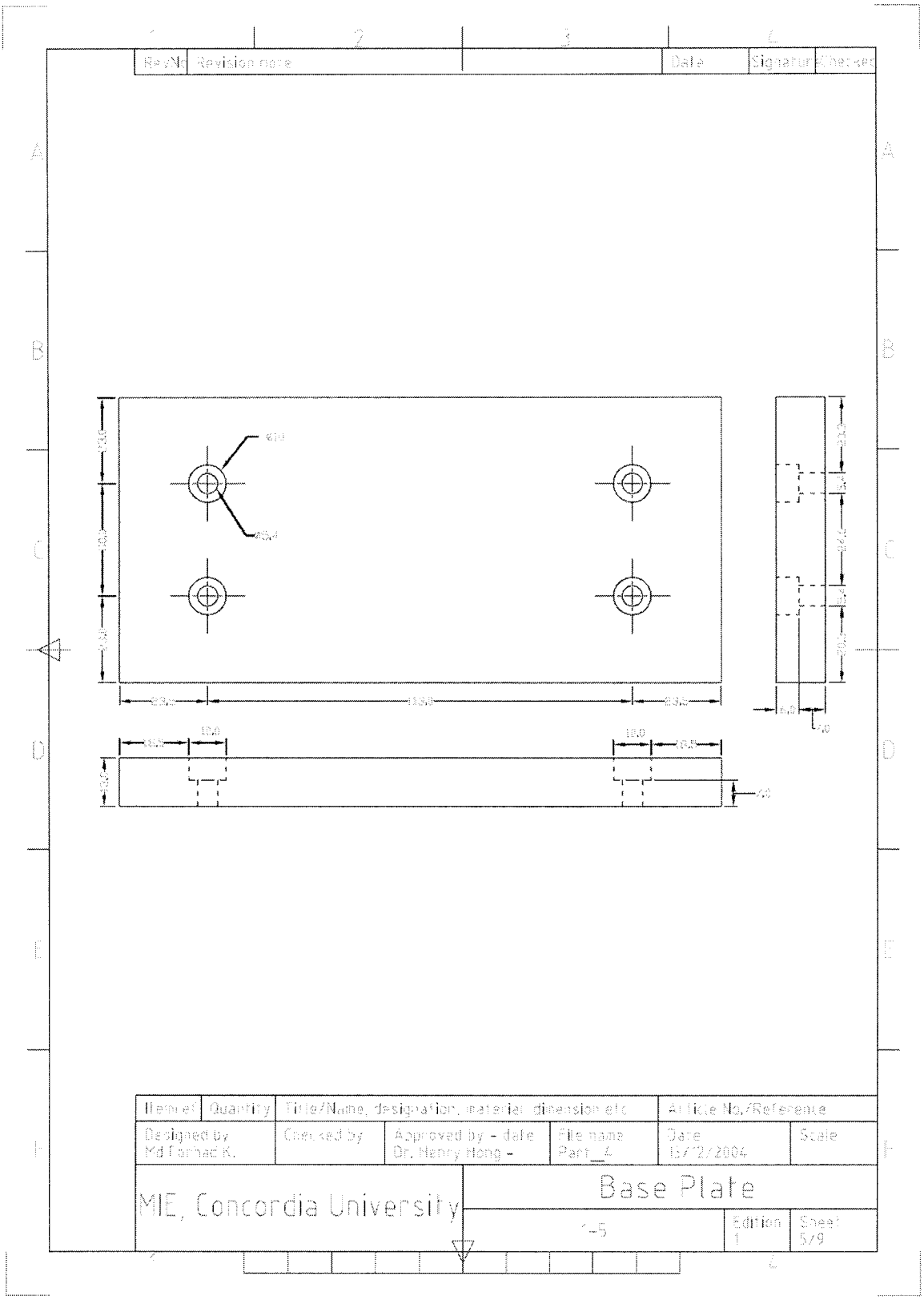

Fig.A-IV.5 Base Plate (Part-4)

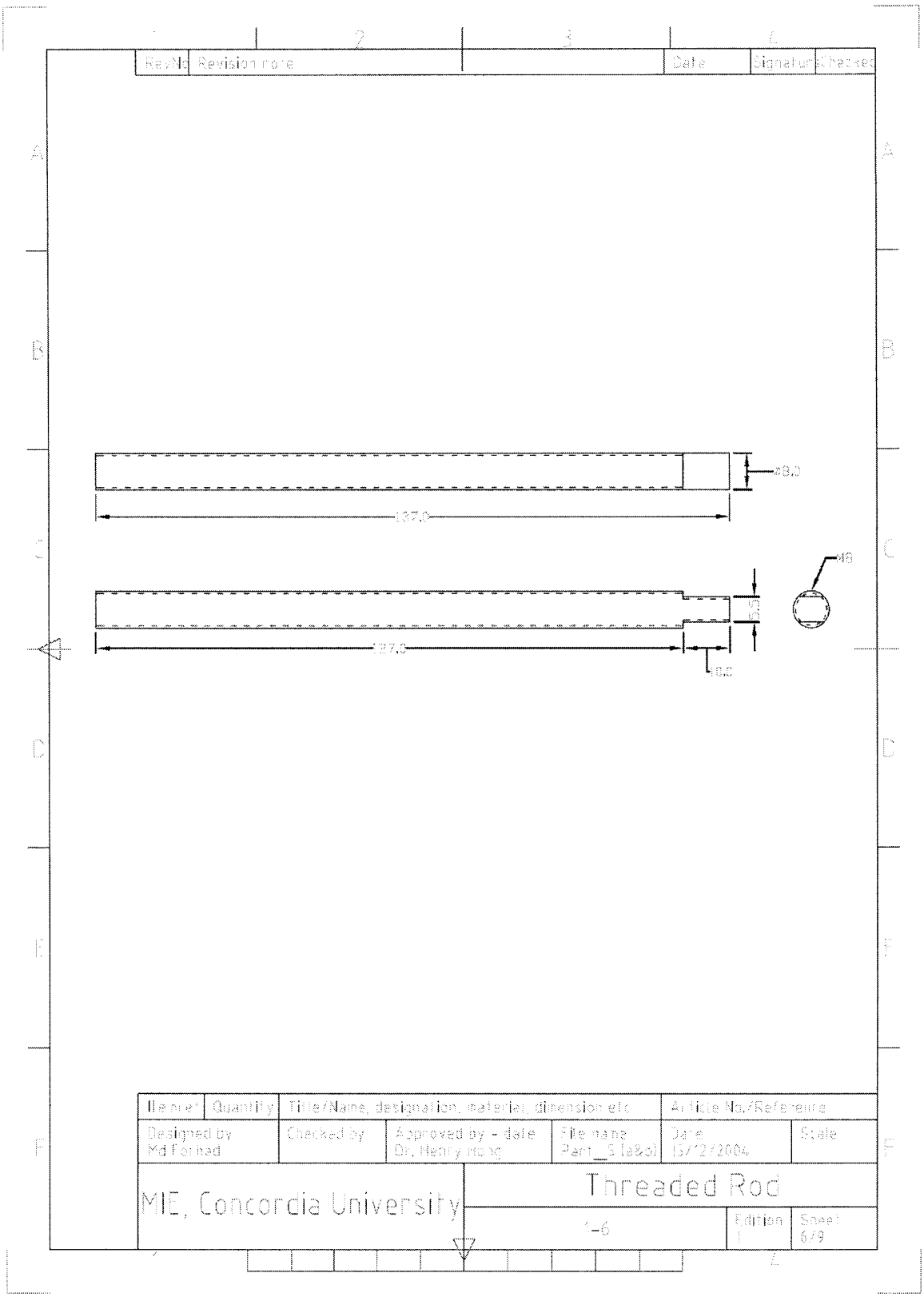

Fig.A-IV.6 Threaded Road (Part-5)

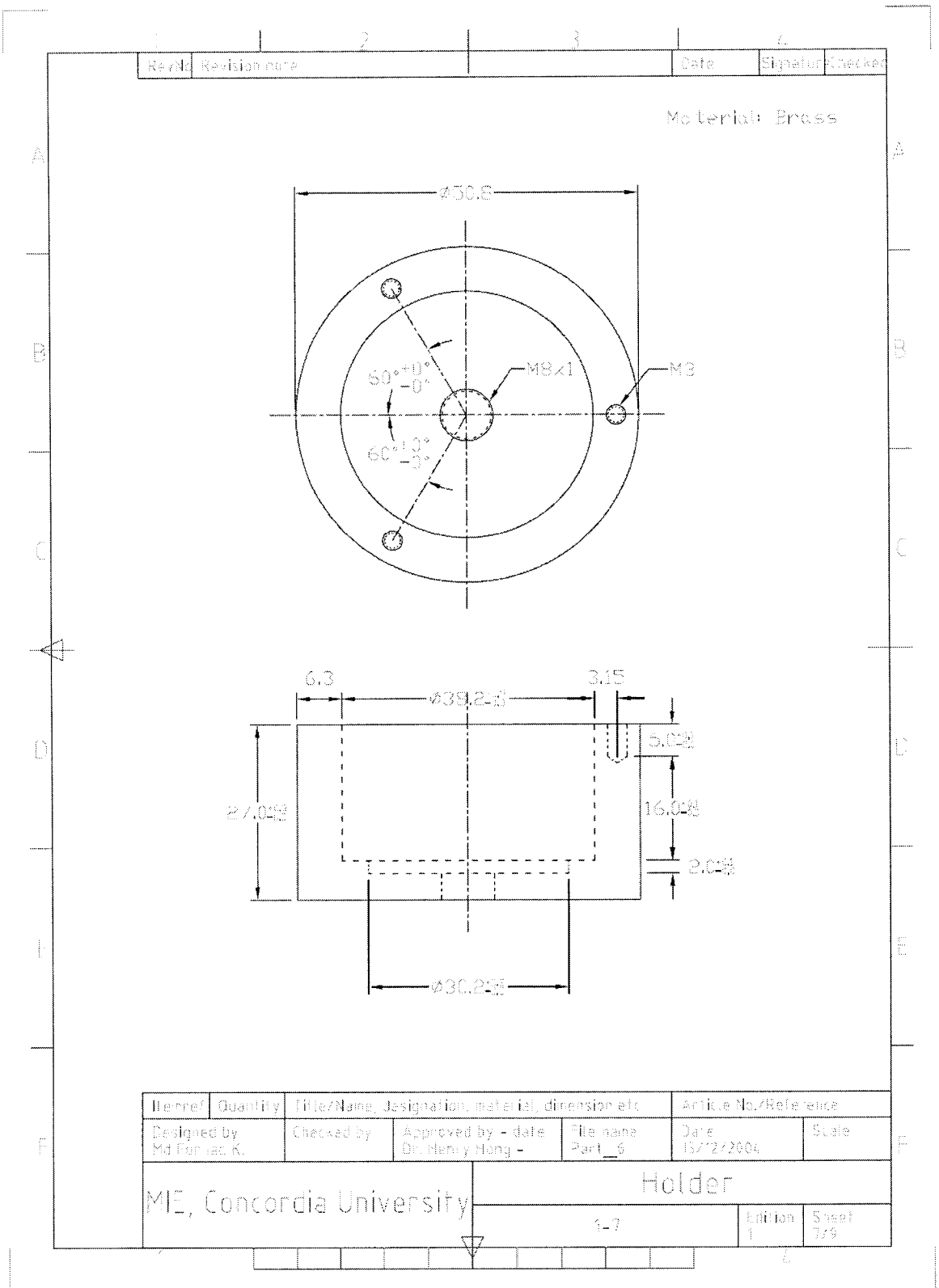

Fig.A-IV.7 Holder (Part-6)

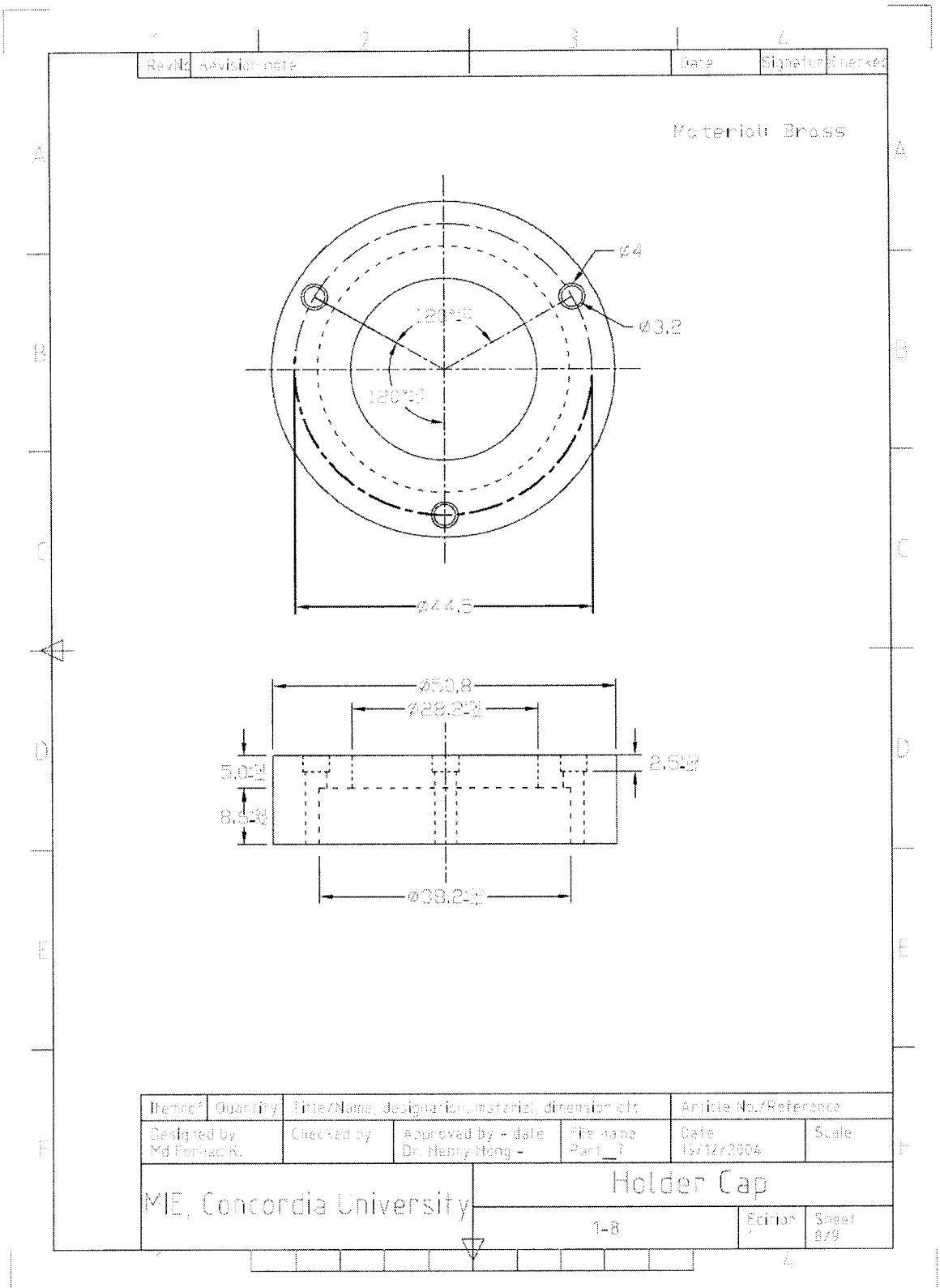

Fig.A-IV.8 Holder Cap (Part-7)

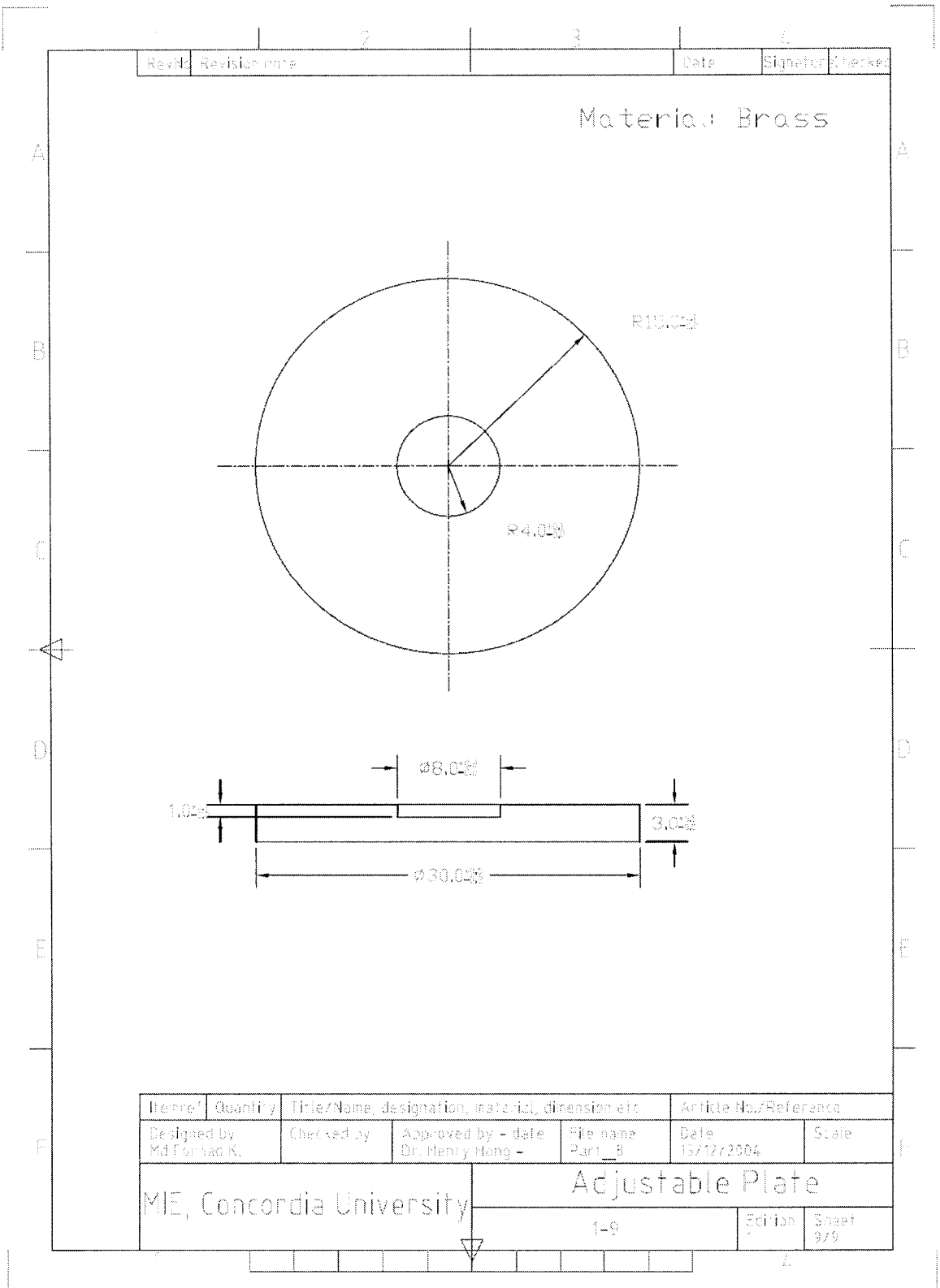

Fig.A-IV.9 Adjustable Plate (Part-8)

APPENDIX-V

The MATLAB program of computer simulation for different voltages (static force and Current) and experimental data plot at 5mm traveling distance is as follows:

```
% Current Response of VCA for different voltages
% Traveling distance 5mm
clc;            clear all;
num_c=1; den_c=[.0014 4.4];
% Transfer function
sys_current=tf(num_c,den_c);
% Step response of the open-loop system
figure(1)

% For PWM voltage 49.3V
t = [0:0.000002:.003];          % Time duration
u = 49.3*stepfun(t,0);          % Step input for desired time duration
lsim (sys_current,u,t);         % Current response
hold on
% Experimental Response of Current
C = 10*csvread('49.3V.2_5_F_C_R.csv', 790,5, [790,5, 1501,5]);
t = csvread('49.3V.2_5_F_C_R.csv', 790,0, [790,0, 1501,0]);
t = t+0.5/1000;
C1=filter (ones(1,25),25, C);
plot (t,C1)
```

```
hold on

% For PWM voltage 36.9V
t = [0:0.000002:.003];          % Time duration
u = 36.9*stepfun(t,0);
lsim (sys_current,u,t);         % Current response
hold on
% Experimental Response of Current
C = 10*csvread('36.9V.2_5_F_C_R.csv', 790,5, [790,5, 1501,5]);
t = csvread('36.9V.2_5_F_C_R.csv', 790,0, [790,0, 1501,0]);
t = t+0.5/1000;
C1 = filter (ones(1,25),25, C);
plot (t,C1)
hold on

% For PWM voltage 24.4V
t = [0:0.000002:.003];          % Time duration
u = 24.4*stepfun(t,0);
lsim (sys_current,u,t);         % Current response
hold on
% Experimental Response of Current
C = 10*csvread('24.4V.2_5_F_C_R.csv', 740,5, [740,5, 1501,5]);
t = csvread('24.4V.2_5_F_C_R.csv', 740,0, [740,0, 1501,0]);
t = t+0.5/1000;
```

```
C1 = filter (ones(1,25),25, C);
plot (t,C1)
hold on

%For PWM voltage 12.3V
t = [0:0.000002:.003];          % Time duration
u = 12.3*stepfun(t,0);
lsim (sys_current,u,t);         % Current response
hold on
% Experimental Response of Current
C = 10*csvread('12.3V.2_5_F_C_R.csv', 745,5, [745,5, 1501,5]);
t = csvread('12.3V.2_5_F_C_R.csv', 745,0, [745,0, 1501,0]);
t = t+0.5/1000;
C1 = filter(ones(1,25),25, C);
plot (t,C1)

title ('Current response of a VCA');
xlabel ('Time(ms)');
ylabel ('Current (Amp)');
legend ('','49.3V','','36.9V','','24.4V','','12.3V',2)
hold off

% For Reverse Direction
figure(2)
```

```
% For PWM voltage -49.3V
t = [0:0.000002:.003];          % Time duration
u = -49.3*stepfun(t,0);         % Step input for desired time duration
lsim (sys_current,u,t);         % Current response
hold on
% Experimental Response of Current
C = 10*csvread('49.3V.2_5_F_C.csv', 790,5, [790,5, 1501,5]);
t = csvread('49.3V.2_5_F_C.csv', 790,0, [790,0, 1501,0]);
t = t+0.5/1000;
C1 = filter (ones(1,25),25, C);
plot (t,C1)
hold on

% For PWM voltage -36.9V
t = [0:0.000002:.003];          % Time duration
u = -36.9*stepfun(t,0);
lsim (sys_current,u,t);         % Current response
hold on
% Experimental Response of Current
C = 10*csvread('36.9V.2_5_F_C.csv', 790,5, [790,5, 1501,5]);
t = csvread('36.9V.2_5_F_C.csv', 790,0, [790,0, 1501,0]);
t = t+0.5/1000;
C1= filter (ones(1,25),25, C);
```

```
plot (t,C1)
hold on

% For PWM voltage -24.4V
t = [0:0.000002:.003];          % Time duration
u = -24.4*stepfun(t,0);
lsim (sys_current,u,t);         % Current response
hold on
% Experimental Response of Current
C = 10*csvread('24.4V.2_5_F_C.csv', 740,5, [740,5, 1501,5]);
t = csvread('24.4V.2_5_F_C.csv', 740,0, [740,0, 1501,0]);
t = t+0.5/1000;
C1 = filter (ones(1,25),25, C);
plot (t,C1)
hold on

% For PWM voltage -12.3V
t = [0:0.000002:.003];          % Time duration
u = -12.3*stepfun(t,0);
lsim (sys_current,u,t);         % Current response
hold on

% Experimental Response of Current
C = 10*csvread('12.3V.2_5_F_C.csv', 745,5, [745,5, 1501,5]);
```

```
t = csvread('12.3V.2_5_F_C.csv', 745,0, [745,0, 1501,0]);

t = t+0.5/1000;

C1 = filter(ones(1,25),25, C);

plot (t,C1)

title ('Current response of a VCA in reverse direction');

xlabel ('Time(ms)');

ylabel ('Current (Amp)');

legend ('','49.3V','','36.9V','','24.4V','','12.3V',3)

hold off
```